

STRUCTURAL DESIGN AND PERFORMANCE OF COMPOSITE
WALL-FOUNDATION CONNECTOR ELEMENTS

By

KRISTIN ANNE DUCHATEAU

A thesis submitted in partial fulfillment of
the requirements for the degree of

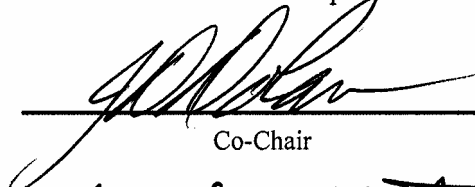
MASTER OF SCIENCE IN CIVIL ENGINEERING

WASHINGTON STATE UNIVERSITY
Department of Civil and Environmental Engineering

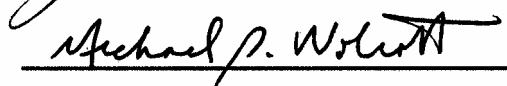
AUGUST 2005

To the Faculty of Washington State University:


The members of the Committee appointed to examine the thesis of KRISTIN ANNE DUCHATEAU find it satisfactory and recommend that it be accepted.



Co-Chair



Co-Chair



ACKNOWLEDGMENT

I would like to thank the many people who provided assistance and support throughout this project. A few groups need to be formally recognized:

- Committee members, Dr. J. Daniel Dolan, Dr. Michael Wolcott, and Dr. David Pollock, for their guidance and engineering insight,
- Office of Naval Research (under contract N00014-03-1-0949) for providing the funding to perform this research,
- Wood Materials & Engineering Lab and Department of Civil & Environmental Engineering faculty and staff for laboratory, technical, and administrative assistance, and
- Family, friends, and fellow grad students for their conversation and encouragement along the way.

STRUCTURAL DESIGN AND PERFORMANCE OF COMPOSITE WALL-FOUNDATION
CONNECTOR ELEMENTS

Abstract

by Kristin Anne Duchateau, M.S.
Washington State University
August 2005

Co-Chairs: J. Daniel Dolan & Michael P. Wolcott

Field observations following extreme earthquake events and laboratory testing identify a key area to improve upon in wood-frame shear walls as maintaining sill plate structural integrity. Due to current load paths through the sill plate when resisting overturning, coupled by construction misalignments, traditional sill plate designs split along the line of anchor bolts and lose lateral resistance. In addition, this location in a structure is susceptible to moisture infiltration. Therefore, structural member degradation from moisture and the required use of potentially hazardous preservative treatments makes it advantageous to develop durable wood thermoplastic composites (WPCs) as structural members for this location.

This paper presents an experimental investigation and proof of concept of the utilization of WPC members as sill plates in wood shear walls. Connection and component testing of one polypropylene hollow section (PP10) identified weakness in the perpendicular-to-extrusion direction, though with the use of reinforcement, performance was improved. Final design configurations showed an improvement of 27-31 kN (6000-7000 lbf) in uplift resistance over traditional end stud-to-sill connections without hold-down hardware. As well, improvements in section design have eliminated rotation and cross-grain bending in sills (forces that have caused brittle splitting of wood sills).

Full scale shear wall tests were performed on one wood sill wall configuration (as the control) and three wall configurations with WPC sills, none of the four configurations used conventional hold-down hardware. Changes in capacities, ductility, and energy dissipation resulted from different sill plate materials and configurations. Cyclic response exceeded monotonic response for walls with WPC sill plates. One WPC section was shown to be a feasible equal substitution to wood sill plates, obtaining similar performance parameters. Another WPC sill plate wall configuration had substantial improvements in capacities and exhibited racking behavior and associated failure modes, developing a completely different load-deformation response. Stiffness degradation for this section was the most gradual, allowing more than a two-fold increase in energy dissipation and retention of its ability to resist deformations in a plastic state.

TABLE OF CONTENTS

ACKNOWLEDGMENT.....	III
ABSTRACT.....	IV
TABLE OF CONTENTS.....	VI
LIST OF TABLES.....	X
LIST OF FIGURES.....	XII
CHAPTER 1 INTRODUCTION.....	1
1.1 Problem Overview.....	1
1.2 Design Modifications.....	4
1.2.1 Code Development.....	4
1.2.2 Experimental Results.....	5
1.3 Motivation.....	8
1.4 Objectives.....	10
CHAPTER 2 MATERIALS AND METHODS.....	11
2.1 Sill Plate Materials.....	11
2.2 Design Methodology.....	14
2.3 Connection Test Materials and Methods.....	17
2.4 Component Test Materials and Methods.....	22
2.5 Shear Wall Test Materials and Methods.....	25
2.5.1 Sill Plate Type.....	26
2.5.2 Fabrication of Specimens.....	26
2.5.3 Test Fixtures and Instrumentation.....	29

2.5.4 Test Procedure	31
CHAPTER 3 CONNECTION AND COMPONENT PERFORMANCE	34
3.1 Connection Tests.....	34
3.1.1 Effect of Varying Sidewall Connection Geometry	34
3.1.2 Effect of Configuration Changes	37
3.1.3 Effect of Reinforcement Methods.....	38
3.1.3.1 Traditional Configuration	39
3.1.3.2 Shifted Configuration.....	40
3.1.4 Finalized End Stud/Sill Connection.....	42
3.2 Component Tests	43
3.3 Connection and Component Test Summary	47
CHAPTER 4 SHEAR WALL PERFORMANCE	48
4.1 Test Parameters.....	48
4.2 Monotonic Test Results	51
4.1.1 Test WOOD4-M	52
4.2.2 Test PE3-M	55
4.2.3 Test PP5-M	57
4.2.4 Test PP10-M	60
4.3 Monotonic Test Conclusions	63
4.4 Cyclic Test Results	68
4.4.1 WOOD4.....	68
4.4.2 PE3.....	70
4.4.3 PP5.....	72

4.4.4 PP10	74
4.5 Cyclic Test Discussion.....	77
4.5.1 Test Group Comparison.....	77
4.5.2 Shear Deformation Contributions	79
4.5.3 Earthquake Performance Evaluation of PP10.....	80
4.5.4 Comparison of Monotonic and Cyclic Results	83
4.5.5 Cyclic Stiffness	84
4.5.6 Cyclic Test Results	87
CHAPTER 5 CONCLUSIONS AND RECOMMENDATIONS.....	89
5.1 Connection and Component Conclusions.....	89
5.2 Shear Wall Conclusions.....	90
5.3 Future Research	92
REFERENCES	95
APPENDIX A: CONNECTION AND COMPONENT TEST RESULTS	99
A.1 Connection Test Fastener Configurations.....	99
A.2 Connection Test Failure Photos	102
A.3 Connection Test Detailed Test Data	104
A.4 Component Test Detailed Test Data	105
APPENDIX B: SHEAR WALL TEST RESULTS	106
B.1 Test Setup.....	106
B.2 Supplement Test Photos: Test PP10-M Failures.....	107
B.3 Cyclic Test Data.....	110

Test WOOD4-1	111
Test WOOD4-2	114
Test PE3-1	117
Test PE3-2	120
Test PP5-2	126
Test PP10-1	129
Test PP10-2	132
B.4 Cyclic Stiffness	135
B.5 Load Washer	136
Monotonic Results	137
Cyclic Results	141

LIST OF TABLES

Table 2.1 Sill plate member properties	12
Table 2.2 Extruder temperature profile.....	13
Table 2.3 Connection Test Variables.....	20
Table 2.4 Shear wall configurations	26
Table 2.5 Framing and sheathing heights for tests	27
Table 2.6 Nail specifications.....	28
Table 2.7 Cyclic wall test reference displacements	31
Table 2.8 CUREE Protocol: Amplitudes of primary cycles (Krawinkler, 2001).....	32
Table 3.1 Connection Test Summary.....	34
Table 3.2. Comparison of stiffness values for connection tests and previous monotonic shear wall tests (2.44 m) (8 feet).....	46
Table 4.1 Monotonic test summary of performance parameters	64
Table 4.2 Comparison of monotonic test parameters	65
Table 4.3 Performance parameters	68
Table 4.4 Amount of wall displacement from shear deformations at point of maximum load.....	79
Table 4.5 Capacities of walls with overturning anchorage.....	81
Table 4.6 Comparison of monotonic and cyclic wall capacities	84
Table A.1 Full connection test data	104
Table A.2 Full component test data	105
Table B.1 Test WOOD4-1 Summary	111
Table B.2 Test WOOD4-1 Energy and damping data	113

Table B.3 Test WOOD4-2 Summary.....	114
Table B.4 Test WOOD4-2 Energy and damping data	116
Table B.5 Test PE3-1 Summary	117
Table B.6 Test PE3-1 Energy and damping data.....	119
Table B.7 Test PE3-2 Summary	120
Table B.8 Test PE3-2 Energy and damping data.....	122
Table B.9 Test PP5-1 Summary.....	123
Table B.10 Test PP5-1 Energy and damping data	125
Table B.11 Test PP5-2 Summary.....	126
Table B.12 Test PP5-2 Energy and damping data	128
Table B.13 Test PP10-1 Summary.....	129
Table B.14 Test PP10-1 Energy and damping data	131
Table B.15 Test PP10-2 Summary.....	132
Table B.16 Test PP10-2 Energy and damping data	134
Table B.17 Cyclic stiffness values.....	135

LIST OF FIGURES

Figure 2.1 Section profiles utilized for sill plates: (a) WOOD4: Pressure treated wood sill, (b) PE3: Solid polyethylene, (c) PP5: Hollow polypropylene three-box, and (d) PP10: Hollow polypropylene.....	11
Figure 2.2 Conceptual sill plate system.....	15
Figure 2.3 Machined stud locations: a) End stud, b) Interior stud.....	16
Figure 2.4 Beam bending of sill plate due to tension from overturning forces	16
Figure 2.5 Compressive forces on sill plate from compression chord (end studs) in wall overturning.....	16
Figure 2.6 Cross-grain bending of sill plate due to eccentricity between sheathing connection and anchor	16
Figure 2.7 Connection forces: (a) End stud connection force direction, (b) Bearing on sill plate from fasteners, (c) Tension perpendicular to extrusion from upward force of fastener.....	17
Figure 2.8 PP10 slot dimensions: (a) Specimens 1-11 and (b) Specimens 12-16 (Shifted Configuration).....	18
Figure 2.9 Typical connection test geometry.....	19
Figure 2.10 Connection test setup.....	21
Figure 2.11 Component design: a) Full section, b) End stud detail.....	23
Figure 2.12 Component test setup: a) Full component, b) End stud detail.....	25
Figure 2.13 PP10 stud configuration (end view)	27
Figure 2.14 Shear wall test frame	30
Figure 2.15 Shear wall test instrumentation	30

Figure 2.16 CUREE loading protocol.....	32
Figure 3.1 Typical failure path in connection tests (Specimen 4 shown).....	35
Figure 3.2 Failure perpendicular-to-extrusion between flange and webs from uplift force transferred to dowels.....	38
Figure 3.3 Comparison of load-deflection behavior from moving end stud position and adding dowels	38
Figure 3.4 Reinforced sill failure photo (Specimen 10)	39
Figure 3.5 Effects of reinforcing sidewall connection.....	40
Figure 3.6 Perpendicular-to-extrusion screw reinforcement between flange and webs	41
Figure 3.7 Effects of reinforcing top flange to web.....	41
Figure 3.8 Beam bending in component tests from dowel uplift.....	44
Figure 3.9 Typical component test flexural failure at end stud slot.....	44
Figure 3.10 Component test load deflection curves: a) Performance parameters and spread of data, b) Structural stiffness calculation.....	45
Figure 4.1 Response curve of monotonic wall test with traditional pressure-treated sill plate (WOOD4-M).....	52
Figure 4.2 Monotonic test failures in sill: (a) Sill plate splitting along edge of plate washer and studs unzipping on loaded end of wall, (b) Split sill plate (end view).....	53
Figure 4.3 Load washer placement for WOOD4, PE3, and PP5	54
Figure 4.4 Test WOOD4-M Load washer readings over time.....	54
Figure 4.5 Response curve of monotonic wall test with solid polyethylene sill plate (PE3- M).....	55

Figure 4.6 Sill failures: (a) Sill bending and flexural cracking at anchor bolt nearest loaded end stud, and (b) Plate washer indentation and anchor bolt hole size increase from bearing.....	56
Figure 4.7 Nail bending and tear-out from sheathing and sill plate at loaded end of wall	56
Figure 4.8 Test PE3-M Load washer readings over time	57
Figure 4.9 Response curve of monotonic wall test with hollow polypropylene three-box sill plate (PP5-M).....	58
Figure 4.10 View of sill bending and splitting: (a) Overall behavior of sill end, (b) View from top of split along strand.....	59
Figure 4.11 View of failure at anchor bolt location, shown from outside bottom edge	59
Figure 4.12 Test PP5-M Load washer readings over time.....	60
Figure 4.13 Response curve of monotonic wall test with polypropylene 100 mm x 152 mm hollow sill plate (PP10).....	61
Figure 4.14 Overall PP10 hollow sill plate behavior (load being applied from right side).....	62
Figure 4.15 Sill failure at end stud: (a) First flexural failure, (b) Failure through section and dowels crushing upper flange and yielding.....	62
Figure 4.16 Test PP10-M Load washer readings over time.....	63
Figure 4.17 Load-displacement curves for monotonic tests	64
Figure 4.18 EEEP curves from monotonic test results	65
Figure 4.19 Racking displacement of walls in monotonic tests.....	66
Figure 4.20 WOOD4 response curves	69

Figure 4.21 WOOD4 failures: (a) Typical sill splitting full length (Test WOOD4-1), (b) Sill end split (Test WOOD4-2), and (c) Sheathing nail pull-out at wall end (Test WOOD4-1)	70
Figure 4.22 PE3 response curves	71
Figure 4.23 PE3 failures: (a) Overall bending during test (Test PE3-2), (b) Failures near end anchor bolt (Test PE3-1), and (c) End anchor bolt plate washer indentation and 45 degree failure (Test PE3-1).....	72
Figure 4.24 PP5 response curves	73
Figure 4.25 PP5 failures: (a) Side box split down length of sill, (b) Bottom view of split box between outside web and flange and flexural failure, and (c) End view of split showing separation between strands	74
Figure 4.26 PP10 response curves	75
Figure 4.27 PP10 failures: (a) Flexural failure at interior anchor bolt, (b) Flexural failure at end stud connection, (c) End view of dowels yielding , (d) Yielded dowels from Test PP10-2, (e) Failure plane along section strands, and (f) Nail pull-through at panel joint (inset photos of yielded fasteners and view of panel joint from outside).....	76
Figure 4.28 Best fit lines for each test group	77
Figure 4.29 Average EEEP curves for wall configurations under monotonic and cyclic loading.....	82
Figure 4.30 Stiffness degradation from cyclic loading	86
Figure A.1 Connection configurations.....	100
Figure A.2 Connection Tests 1-12 failure photos	102
Figure A.3 Connection Tests 13-16 failure photos.....	103

Figure B.1 Shear wall test setup photos.....	106
Figure B.2 Test PP10-M sill failure and overall behavior.....	107
Figure B.3 Interior stud-to-sill connection behavior: (a) Nail bending with sheathing racking, (b) Stud splitting from screw connectors, and (c) Interior stud movement in slot and crack in bottom flange.....	107
Figure B.4 Illustration of sheathing racking: (a) Bearing on sill top, (b) Displacing 13-19 mm (0.5-0.75 inches) past end of sill, and (c) Racking at panel joint.....	108
Figure B.5 End stud failed connection (top view): dowels yielded, top flange crushed, sill cracked through.....	109
Figure B.6 Flexural failure at second anchor bolt: (a) Location along sill, (b) Failure exposes anchor bolt within.....	109
Figure B.7 Test WOOD4-1 Hysteresis: Reference Displacement = 41 mm (1.61 in).....	112
Figure B.8 Time history for Test WOOD4-1.....	112
Figure B.9 Test WOOD4-2 Hyteresis: Reference Displacement = 41 mm (1.61 in).....	115
Figure B.10 Time history for Test WOOD4-2.....	115
Figure B.11 Test PE3-1 Hysteresis: Reference Displacement = 36 mm (1.40 in).....	118
Figure B.12 Time history for Test PE3-1.....	118
Figure B.13 Test PE3-2 Hysteresis: Reference Displacement = 36 mm (1.40 in).....	121
Figure B.14 Time history for Test PE3-2.....	121
Figure B.15 Test PP5-1 Hysteresis (Reference Displacement = 18 mm (0.70 in)).....	124
Figure B.16 Time history for Test PP5-1.....	124
Figure B.17 Test PP5-2 Hysteresis (Reference Displacement = 18 mm (0.70 in)).....	127
Figure B.18 Time history for Test PP5-2.....	127

Figure B.19 Test PP10-1 Hysteresis (Reference Displacement = 35 mm (1.39 in)).....	130
Figure B.20 Time history for Test PP10-1	130
Figure B.21 Test PP10-2 Hysteresis (Reference Displacement = 35 mm (1.39 in)).....	133
Figure B.22 Time history for Test PP10-2	133
Figure B.25 Test WOOD4-M load washer data	137
Figure B.26 Test PE3-M load washer data	137
Figure B.27 Test PP5-M load washer data	138
Figure B.28 Test PP10-M load washer data	138
Figure B.29 Load washer 1 test data.....	139
Figure B.30 Load washer 2 test data.....	139
Figure B.31 Load washer 3 test data.....	140
Figure B.32 Test WOOD4-1 load washer time history	141
Figure B.33 Test WOOD4-2 load washer time history	141
Figure B.34 Test PE3-1 load washer time history	142
Figure B.35 Test PE3-2 load washer time history	142
Figure B.36 Test PP5-1 load washer time history	143
Figure B.37 Test PP5-2 load washer time history	143
Figure B.38 Test PP10-1 load washer time history	144
Figure B.39 Test PP10-2 load washer time history	144

CHAPTER 1 INTRODUCTION

To improve upon lateral load resistance and durability of wood building envelopes, research is currently being conducted on “Durable Wood Composites for Naval Low-Rise Buildings” at Washington State University. This work is funded by the U.S. Navy’s Office of Naval Research. The U.S. Navy has considerable inventory in low-rise timber construction. The coastal location of these buildings results in significant exposure to moisture, causing large maintenance problems and potentially high costs for ownership. Additionally, these facilities are often located in areas of high seismic or hurricane risk, requiring an increased level of structural performance. The need for durable materials used in engineered applications provides the opportunity to research wood thermoplastic composites utilized as structural members.

This study investigates the application of wood plastic composites (WPCs) in wall-to-foundation connections of wood-frame buildings. A literature review will identify current structural problems in lateral force systems, outline design requirements, present previous experimental results, and establish advantages of utilizing WPC material. Following the literature review, the objectives and scope of this research will identify necessary experimental investigations in designing a prototype wood-to-foundation connection system.

1.1 Problem Overview

Wood-frame buildings were perceived to perform relatively well in earthquake loadings due to their highly redundant structural systems. Northridge earthquake in 1994 contradicted this perception and shifted attention in the structural community towards improving seismic performance of these buildings. Wood-frame building failures accounted for \$20 billion in property loss, outweighing losses incurred by any other single type of building construction.

This damage resulted in 100,000 residents temporarily displaced, and an additional 50,000 residents unable to return to their homes. Numerous injuries, and 24 out of 25 fatalities occurring in the Northridge earthquake, were attributable to failures in wood-frame buildings (Mahaney and Kehoe, 2002). These losses contributed to the most costly natural disaster in United States history (Moehle, 1994).

Wood-frame construction comprises a substantial portion of building inventory in the United States—80-90% of all structures. In Los Angeles County alone, wood-frame construction accounts for 81% of total structures and 99% of residences. (Mahaney and Kehoe, 2002). With such a large percentage of the nation's population occupying wood-frame structures, the consequences of the Northridge earthquake present widespread concern.

Shear wall and lateral force resisting systems were particularly prone to failure during the Northridge earthquake, contributing to 167 dwellings being demolished (Schierle, 2002). Field observations found signs of failure including exterior cracking at sill-foundation connections, significant deformation at wall boundaries, sliding of walls along foundations, and splitting of sill plates (Day, 1996). Cases of limited shear resistance result from hold-down connections stretching where shear and overturning forces concentrate, from bolt holes being spaced too close or too far apart, having over-drilled bolt holes, or inadequate number of anchors. Resulting slip and deformation reduce lateral force capacity after sill plates split longitudinally (Hamburger, 1994). The concealed nature of these structural failures makes damage difficult to identify and costly to repair after a large loading event (Schierle, 2002). Immediately, damages in walls at the base of structures may have detrimental effects on the remaining structure—causing further deformations, or even collapse.

Improper installation methods were identified as a factor in poor sill plate behavior when subjected to high stresses. Misalignments in foundation wall placement frequently cause sill plates to be installed off-center of anchor bolts. This creates larger eccentricities between anchorage and uplift forces when resisting overturning. Additionally, errors in anchor bolt installation require countersinking of bolt holes, which reduces sill plate thickness. Both of these factors reduce resistance to cross-grain bending (Kiefer, 1998).

Wood degradation compounds weaknesses in structural members. According to personal correspondence with Los Angeles County officials, in multiple cases of collapse it was shown that approximately the bottom six inches of sheathing had decayed due to moisture (Delli Quadri, 2003). Factors contributing to infiltration of moisture at shear wall bases are: proximity to the ground, vegetation, and sprinklers; contact with concrete; condensation on metal connectors; lack of or improper overhang, siding cover, or improper bottom flashing; and moisture barrier installation. Moisture protection is frequently overlooked or is omitted in order to reduce costs. The resulting sheathing degradation prevents complete lateral resistance from nailed connections between sheathing and framing.

Structural damage from moisture infiltration is widespread, and moisture problems in lateral force resisting systems have caused billions of dollars in damages in the last decade.

Some of the more notable losses are (CRD, 2003):

- CDN \$1 billion in damages of framing and sheathing for leaky condos in Vancouver, British Columbia.
- US \$20 million for a class action settlement for decay in sheathing in North Carolina
- US \$100 million and more for damage to framing and sheathing in leaky condos in Seattle, Washington

The magnitude of this problem was well stated by Kubal (2000): moisture problems “damage or completely destroy more buildings and structures than war or natural disasters” (Kubal, 2000),

and cause the overall construction lumber industry in the United States to use more than 5% of newly manufactured wood to replace decayed wood in service every year (Smulski, 1996). Because of the widespread problem of wood degradation and its implications on structural performance of shear walls, this research focuses on improving moisture resistance along with structural behavior.

1.2 Design Modifications

1.2.1 Code Development

Sill plate failures in the Northridge earthquake helped engineers recognize the significance of poorly designed sill plates and, consequently, following this event design requirements were changed. Code changes submitted to the 1994 Editions of the Uniform Codes proposed panel edge nailing distances to be increased and sills to be increased to 76 mm (3x) nominal thickness lumber for high shear loads (ICBO, 1994). This was challenged because it was felt that 63 mm (3x nominal) sill plates would increase costs and challenge standardization in the construction industry. Additionally, 102 mm (4-inch) nominal width members, if set flush against outside rim joists, would not allow anchor bolts to be centered in foundation walls nor achieve the required clearance for bolts relative to concrete or masonry foundation wall faces. The International Building Code (IBC) continues to require 76 mm (3x) nominal thickness members for sill plates resisting an ASD design load greater than 5.1 kN/m (350 plf), though with an exception brought forth by the Redwood Empire Chapter. The amendment, submitted and passed, allows using 51 mm (2x) sill plate members with twice the amount of anchor bolts and with the use of square-cut plate washers (ICBO, 2000b). Permitting use of 51 mm (2x) members avoids mixing 51 mm (2-inch) and 76 mm (3-inch) plates in a building which cause

detailing difficulties and increases the incidence of overdrilling sill plate anchor bolt holes (ICBO, 1996).

1.2.2 Experimental Results

Following the events of the Northridge earthquake, an extensive effort toward improving wood-frame performance was organized as the CUREE-Caltech Wood-frame Project. CUREE, the Consortium of Universities for Research in Earthquake Engineering, is comprised of universities, consulting engineers, government agencies, trade groups, and others to advance earthquake engineering (Hall, 2002).

Within CUREE, Task 1.4.1.1 *Anchorage of Wood-Frame Buildings* performed extensive testing on variables affecting sill plate performance. This work, completed by Mahaney and Kehoe (2002), included the following variables: sill width, sill thickness, sill species, anchor bolt size, amount of dead load, shear connection type, bolt washer size and type, anchor bolt location, anchor bolt hole size, and hold-down type. A force-controlled loading protocol based on developments in CUREE Task 1.3.2, *Cyclic Response of Wood-frame Shearwalls: Loading Protocol and Rate of Loading Effects* (Gatto and Uang, 2002), was utilized in testing specimens.

Results from CUREE anchorage tests provide insight on shear wall failure modes and ductility response. Out of sixty-three valid tests, thirty-four failed in the sill plate. Of those tests lacking hold-down connectors, where failures in the sill plate occurred, lower load capacities and lower number of cycles were achieved—compared to walls having other failure mechanisms. Those tests using hold-down anchors and failing in the sill plate achieved higher loads but lower cycles than those with plywood or blocking failures (Mahaney and Kehoe, 2002).

Specific failures observed in sill plates occurred due to combined bending and twisting (for reference, greater than 10 mm (3/8 in) upward and cross-grain rotation of 0.1 radians)

coupled with stress concentrators along the grain from sheathing nails. By limiting sill plate bending and twisting, failure of shear walls can be shifted from brittle sill-to-foundation connection damage to a more ductile failure associated with anchor bolts or plywood/framing connections yielding (NDS Mode III_s failure). Testing has shown that when failure modes occur in the plywood rather than sill plates, ductility and wall performance are improved.

CUREE Task 1.4.1.1 also identified specific variables that prevent or delay sill plate bending and twisting. Limiting a wall's height to width ratio and supplying hold-downs with sufficient strength and stiffness can increase wall performance significantly. Anchor bolt washers, approximately the width of the sill plate and with adequate thickness to prevent yielding, are also ways to improve performance. Additionally, increasing the thickness of sill plates to 76 mm (3x) nominal thickness, inserting 76 mm (3x) nominal blocking between studs into which sheathing would be nailed, or by installing sheathing on both sides of the wall leads to performance improvements. Other factors such as wood species, applied dead load, end distance of first anchor bolt, sill plate width, slanted bolts and oversized holes (or epoxy-filled), bolt diameter, or concrete strength play minor roles in sill plate and, consequently, shear wall performance.

Final design recommendations from CUREE Task 1.4.1.1 suggest increasing sill plate thicknesses to nominal 76 mm (3 in) and using square plate washers—both design recommendations parallel code changes after Northridge earthquake. In addition, it was recommended that end studs be 102 mm (4 in) nominal posts connected to stiff hold-downs, and 76 mm (3 in) nominal framing be provided at plywood panel joints.

The effectiveness of square plate washers to counteract cross-grain bending and subsequent sill splitting has been further investigated. The International Residential Building

Code requires the use of plate washers with minimum dimensions of 50 mm x 50 mm x 5 mm (2 in. x 2 in. x 3/16 in.), as opposed to round, cut washers (ICBO, 2000a). The American Plywood Association (APA) reported no splitting failures and a shear wall strength of 12.7 kN/m (870 plf) in tests on walls with 38 mm x 89 mm (2 in x 4 in nominal) sill plates restrained with large, 76 mm x 102 mm x 19 mm (3 in. x 4 in. x 3/4 in.) plate washers (Martin, 2004). Recently (May 2004), Oregon State University (OSU) prepared reports for the American Forest and Paper Association (AF&PA) considering different plate washer sizes for engineered shear walls. Using 50 mm x 102 mm (2 in. x 4 in.) nominal Dougl-fir and Simpson PHD hold-downs, four different test set-ups investigated wall response with 50 mm x 5 mm thick (2 in. x 3/16 in.), 64 mm x 6 mm thick (2-1/2 in. x 1/4 in.), and 76 mm x 10 mm thick (3 in. x 3/8 in.) square plate washers, and standard round washers—44 mm diameter x 3 mm thick (1-3/4 in. x 1/8 in.). In this testing, walls with standard round washers were shown to carry higher maximum loads with smaller deflections, resulting in lower energy dissipation than square plate washers. Despite different ultimate loads, statistically these differences were found to be insignificant based on analysis of variance values for mean peak capacities. Failure modes were consistent throughout testing—failing in sheathing fasteners for walls using square plate washers and in sill plates for walls using round cut washer (Rosowsky et al, 2004). This implies walls constructed with standard round washers, under extreme loading, absorb less energy, creating less desirable, brittle failures in shear walls. These results are consistent with behavior in CUREE tests where square washers tend towards slightly lower ultimate loads (Mahaney and Kehoe, 2002).

Retrofit solutions for sill plate splitting along the line of anchor bolts have been researched at Texas A&M. Two methods proposed were thin metal reinforcing straps or reinforcing clamps, both which provide extra resistance against perpendicular-to-grain splitting

across sill plates. The strap, adjustable and post-tensioned with metal hose clamps, confines sill plates around anchor bolts to enable lateral forces to be transferred even in cases where sills split. The second method, reinforcing clamps, achieves improved strength and deformation capacity of connections by placing galvanized steel or composite material over the sill plate, around the anchor bolt, partially wrapping around sill plate sides, and nailing. Anchor bolts are able to bear on clamps, rather than crushing and splitting wood. If sill failure would occur, clamps buckle locally or anchor bolts deform, while clamps contain members to ensure bearing and to prevent brittle failure (Bracci et al, 1996).

1.3 Motivation

Sill plate performance is dependent not only on structural form but also material behavior. Due to their proximity to water sources, sill plates undergo moisture stresses and are required to be made of naturally durable material or be pressure-treated with chemical preservatives. Chromated Copper Arsenate (CCA), a common preservative for treated lumber, was banned for residential use by the Environmental Protection Agency at the end of 2003 due to arsenic and chromium having evidence of human carcinogenicity and copper being toxic to some organisms (Cox, 1991). Replacements for CCA such as Alkaline Copper Quaternary (ACQ) and Copper Azole (CA) (CWC, 2004) have been formed by adding more copper, thus raising prices and increasing corrosion potential of fasteners (Morrison, 2004). An alternative to chemically preserved wood is wood plastic composite material—these naturally durable systems composed of wood fibers and thermoplastics are inherently resistant to moisture and biological decay (Pendleton et al, 2002). This material has higher raw material costs than traditional wood, but, because of the switch in chemical preservatives and probable price increases, the resulting price

gap between chemically treated wood and wood plastic composites narrowed (Smith, 2001; Clemons, 2002).

Wood plastic composite (WPC) materials traditionally have been introduced for non-structural applications due to low stiffness. Research shows formulations of higher percentages of wood (50 to 80%) having improved stiffness (Adcock et al, 2001; Slaughter, 2004). These formulations have proven suitable for structural applications as they are able to provide increased stiffness with strength. The use of both wood and plastic in WPC members is complimentary in their structural performance—the polymer has a negative influence on stiffness and positive influence on strength, while wood has a positive influence on stiffness and negative influence on strength (Adcock et al, 2001). The assemblage of these studies has proven wood plastic composite members to be feasible for use in structural applications (e.g. dock and fender systems), and for the same reasons could be beneficial for use in building wall-to-foundation connections. WPC members naturally resist decay in moist environments, eliminating the need for chemical preservative treatments and making it an attractive choice for wall-to-foundation connections. As well, material volume can be minimized with the production of hollow sections (Mapleston, 2001; Clemons, 2002). Current research is compiling design values for various formulations of WPC members to fully utilize this material in structural design (Slaughter, 2004; Kobbe, 2005).

Processing of WPCs allows the material to be extruded in complex, intricate shapes—efficiently utilizing material to develop advantageous section properties (i.e. moment of inertia). Specific load applications may also be met with increased component properties from section design or surface modifications. With flexibility in member design, WPC members provide the

necessary load resistance and encourage integrating structural members for reduced construction time.

Future goals of the wood products industry aim to create structural systems, rather than individual members, to increase durability, performance, and disaster resistance, reduce construction time, labor, and environmental impact of wood and wood-based products (Showalter et al, 2003). With the capabilities described for WPC structural components, WPC wall-to-foundation connection systems will meet the future goals of the wood products industry and help push forward improvements upon wood-frame shear wall behavior.

1.4 Objectives

For this study, development of a prototype wall-to-foundation connector system will apply specifically to slab-on-grade construction. This project will evaluate previously developed sections (modified by machining) through component and wall tests. The intent will be to identify specific improvements in the structural shape, demonstrating a conceptual use of the durable wood-plastic material in a wall system. The objectives of this research are as follows:

- 1) Assess performance of isolated end stud-to-sill connections when varying fastener layout, configuration, and section reinforcement,
- 2) Verify load-deformation behavior of optimal sill plate design for full-size components, testing with representative field loading conditions, and
- 3) Evaluate and compare system performance of prototype sill plates and traditional shear wall construction in full-scale shear wall testing.

CHAPTER 2 MATERIALS AND METHODS

2.1 Sill Plate Materials

Wood plastic composite material was extruded and machined into three different section profiles, shown with nominal dimensions, along with a traditional solid wood sill in Figure 2.1. Referring to the profiles below, this chapter discusses three different investigations necessary for producing prototype composite stud-to-sill connection elements:

- Connection tests
- Component tests
- Shear wall tests

General processing details along with sill plate design methodology are presented first as it is applicable to all sill plate sections, followed by detailed materials and methods, presented separately for each investigation listed above.

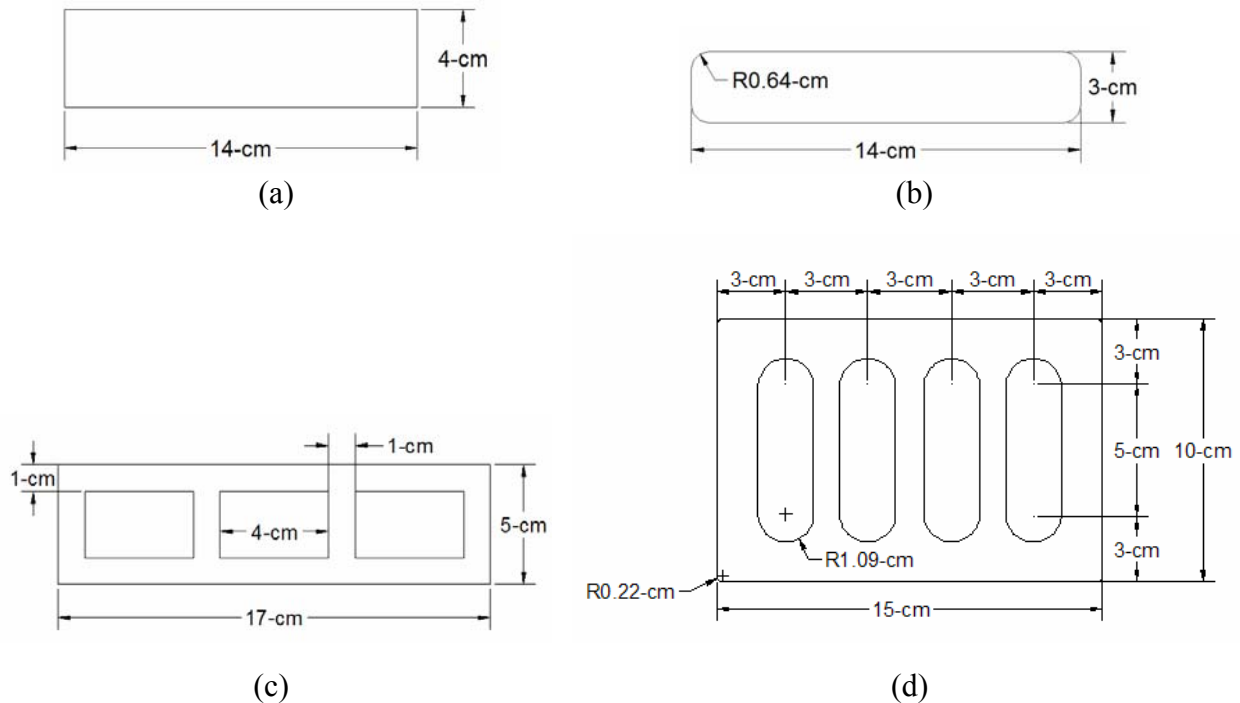


Figure 2.1 Section profiles utilized for sill plates: (a) WOOD4: Pressure treated wood sill, (b) PE3: Solid polyethylene, (c) PP5: Hollow polypropylene three-box, and (d) PP10: Hollow polypropylene

Sections in Figure 2.1 all have approximately nominal 150 mm widths. Therefore, sections will be referred to by material type and nominal depth in centimeters (e.g. WOOD4 is a wood sill plate with nominal depth of 4 cm). Section and material properties for the utilized sections are found in Table 2.1.

Table 2.1 Sill plate member properties

	Section Properties			Material Properties	
	I (cm ⁴)	S (cm ³)	A (cm ²)	MOR (kPa)	MOE (kPa)
WOOD4*	64.4	33.8	53.2	34,359 (35.0%)	8,513,650 (25.0%)
PE3	18.6	14.7	35.1	20,850 (2.4%)	3,430,149 (1.7%)
PP5	114.5	50.1	43.9	29,778 (6.8%)	4,544,211 (14.6%)
PP10	1167.9	225.7	97.5	NA	NA

Values in parenthesis: Associated coefficient of variation

*Based on design value of incised hem-fir, 10 minute load duration, and assumed coefficient of variation (NDS, 2001)

Connection and component testing only used the hollow section, PP10, whereas all sections were used in shear wall tests. The solid deck board (PE3) is intended as a direct substitution for prescriptive wood sill plates. The hollow three-box (PP5) is also intended as a direct substitution, only using a more efficient section shape. The deeper hollow section (PP10) is intended to improve upon prescriptive shear wall design, incorporating hold-down behavior between end studs and sills. This section was developed and modified to most significantly improve traditional end-grained nailing and reduce sill plate splitting in shear walls. It is the subject of discussion in design methodology and connection and component testing.

The solid deck board section is a polyethylene formulation, with the following constituents:

57.0%	60 Mesh Pine flour, <i>Pinus spp.</i> (#6020 American Wood Fibers)
30.0%	HDPE (Equistar LB0010 00)
6.0%	White Talc (Luzenac Nicron 403)
2.0%	Zinc Stearate (Ferro Chemicals Synpro DLG-20B)
2.0%	Zinc Borate (US Borax Boroguard)
2.0%	Pigment (Ciba)
1.0%	EBS Wax (GE Specialty Chemicals N, N'-thylene-bisstearamide)

Both hollow sections were a polypropylene formulation, chosen based on results from a previous polypropylene formulation study (Slaughter, 2004). This formulation maximizes mechanical and physical properties while providing quality extrusion characteristics. The following is the list of formulation constituents:

58.83%	Isotactic Polypropylene Homopolymer (Solvay HB9200)
33.83%	60 Mesh Pine flour, <i>Pinus spp.</i> (#6020 American Wood Fibers)
4.0%	White Talc (Luzenac Nicron 403)
2.3%	MAPP, Maleated Polypropylene Copolymer (Honeywell A-C 950P)
1.0%	OptiPak-100, Polyester-based wax (Honeywell OP-100)

Wood flour was dried using a steam tube dryer to 2% or less moisture content. Formulations were then dry blended in 25-kg batches using a drum mixer and extruded using an 86-mm conical intermeshing twin-screw extruder with crammer feed (Cincinnati-Milacron TC86) with the temperature profile listed in Table 2.2.

Table 2.2 Extruder temperature profile

Zone	Temperature (°F)
Barrel Zone 1	370
Barrel Zone 2	370
Barrel Zone 3	365
Barrel Zone 4	360
Screw	360
Die Zone 1	360
Die Zone 2	370
Die Zone 3	370

The screw rotational rate was 10 rpms for PE3, 5-12 rpms for PP10, and 8 rpms for PP5, with both PP10 and PP5 utilizing stranding plate technology (Laver, 1996). The extrudate was cooled in a water bath after exiting the die.

2.2 Design Methodology

Current shear wall design methods concentrate overturning forces at the sill plate. In conventional construction, walls are anchored to foundations using shear bolts or nails. The uplift forces are then transferred from the end stud and sheathing into the sill plate through sheathing nails, because the framing nails have zero force resistance when oriented in the end-grain of the lumber. From the sill plate, loads are transferred into foundations through anchor bolts or nails. However, engineered construction includes additional hold-down hardware to directly transfer uplift forces from end studs into foundations.

In developing a prototype of our composite sill plate, certain restrictions and design goals had to be met. To use conventional stud lengths, it was necessary to maintain 38-mm (2x nominal) thicknesses in the sill plate at stud locations. At the same time, the sill plate should allow placement of sheathing 152-mm (6-in) up from bottom edges to avoid moisture contact. By approaching the design from a system stand point, the need for measuring in the field may be eliminated along with the need for foundation anchors, large washers, and hold-down hardware. To accomplish design goals, the prototype WPC sill plate will conceptually have an L-shaped cross section. Ideally, the bottom surface would be 38-mm (2x nominal) thickness and the side section would stand 152-mm (6-in). The prototype used existing cross-sections; therefore, dimensions represent intended design. The basic concept, illustrated in Figure 2.2, provided the necessary dimensions at studs, clearance of sheathing, and additional connection options between studs and sills to accomplish performance requirements. Hold-down hardware in

engineered construction, limits the uplift sill plates undergo. However, it also increases construction expense as well as the need for quality control. Therefore, the prototype sill plate incorporates the hold-down behavior within the stud-to-sill connections.

Members were machined to create slots at stud locations providing a place for studs and an ability to fasten through side walls into stud edges as shown in Figure 2.3. Uplift resistance was achieved by the lateral resistance of fasteners installed through the sill side into studs, perpendicular to stud lengths, improving upon traditional end nailed connections (having negligible withdrawal/uplift resistance). Based on this conceptual design, the following forces must be considered in design of a composite sill plate system:

- Beam bending from uplift forces in end studs (tension), illustrated in Figure 2.4.
- Compression from opposite chord in overturning resistance (end stud), illustrated in Figure 2.5.
- Cross grain bending due to the eccentricity between upward forces from sheathing nails and restraint of anchor bolts, illustrated in Figure 2.6.
- Bearing and tension perpendicular-to-extrusion at connections, illustrated in Figure 2.7.

Calculations based on simple mechanics' assumptions indicate that the highest stresses will occur in tension perpendicular-to-extrusion at connections.

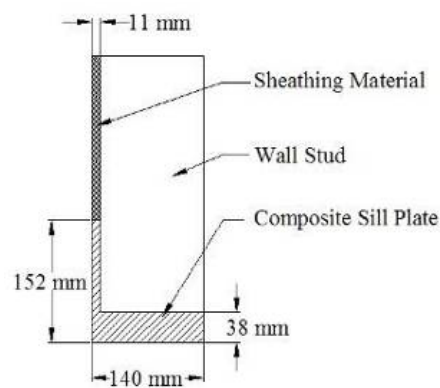


Figure 2.2 Conceptual sill plate system



(a)



(b)

Figure 2.3 Machined stud locations: a) End stud, b) Interior stud

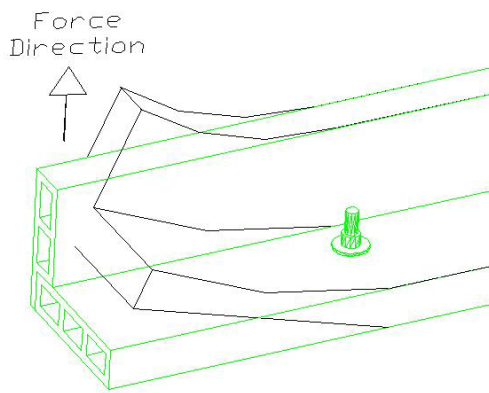


Figure 2.4 Beam bending of sill plate due to tension from overturning forces

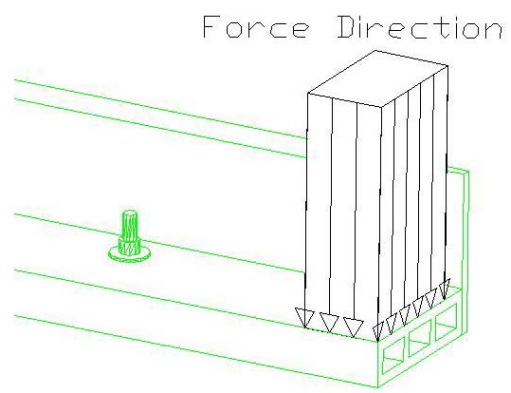


Figure 2.5 Compressive forces on sill plate from compression chord (end studs) in wall overturning

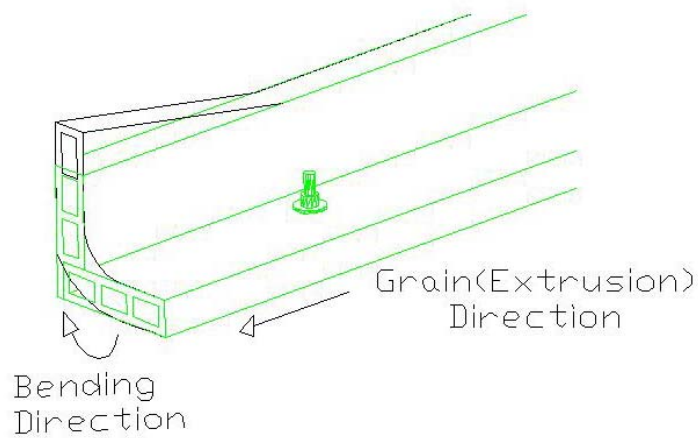


Figure 2.6 Cross-grain bending of sill plate due to eccentricity between sheathing connection and anchor

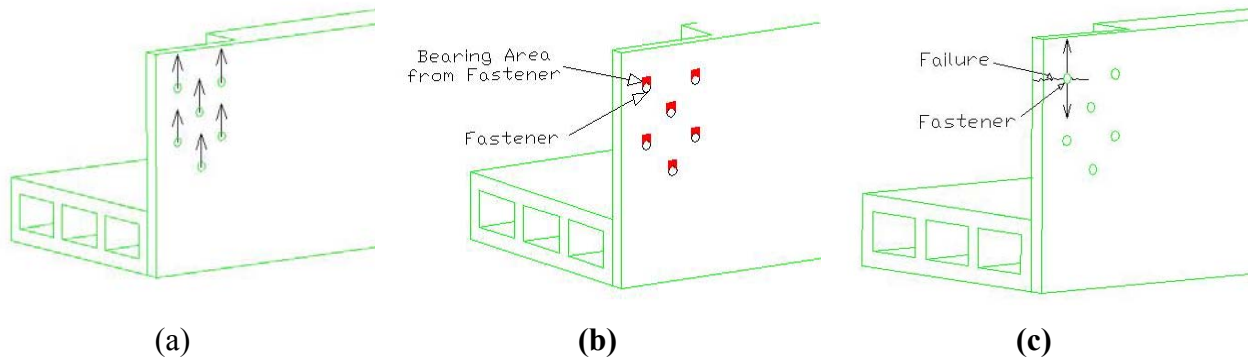


Figure 2.7 Connection forces: (a) End stud connection force direction, (b) Bearing on sill plate from fasteners, (c) Tension perpendicular to extrusion from upward force of fastener

2.3 Connection Test Materials and Methods

Design of the connection between double end studs and the hollow composite sill plate (PP10) required design values for the sill for tension in the perpendicular-to-extrusion direction. Because these values have not been determined for the formulation used, design became difficult.

Connection tests were required to isolate this end stud/sill connection. Tests investigated:

- Methods of attachment (e.g. number of fasteners, amount of edge distance, toe nails)
- Configuration changes (e.g. end stud location, anchor bolt locations)
- Transverse reinforcement effects (e.g. installing screws, fiberglass/PP tape)

Connection tests were conducted on PP10, in which specimens were cut to 254-mm (10-in) in length. Slots for end studs had dimensions as shown in Figure 2.8, with 11 specimens having slots machined in one end, and 5 specimens having a shifted configuration with slots machined 127-mm (5-in) O.C. from the end.

Wood members for end studs were two 381-mm (15-in) long pieces of 38-mm x 140-mm (2-in x 6-in nominal) dimensional lumber graded as Select Structural Douglas-fir. Because of limitations in machining rounded interior corners in composite sections, bottom corners of end studs were cut at 45 degrees, approximately 6-mm ($\frac{1}{4}$ in) up from the end.

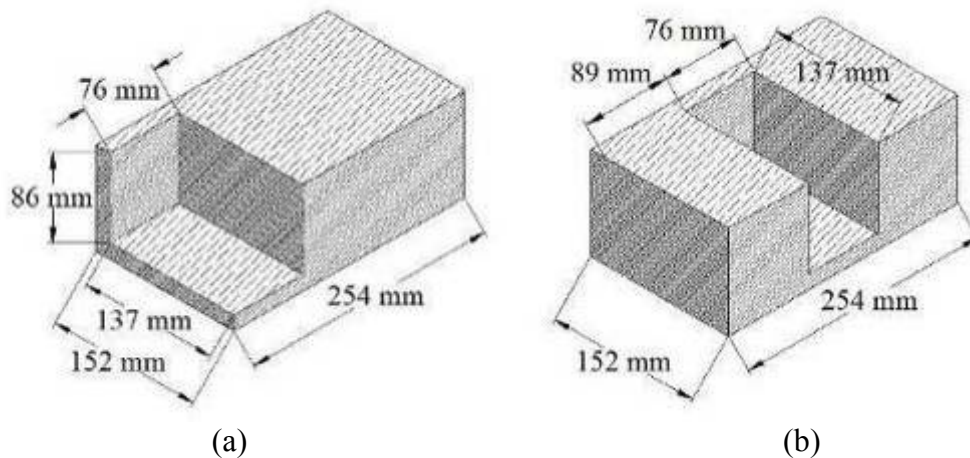


Figure 2.8 PP10 slot dimensions: (a) Specimens 1-11 and (b) Specimens 12-16 (Shifted Configuration)

Connections of the studs to specimens were through the 15-mm (0.6-in) thick vertical wall remaining of the composite sill after machining. A typical connection is shown in Figure 2.9, with the only connection occurring through section sidewalls. The end stud/sill connection geometry and type of fastener is specified for each test in the summary table located in Appendix A. Stud-to-sill connections used wood screws and helical threaded nails. Helical threaded nail diameters were approximately 50% less than wood screws (3.4-mm (0.135-in)), with similar stiffness. When installing the screws, a pilot hole equal to the fastener diameter prevented splitting of the WPC and allowed fasteners to insert completely. Pre-drilling the wood studs with a 4-mm ($\frac{9}{64}$ -in) hole facilitated completely inserting screws while preventing splits. Predrilled holes in WPC specimens for utilizing helical threaded nails had a diameter of 3.1-mm (0.125-in.).



Figure 2.9 Typical connection test geometry

The configuration for Specimens 1-11 had the end stud located at the end of the sill, as traditionally would be done. On the contrary, Specimens 12-16 had end studs located 127-mm (5-in) O.C. from ends of sills, leaving 89-mm (3-1/2 in) from outside stud face to the end of the sill, to allow an adjacent 38-mm x 89-mm (2-in x 4-in nominal) wall to be framed at the corner. This shifted configuration also provides more surface area for connections to fully utilize the WPC section when transferring tensile forces, compared to the configuration of Specimens 1-11, primarily having only the sidewall into which to fasten. Two 254-mm (10-in) diameter A36 steel dowels were inserted through the two center cavities of the WPC section and through the end stud—allowing 89-mm (3-1/2 in) of dowel extend from either side of end studs. Dowels were able to bear on the sections' top flanges from inside the hollow cavities.

Two reinforcing methods were used to improve transverse properties. The first, used fiberglass reinforced PP tape which was melt bonded to the sill surface, with fibers oriented parallel to the tension force direction. The second method consisted of fine thread drywall screws with length of 64 mm (#8 x 2-1/2 in) inserted through sill flanges and into webs (predrilled to 3.1 mm (1/8-in) diameter).

A summary of test variables is in Table 2.3.

Table 2.3 Connection Test Variables

Test	Stud/Sill Attachment Method	Configuration	Reinforcing
1	Wood screws	Traditional	NA
2			
3			
4			
5			
6			
7	Helical nails		
8	Wood screws		
9	Helical nails		
10	Wood screws	Drywall screws	
11		Fiberglass/PP screws	
12			
13	Wood screws, dowels	Shifted end stud and anchor bolt location	NA
14			
15			Drywall screws
16			Dowels

Monotonic testing of end stud-sill connections was conducted under displacement-controlled loading after conditioning for WPC sill plates took place for a minimum of 160 hours at 50% RH and 21.1 degrees Celsius. End studs were conditioned for a minimum of 184 hours at 65% RH and 20 degrees Celsius until moisture contents were near 12%. Loading rates determined by ASTM D790 (Flexural Properties of Reinforced and Unreinforced Plastics) were difficult to apply to this unique section shape. The loading rate was modified from Bolted Connections in Wood and Wood-Based Products (ASTM D 5652) and Standard Test Methods for Mechanical Fasteners in Wood (ASTM D1761-88) to be 5 mm/min (0.20 in/min). Previous testing by Smart (2002) at Virginia Tech showed no appreciable difference in strength when increasing the load rate from 2.5 mm/min (0.10 in/min).

Tensile loads were applied with a 30-kip universal electromechanical test machine (Instron 4400R), simulating tension forces that occur in end studs as walls overturn. The test setup is illustrated in Figure 2.10. The end studs were positioned between two steel plates

attached to the loading ram, through which a 19-mm ($\frac{3}{4}$ -in) bolt transferred uplift forces from the fixture to specimens. Specimens were held down against uplift by a steel HSS 127-mm x 76-mm x 8-mm (5-in x 3-in x $\frac{5}{16}$ -in) section on its side. Forces were transferred from the hold-down to the test machine base with four 12-mm ($\frac{1}{2}$ -in) A36 steel threaded rods anchored into T-slots. The lateral distance between the HSS section edge and end studs was 76-mm (3-in) for the first test, though altered for subsequent tests to 6-mm ($\frac{1}{4}$ -in) distance to minimize added moment induced from the eccentricity between the load and reaction. Tests #8, 10 and 11 required approximately 50-mm (2-in) between the hold-down section and the stud to permit room for toenailed screws. Tests #15-16 had 64-mm (2- $\frac{1}{2}$ -in) distance to the stud face to allow room for perpendicular-to-extrusion reinforcing screws.



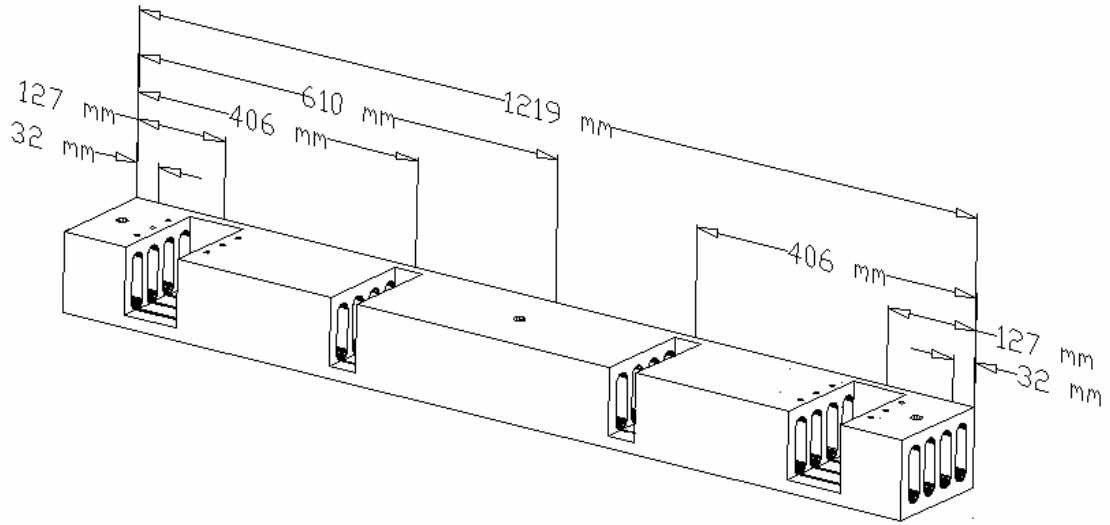
Figure 2.10 Connection test setup

Displacement measurements were used to monitor stud/sill separation and sill uplift. A linear variable displacement transducer (LVDT), attached to the end stud within one inch of the connection face, measured the displacement between the stud and bottom thickness of the WPC

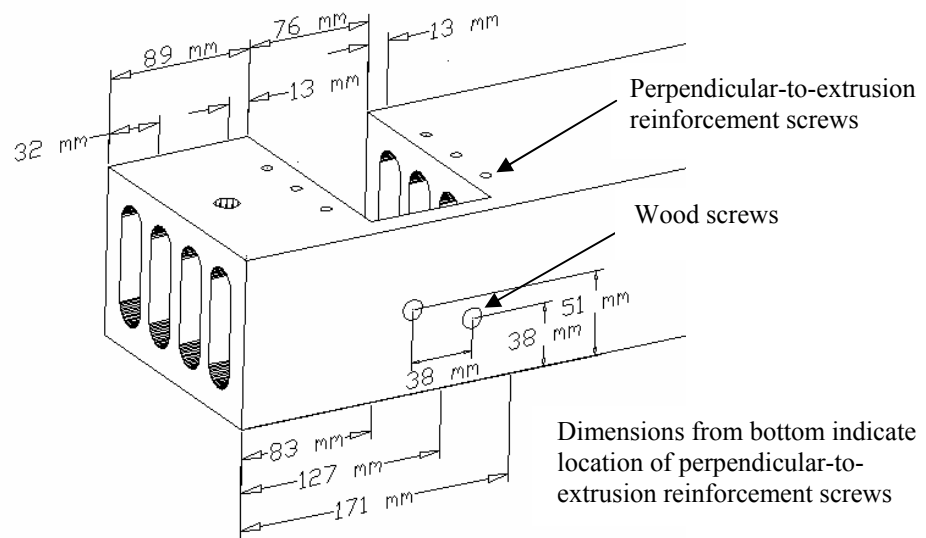
sill to quantify stud and sill separation. The crosshead extension reading of the test machine was used to measure total uplift. Testing continued until a visual connection failure occurred and load resistance reached 80% post-peak load.

2.4 Component Test Materials and Methods

Component tests used the optimum end stud-sill design from connection tests. They were tested under loading and restraint conditions most closely resembling that in full-scale walls to verify load-deformation behavior. As well, these tests helped better predict the damage the sill plate would undergo and its uplift resistance without constructing full-scale walls. Components were made from PP10 and were 1.22-m (4-ft) in length. The final dimensioned design is shown in Figure 2.11. The design utilized the end stud-sill configuration which shifted the end stud in from the sill end. End slots were 76-mm (3-in) along the length to accommodate double end studs (38-mm x 140-mm) as in preliminary connection tests and 38-mm (1-¹/₂-in) for interior slots. The end stud slot was located 127-mm (5-in) on center from component ends and interior slots are located 406-mm (16-in) on center. This configuration had specimens anchored at 32-mm (1-¹/₄-in) from ends and one centered along the 1.22-m (4-ft) length. To achieve the actual connection between end studs and sills, two steel dowels (12-mm (¹/₂-in) diameter) were installed in the center hollow voids of the WPC.



(a)



(b)

Figure 2.11 Component design: a) Full section, b) End stud detail

Utilizing reinforcement aimed to improve transverse properties. Tension forces perpendicular-to-extrusion direction were countered with three drywall screws in interior webs on both sides of end studs, along with the bottom outside wall at the end stud sidewall connection.

Lumber for studs was No. 2 and Better grade Douglas-fir, with 38-mm x 140-mm (2-in x 6-in nominal) dimensions. Interior studs were 127-mm (5-in) long, acting only as placeholders in machined slots as they did not resist or apply load to specimens—only accounting for stiffness changes and localized stresses where interior portions of webs were removed from net cross sections. End studs were doubled and 381-mm (15-in) in length.

Test setups were similar to those used for the connection tests and are shown in Figure 2.12. The loading ram was connected to end studs using a 19-mm ($\frac{3}{4}$ -in) bolt, 152-mm (6-in) from the upper end of studs, using four wood screws (two on each side). Uplift reactions were 12-mm ($\frac{1}{2}$ -in) A36 anchor bolts extending from beneath the steel double channel sections on the test machine to the top of WPC sections. Initial testing used only one bolt at 32-mm ($1\frac{1}{4}$ -in) at each end, though unrealistic upward bending was occurring at mid-span from no restraint from studs, so a middle bolt was added for remaining replicates. Holes for anchor bolts were 14-mm ($\frac{9}{16}$ -in) and were secured with a nut and plate washer. As anchor bolts were inserted in both sill plate ends for each test, only the loaded end resisted the majority of the uplift and allowed twenty-eight tests to be completed from fourteen 1.22-m (4-ft) long specimens.

Methods for component tests followed ASTM E529-94. Displacement was applied at 5 mm/min (0.2 in/min) similar to previous connection tests, and applied in tension in the 30-kip universal electromechanical test machine (Instron 4400R). Displacement was applied until load decreased to 80% of peak load. Displacement measurements were taken with the crosshead extension for overall displacement and with two string pots to determine rotational behavior of sills. String pot measures were centered at end studs (center of load application) on opposite edges of WPC sill plates.



(a)



(b)

Figure 2.12 Component test setup: a) Full component, b) End stud detail

2.5 Shear Wall Test Materials and Methods

Full-scale tests of shear walls constructed with wood-plastic composite (WPC) sill plates provided final data needed to characterize prototype wall-foundation connector elements. Wall configurations included sill plates described previously in this chapter, testing a control wall, two walls with equal replacement sills, and one with expected performance improvements from stud-sill connection improvement. Tests of various wall configurations allowed comparison of wall deflection and load capacity with current shear wall designs. As well, tests demonstrated changes in sill plate behavior, in distribution of uplift forces to anchor bolts, and in wall failure modes.

The following discussion outlines test materials and procedures used.

2.5.1 Sill Plate Type

Shear wall tests utilized four different sill plates described in Table 2.4. Each wall configuration will be classified as its sill name for purposes of discussion.

Table 2.4 Shear wall configurations

	No. of Tests	Sill Dimensions	Cross-Section Description	Material Type	End Stud Connection	Rationale
WOOD4	2	38 mm x 140 mm (1½ in x 5½ in)	Solid	Preservative Treated Wood	End-nailed	Control specimen
PE3	2	25 mm x 140 mm (1 in x 5½ in)	Solid	Polyethylene/Pine	End-nailed	Equal substitute
PP5	2	46 mm x 165 mm (1.8 in x 6.5 in)	Hollow	Polypropylene/Pine	End-nailed	Equal substitute, with efficient material use
PP10	2	104 mm x 150 mm (4.1 in x 5.9 in)	Hollow	Polypropylene/Pine	Dowels + Side Screws	Section that improves constructability and uplift resistance without hold-downs and allows sheathing to be lifted for moisture resistance purposes

2.5.2 Fabrication of Specimens

Framing for each specimen consisted of 38-mm x 140-mm (2-in x 6-in nominal) Douglas-fir, graded No. 2, No. 1, or machine rated to 1950 F_b 1.7 E or 2100 F_b 1.8 E. All lumber was purchased at the local building supply. For half of the specimens, lumber was delivered as MSR graded when No. 2 or better was ordered. Lumber was conditioned at 70% relative humidity, 70° Fahrenheit for more than a month before first wall fabrication. Moisture content readings for lumber were taken at time of fabrication and at time of testing with an electric resistance meter. After fabrication, walls were allowed to relax for a minimum of two weeks in the laboratory environment.

Studs were spaced 406-mm (16-in) on center, with the exception of PP10 having end studs located at 127-mm (5-in) from end of sills. In order to keep constant 2.4-m (8-ft) wall

heights, stud length varied for each test, depending on sill plate thickness. Sheathing was connected to sill plate edges for all tests, except PP10, which had 102-mm (4-in) of sheathing removed to allow the sheathing to set on the sill top edge as shown in Figure 2.13. Framing and sheathing heights for each test are listed in Table 2.5.

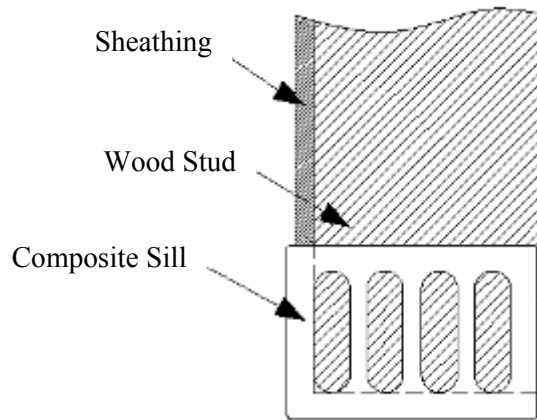


Figure 2.13 PP10 stud configuration (end view)

Table 2.5 Framing and sheathing heights for tests

Test Group	Sill Thickness		Stud Length		Sheathing Height		End Stud Location	Anchor Bolt Location	
	<i>mm</i>	<i>in</i>	<i>m</i>	<i>in</i>	<i>m</i>	<i>in</i>		<i>mm</i>	<i>in</i>
WOOD4	38	1.5	2.32	91.5	2.4	96	End of sill	0.31, 0.91, 1.52, 2.13	12, 36, 60, 84
PE3	38	1.5	2.32	91.5	2.4	96	End of sill	0.31, 0.91, 1.52, 2.13	12, 36, 60, 84
PP5	46	1.8	2.32	91.2	2.4	96	End of sill	0.31, 0.91, 1.52, 2.13	12, 36, 60, 84
PP10	15	0.6	2.35	92.4	2.34	92	Shifted inward 127 mm	0.038, 0.61, 1.83, 2.40	1.5, 24, 72, 94.5

Fastener type and dimensions are listed in Table 2.6. Framing for end studs consisted of two 38-mm x 140-mm (2-in x 6-in nominal) members nailed together with 2-16d nails 610-mm (24-in) on center. Double top plates (nailed together with 16d common nails, 406-mm (16-in) on center) were end-nailed to studs using 2-16d common nails. Studs were then end-nailed to the single bottom sill plate by 2-16d nails for WOOD4, PE3, and PP5. Holes were predrilled in the WPC slightly smaller than the nail diameter for PE3 and PP5. For PP10, connections of the end studs to the sill were made as in component tests, with 6-mm x 51-mm (¼-in x 2-in) wood

screws and A36 steel dowels. Intermediate studs in PP10 were also connected to sill using two wood screws.

Table 2.6 Nail specifications

	Manufacturer	Diameter	Length
8d—common smooth shank	Stanley Bostitch Fasteners	3.3 mm (0.131 in)	64 mm (2-1/2 in)
16d—common smooth shank	Fanaco® Fasteners	4.1 mm (0.162 in)	89 mm (3-1/2 in)

Sheathing was applied to framing with the long dimension parallel to the studs on only one side of the wall, allowing a 3.2-mm ($1/8$ -in) gap at sheathing panel joints for all walls, and also at the bottom edge in PP10. Sheathing was 11-mm ($7/16$ -in) OSB, Exposure 1 rated sheathing attached with 8d common nails, with 76-mm (3-in) on center edge nailing and 305-mm (12-in) on center field nailing on intermediate studs, providing ASD shear design capacity of 7.2 kN/m (490 plf) (AF&PA, 2001). PP10 did not have edge nailing along the bottom of the sheathing since blocking was not used. Edge distances of 19-mm ($3/4$ -in) were achieved at outside edges and were 10-mm ($3/8$ -in) at interior panel joints.

Anchor bolts for WOOD4, PE3, and PP5 were placed 305-mm (12-in) and 914-mm (36-in) from each sill end. Due to PP10's end stud location, which was developed from previous component testing, the location of anchor bolts was altered as compared to traditional wall design. The locations of these bolts, which transfer both shear and uplift to the foundation, were 38-mm ($1\frac{1}{2}$ -in) and 610-mm (24-in) from the end of sills. For all tests, anchor bolts were 16-mm ($5/8$ -in) diameter, Grade 8 steel. Steel plate washers, with dimensions 51-mm x 51-mm x 6-mm (2-in x 2-in x $1/4$ -in), were used for all bolts. Table 2.5 summarizes the bolt locations for all tests.

End stud slots were cut to 80-mm ($3\text{-}\frac{1}{8}\text{-in}$) width and intermediate slots at 40-mm ($1\text{-}\frac{9}{16}\text{-in}$) width to accommodate 76-mm (3-in) and 38-mm ($1\text{-}\frac{1}{2}\text{-in}$) width studs, respectively. Holes for wood screws were predrilled to 6-mm ($\frac{1}{4}\text{-in}$) for WPC material and 4-mm ($\frac{9}{64}\text{-in}$) for wood. Holes for 12-mm ($\frac{1}{2}\text{-in}$) dowels in end studs were 14-mm ($\frac{9}{16}\text{-in}$). Anchor bolt holes had no overdrilling for Test Group A, had 1.6-mm ($\frac{1}{16}\text{-in}$) overdrilling for PE3 and PP5, and had 3-mm ($\frac{1}{8}\text{-in}$) overdrilling for PP10.

2.5.3 Test Fixtures and Instrumentation

Walls were tested in a vertical position, loading occurring parallel to the top of the wall. The hydraulic-controlled actuator had a ten-inch stroke and 100 kip capacity. The test setup is shown in Figure 2.14. Walls were supported by a steel 102-mm x 152-mm (4-in x 6-in) HSS section, with the bolts offset from the center in order to inset the steel section from the sheathing to allow sheathing to have free rotation at wall bottoms. The HSS section set, with the 152-mm (6-in) dimension as the width, on a steel I-beam which was bolted to the strong-floor. Wall anchor bolts extended through sill plates, through the HSS section, and top flange of the I-beam. Holes in the steel were overdrilled 1.6-mm ($\frac{1}{16}\text{-in}$). To distribute the applied racking load, a steel channel section was attached to wall top plates with 12-mm ($\frac{1}{2}\text{-in}$) bolts between each stud. Holes in wall top plates had no oversizing to minimize slip, and holes in the steel channel were over-drilled 1.6-mm ($\frac{1}{16}\text{-in}$). Spacers were placed between the channel section and wall top plates to avoid impingement of the sheathing when racking. The top steel beam was connected to the actuator with a hinge connection to eliminate moment transfer to the load cell. Lateral displacement out-of-plane of the wall was prevented by steel plates, oriented perpendicular to the wall face. Edges were covered in Teflon sheets and slid along steel angle brackets extended down from the test frame. No gravity loads were applied to any of the walls.

Load and deflection measurements were taken at the locations identified in Figure 2.15. Load measurements for tension in anchor bolts were made with Omega LC901-3/4-65k bolt force sensors wired through digital strain indicators. Load washers were placed on top of plate washers (code-required), below bolt heads. Displacement measures were all taken with resistance potentiometers (string pots) with maximum 254-mm (10-in) displacement ranges. The exception was Displacement Measure 9, which used a 51-mm (2-in) displacement pot.

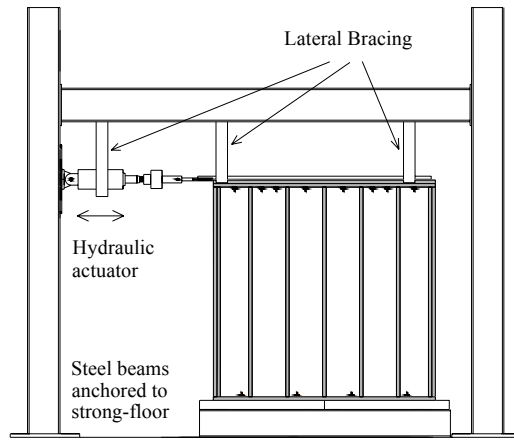


Figure 2.14 Shear wall test frame

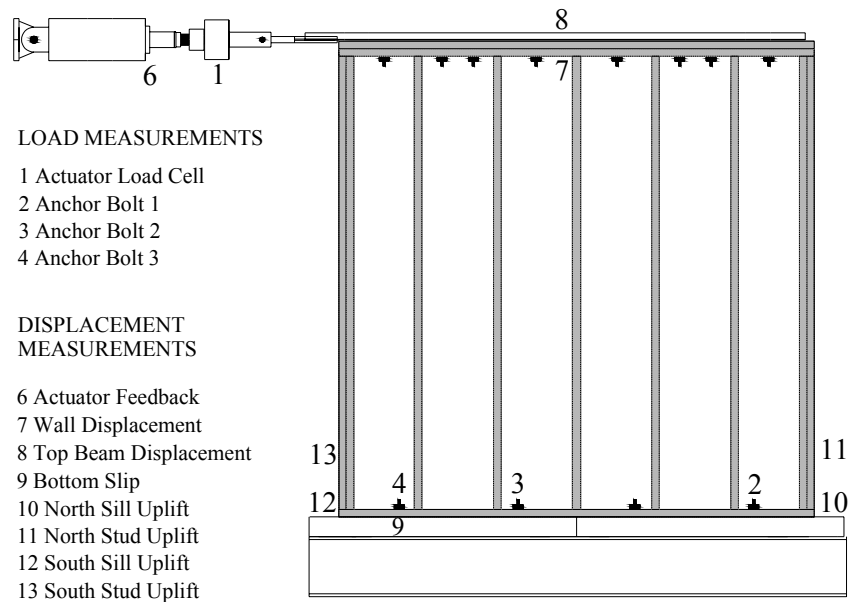


Figure 2.15 Shear wall test instrumentation

2.5.4 Test Procedure

Monotonic tests followed ASTM E564 (2000), loading walls at 15 mm/min (0.6 in/min). One monotonic test was performed for each test group to determine the reference displacement for following cyclic test protocols. A string pot mounted to the actuator monitored the displacement for controlling the hydraulics. Test methods were altered to apply a constant displacement rate until failure (80% peak load capacity), not incorporating sequences of loading and unloading as directly specified in the standard.

Cyclic tests followed ASTM E2126 *Standard Test Methods for Cyclic (Reversed) Load Test for Shear Resistance of Framed Walls for Buildings* (2002), following the CUREE-Caltech Standard Protocol (CUREE). Two tests were completed for each test group. Reference displacements for each test group are listed in Table 2.7.

Table 2.7 Cyclic wall test reference displacements

Test Group	Reference Displacement, Δ
A	41 mm (1.61 in)
B	36 mm (1.40 in)
C	18 mm (0.70 in)
D	35 mm (1.39 in)

The reference displacements, Δ , were calculated by first determining the displacement at 80% of ultimate load on the degradation part of monotonic load-deflection curves, Δ_m . Cyclic loading protocol references Δ , which is defined as 60% of Δ_m . The CUREE protocol then loads as a fraction of Δ , beginning with small amplitude cycles simulating small tremors, followed by large amplitude cycles. These cycles are characterized by trailing cycles, having amplitudes of

75% of the primary one, which may be more closely representing actual seismic behavior (Krawinkler et al., 2001). The amplitudes of primary cycles are presented in Table 2.8 and the representative loading time history is illustrated in Figure 2.16. This protocol, when compared to results of wall tests under other protocols, produces failure modes most closely resembling that which would occur in actual seismic events (Gatto and Uang, 2002).

Table 2.8 CUREE Protocol: Amplitudes of primary cycles (Krawinkler, 2001)

Pattern	Step	Minimum Number of Cycles	Amplitude of Primary Cycle, Δ
1	1	6	0.05 Δ
2	2	7	0.075 Δ
	3	7	0.1 Δ
3	4	4	0.2 Δ
	5	4	0.3 Δ
4	6	3	0.4 Δ
	7	3	0.7 Δ
	8	3	1.0 Δ
	9	3	(1.0+1.0 α^*) Δ
	10	3	Additional increments of 1.0 α (until wall failure) followed by two trailing cycles

* $\alpha < 0.5$

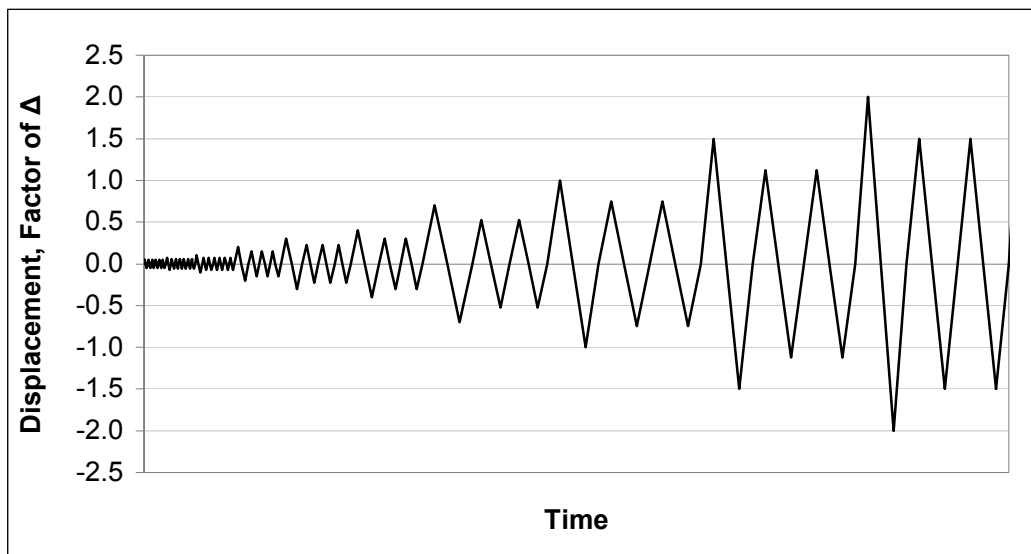


Figure 2.16 CUREE loading protocol

A constant rate of loading, 437 mm/min (17.2 in/min), was followed for this protocol for all wall tests, up to the point of instrument limitation. Because of the range of amplitudes required for the full loading program, this constant rate of loading caused frequencies to extend outside the range required by the standard (0.2-1.0 Hz). When exceeded on the high frequency side, amplitudes were low, in initiation cycles, and should not have caused inertial effects. As well, for higher displacement amplitude cycles, frequencies were required to drop below 0.1 Hz, though due to limitations in the 407 controller, a frequency of 0.1 Hz was employed and rate of loading was adjusted accordingly.

Tests continued until the primary cycles' maximum load dropped below 80% peak capacity. An exception was for Test 4-2, which was stopped after the 2.5 Δ cycle when the actuator stroke capacity limited further cycling.

CHAPTER 3 CONNECTION AND COMPONENT PERFORMANCE

3.1 Connection Tests

Interpretation of connection test results identified several factors affecting end stud-to-sill connection performance. Loads and deflections obtained reflect improvements in isolated end stud-to-sill connections, but only estimate full-scale wall behavior, as loading was purely in tension and did not account for bending which occurs in the field application.

Results are summarized in Table 3.1 and the following discussion will identify performance changes as a result of connection type, configuration, and reinforcing methods. Presented interpretation was based on only one specimen per fastener layout, so results are not statistically validated. Geometries and configurations notes for each test can be found in Figure A.1. Failure photos for each specimen are also in Appendix A (Figures A.2 and A.3).

Table 3.1 Connection Test Summary

Test Group	Stiffness (kN/mm)	Max Load (kN)	Deflection (mm)		Work (kN-mm)	Ductility ($\Delta_{failure}/\Delta_{max}$)
			@ Max Load	@ Failure		
Sidewall Connection Only	1.4	7.9	5.7	6.0	29	1.06
Shifted Configuration	5.1	19.5	4.8	5.5	70	1.22
Reinforced Sidewall Connection	2.0	15.5	7.5	8.5	87	1.15
Reinforced Shifted Configuration	5.2	28.3	6.4	9.7	184	1.52

3.1.1 Effect of Varying Sidewall Connection Geometry

Fastener layout and fastener type varied to obtain results on how edge distance, net section, and amount of fasteners affected connection capacity. Specimens 1-6 had the connection between the stud and sill only through the sidewall of the section, relying on its transverse properties. Typical failure occurred along the bottom row of fasteners, propagating from the end of the sill along the section strands, and shifting upward at a 45-degree angle after passing the end stud slot (Figure 3.1). The weakness is clearly in properties in the perpendicular-

to-extrusion direction. It is at this bottom fastener where no fasteners are below to put compressive forces on this weak plane.



Figure 3.1 Typical failure path in connection tests (Specimen 4 shown)

Increased edge distance of the bottom fastener row achieved greater load and displacement capacity. This is because it was able to provide greater resistance to perpendicular-to-extrusion tension forces between strands that are clearly weak planes in the sections. The difference is apparent between Specimens 2 and 3, where number, size, and end distances are similar, though the middle column had been shifted to increase the edge distance of the bottom fastener. By increasing the edge distance, the amount of material without any penetrations is greater to resist tension forces.

By substituting helical threaded nails for wood screws, the amount of remaining net section resisting tension is maximized. Comparisons were made between Specimens 3 and 7 and Specimens 5 and 9, both having fasteners with relatively high stiffness. Specimens 7 and 9 had identical configurations as Specimens 3 and 5, respectively, except helical threaded nails were used instead of screws. As a result of smaller diameter fasteners, the load capacity and connection stiffness decreased, subsequently lowering the amount of work done in the connection. A probable reason for load capacity reductions may be due to larger stress

concentrators at fasteners, initiating premature failure. Reductions in connection stiffness may arise from greater stress per width of fasteners, having increased crushing around the nail in the wood stud. Knowing this PP formulation has superior compressive strength properties (Kobbe, 2005) and not observing local failure, crushing around the fastener in the WPC most likely does not occur and is not likely a cause for reduced stiffness.

Another possible factor affecting capacity may be unit load per screw as shown in Specimens 5 and 6. Both used same configurations along with same edge distances, though Specimen 6 had four connectors instead of six. An advantage of fewer screws may be greater deflection capacities, ultimately affecting wall drift. Though, less load capacity coupled with decreased stiffness reduces the amount of work done by the connection. This is confirmed when comparing Specimens 15 and 16, where connection configurations are different than Specimens 1-6, though sidewall screws were reduced to two (for Specimen 15) and eliminated (for Specimen 16). Deflection capacities at peak loads were comparable, though remaining capacity until failure (measured by ductility) decreased substantially for the specimen without sidewall fasteners. There was also a dramatic decrease in the amount of work done in the connection. Although the data is not statistically conclusive, it would suggest retaining the use of sidewall screws.

As failure in the sidewall was limiting load capacities for the isolated end stud/sill connection, an attempt to distribute the load into the entire section was done by installing wood screws, toe-nailed from the top of the sill into interior stud faces. Connection tests with this geometry showed no appreciable increases in load capacity (comparing Specimens 5 and 8). Ultimate deflection capacity noticeably decreased, though the amount of ductility increased

slightly as the proportion of deflection post-peak increased. This is from a greater distribution of load throughout the section, creating redundancy in tension resistance.

3.1.2 Effect of Configuration Changes

Those test specimens with the shifted configuration (#12-16) altered the traditional sill plate/end stud configuration to further increase load and deflection capacities. The specimen configuration is shown in Figure 3.2, having the end stud shifted in 89 mm (3-1/2 in) and dowels inserted through WPC hollow cavities to attach the end stud. Tests on this shifted configuration also varied the configuration of the dowels.

Substantial changes in load-deflection behavior occurred when changing the end stud configuration from its traditional end-of-sill location. This can be seen in the load-deflection response in Figure 3.3. From having a symmetric connection to the stud, transferring the load from both stud faces as well as being centered in the width, the connection stiffness increased dramatically—triple that of connections between the stud and only the sidewall. Load capacities also doubled, likely due to engaging the full sill plate section rather than solely the sidewall. Subsequently, the work done by the connection more than doubled. The range of deflection capacities were similar to traditionally located end studs, as the load capacity increase was coupled with increased stiffness. Though, due to small changes in the deflections at peak and failure loads, the ductility increased with switching configurations (by approximately 15%). The largest increase in ductility and work done by the connection was when dowels were located in the center of the section, most efficiently transferring uplift force to the anchor bolt washer and into the foundation (minimizing the load path). The configuration in this specimen (#14) also included a plate washer which helped delay failure and allow dowel yielding, so the exact contribution of dowel location towards ductility and work done cannot be identified.



Figure 3.2 Failure perpendicular-to-extrusion between flange and webs from uplift force transferred to dowels

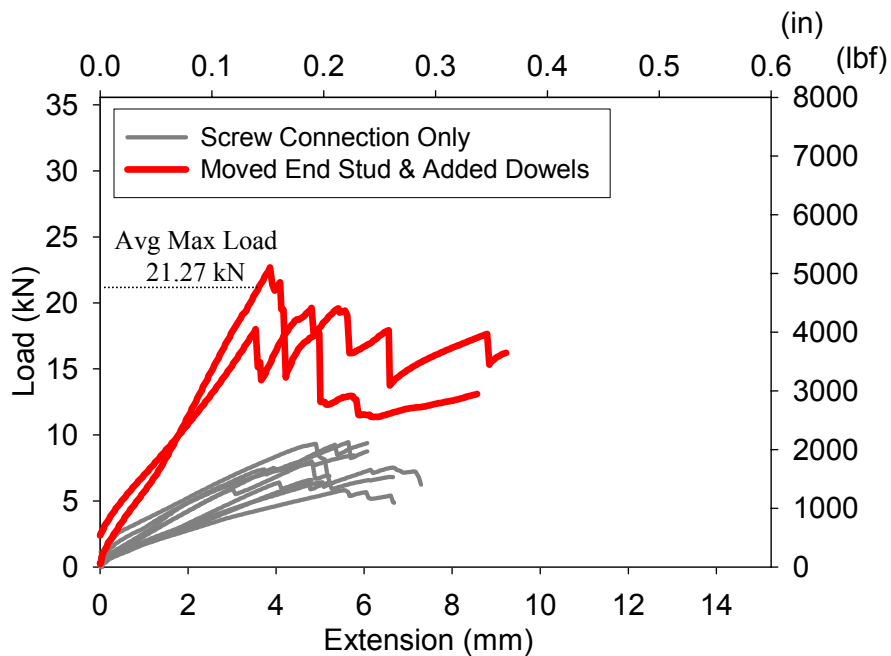


Figure 3.3 Comparison of load-deflection behavior from moving end stud position and adding dowels

3.1.3 Effect of Reinforcement Methods

For specimens in both end stud configurations, transverse weaknesses were apparent at the location of the bottom fastener in the sidewall for the traditional configuration, and at the intersection of the section webs and flange in the shifted configuration. Because these failures limited the amount of load carried and the full utilization of the entire member cross-section, reinforcing methods were applied (in the form of drywall screws and fiberglass/PP tape).

3.1.3.1 Traditional Configuration

The effects of reinforcing were apparent in changing failure modes. The failure was most likely shifted to the next weak point in the connection system. For reinforced sidewalls, the failure along the strands at the end of the sill was eliminated. Instead, the failure initiates at the stress concentration the reinforcing screw creates and propagates up the section as before. This change in failure is shown in Figure 3.4. For the section reinforced with fiberglass/PP tape, the ultimate failure still occurred along the line of the bottom fastener, though it was delayed as the bond strength between the tape and sill had to be attained first. For those reinforced locations between the flange and webs in the sills in shifted configurations, the failure mode switched to flexural failure at the end stud location. Local crushing around reinforcing screws also occurred from the bending caused by the upward force of the dowels underneath the flange. Essentially, the shifted configuration with screw reinforcement eliminated the weakness perpendicular-to-extrusion in the section.

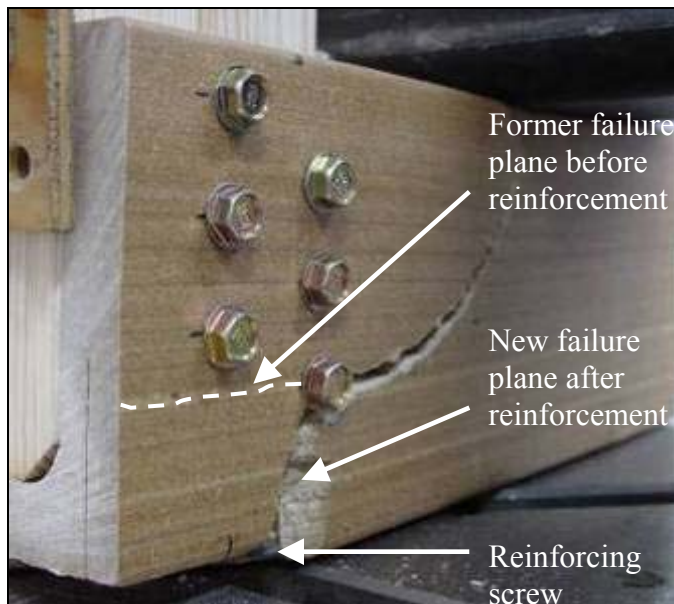


Figure 3.4 Reinforced sill failure photo (Specimen 10)

Reinforcing the sidewall connection created a better performing connection as shown in the load-deflection plots in Figure 3.5. Loads doubled and the work done almost tripled. Stiffness of the connection increased as tension loads were transferred to stiff screws and reinforcing tape, reducing the amount of separation between section strands. The maximum deflection capacity increased by 30%, with slightly higher increases in ultimate deflection capacities, thus improving ductility in the connection (approximately 10% increases—greatest for connections with tape reinforcing).

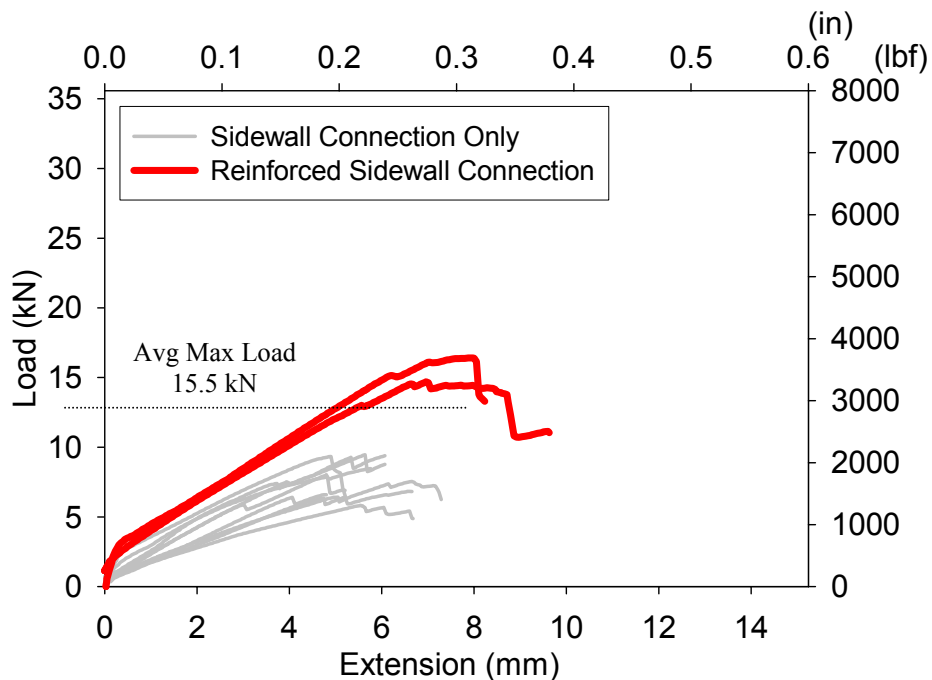


Figure 3.5 Effects of reinforcing sidewall connection

3.1.3.2 Shifted Configuration

With all parameters increasing for reinforcing the weak sidewall, it is an obvious improvement and that which can be applied to weaknesses occurring between strands in the shifted configuration. Screws were the most effective means to transfer tension forces from the section top flange and down into the section webs, as shown in Figure 3.6. As expected, loads

increased (by 50%) and the work done increased by 2.5 times. This particular location of reinforcement did not affect stiffness dramatically, but increased the deflection at peak load by 30% and more substantially at failure. Therefore, increases in ductility reached 25%, creating more ideal connection behavior. The improvements in behavior from this reinforcing applied to the sidewall is illustrated in Figure 3.5, and that applied to the shifted configuration can be seen in Figure 3.7.



Figure 3.6 Perpendicular-to-extrusion screw reinforcement between flange and webs

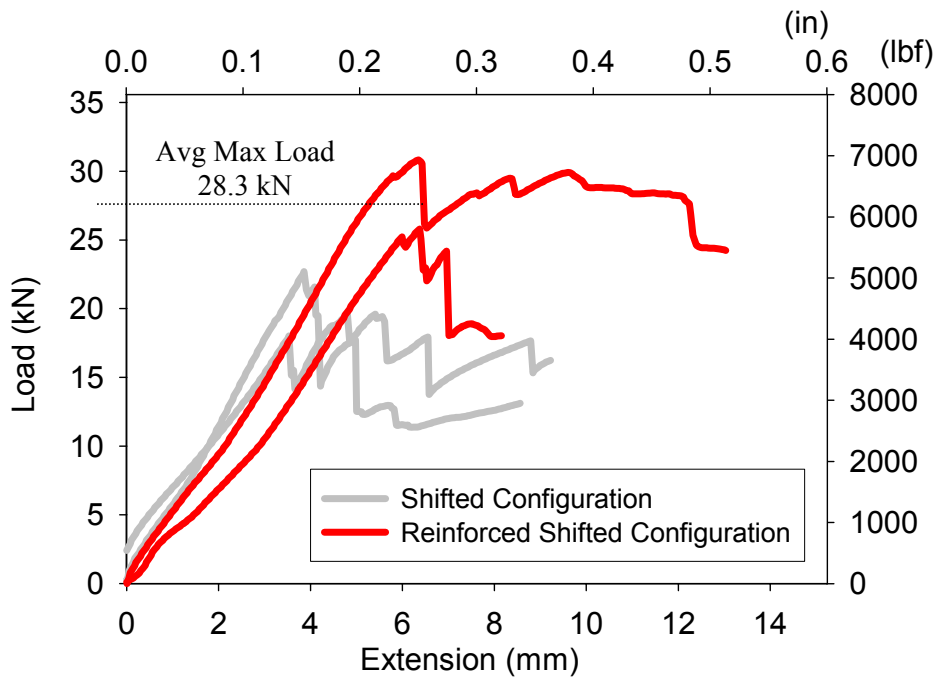


Figure 3.7 Effects of reinforcing top flange to web

Testing proves a change in behavior when reinforcement methods are applied. Failure modes shift to the next weakest point in the section. Higher capacities and stiffness and ductility prove both reinforcing methods to be effective in delaying perpendicular-to-extrusion failure and improving connection performance.

3.1.4 Finalized End Stud/Sill Connection

Initial connection tests show that the most effective fastener configurations have greater edge distances to the bottom fastener—allowing more material to resist perpendicular-to-extrusion forces. The amount of fasteners can be used to alter the deflection capacities. Less fasteners decrease the connection stiffness and load capacity, but increase the deflection. To maximize the loads achieved, the screw fasteners were preferred over helical threaded nails. Switching to a non-traditional configuration (shifting end studs inward) proved to supply substantially greater stiffness and resistance to uplift by engaging the entire cross section. By shifting the configuration and reinforcing the section with screws, capacities increased and provided 26.7-31.1-kN (6000-7000-lbf) more uplift resistance than traditional stud-to-sill end-nailed connections (considered zero) and had desirable ductile performance. Where loads still exceed the composite material capacities (primarily in the transverse direction), reinforcement dramatically improves performance. Screw reinforcement as opposed to polypropylene/glass fiber reinforcement proved to be the most reliable to install at this time and completely shifted the failure mode from failure perpendicular-to-extrusion, allowing the greatest increases in performance.

Based on these property increases observed from varying the sidewall connection, changing the connection configuration, and applying reinforcement, the final end stud/sill connection utilized in the remaining tests incorporated:

- Maximum edge distance,
- Minimal sidewall penetrations,
- Shifted configurations with dowel attachment, and
- Reinforcing between flange and webs of sections.

3.2 Component Tests

Data collection for component tests included crosshead load, crosshead displacement, and sill plate displacement on either side of end stud slots. Detailed data for these tests is located in Appendix A. Figure 3.8 shows sills bending between anchor bolts as dowels imparted upward force on sills when loaded. Ultimate failure was brittle and occurred from flexure in the side walls at the location of end stud connections. Failure propagated from the inside corner of stud slots for a majority of the specimens (Figure 3.9). Few tests demonstrated additional shear failures in webs near the bottom flange. Resulting load-displacement curves in Figure 3.10 yield a mean capacity of 18.4-kN (4131-lbf) with a 12.2% COV, and mean crosshead deflection at failure of 5.6-mm (0.22-in) with 21.6% COV. The higher COV for failure deflections and the range of data, indicated in Figure 3.11a, results from initial slack in connections between the dowels and WPC members. Simply shimming studs upward would reduce this spread in data and reduce initial displacement required to seat the dowels in the connections and initial stiffness differences.

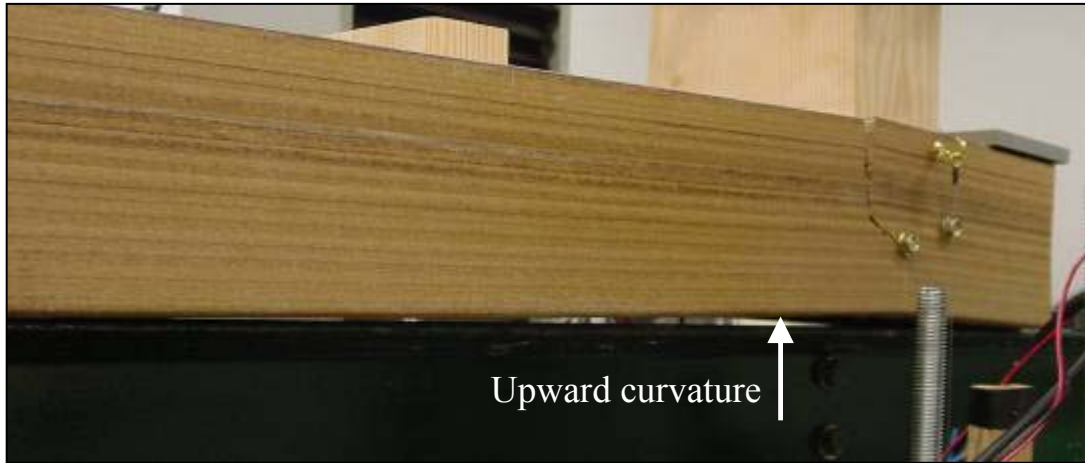


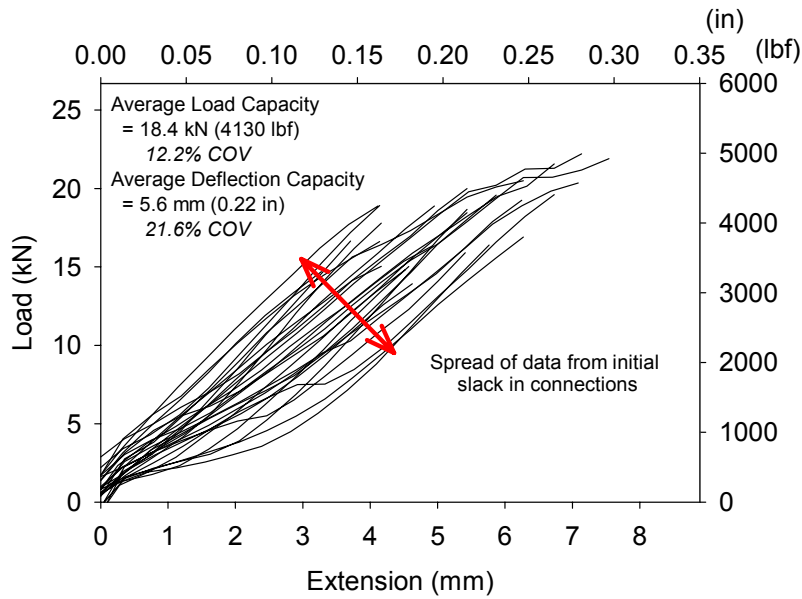
Figure 3.8 Beam bending in component tests from dowel uplift



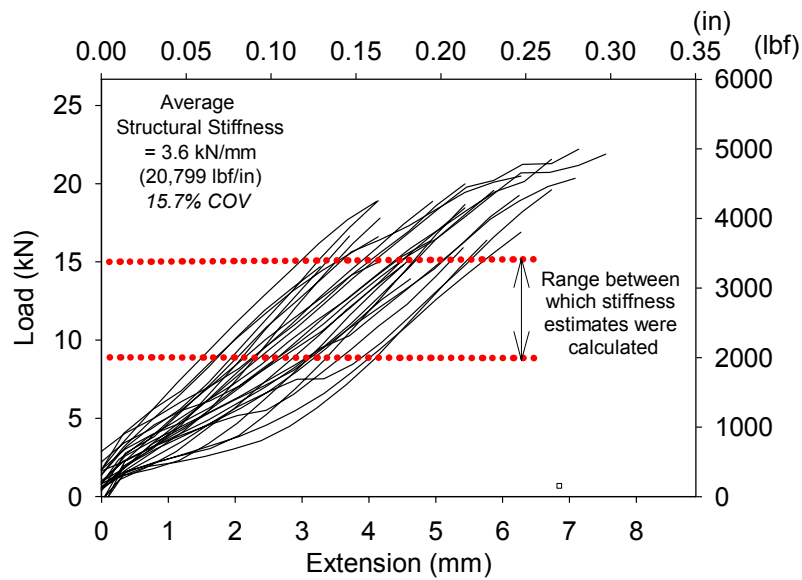
Figure 3.9 Typical component test flexural failure at end stud slot

Load capacity was not affected by connection slack, and by assuming a direct correlation between this capacity and expected shear wall behavior, an estimate of wall design capacity could be calculated. Assuming a 2.44-m (8-ft) shear wall, 18.4-kN (4131-lbf) of uplift equates to 7.9 kN/m (540 plf); assuming a safety factor of three, an ASD design wall capacity of 2.6 kN/m (180 plf) is estimated. The average structural stiffness was calculated as the slope of the load-deflection curve and is equal to 3.6 kN/mm (20,799 lbf/in) with 15.7% COV. Because of differences in initial stiffness from connection slack, the reported stiffness was calculated where

all tests reached a consistent stiffness shown in Figure 3.10b (in the range of 2.5-5.1-mm (0.10-0.20-in)).



(a)



(b)

Figure 3.10 Component test load deflection curves: a) Performance parameters and spread of data, b) Structural stiffness calculation

Compared to initial stiffness measures at 40% peak load of monotonic wall test results, component test structural stiffness is higher. Shown in Table 3.2, Langlois (2002) tested 2.4-m (8-ft) walls with 38-mm x 89-mm (2-in x 4-in nominal) framing and 12-mm (15/32-in) OSB with 102-mm/305-mm (4"/12") nail spacing, averaging initial stiffness values of 1.97 kN/mm (11,249 lbf/in). Salenikovich, testing eight-foot walls with varying amounts of anchorage, computed stiffness values to be 0.69 kN/mm (3953 lbf/in) for walls with no anchorage, to 1.62 kN/mm (9252 lbf/in) for walls with full hold-down anchorage. Component test results suggest stiffness measures to be overestimated, attributable to the additional anchor mid-span to correct for unrealistic bending.

Table 3.2. Comparison of stiffness values for connection tests and previous monotonic shear wall tests (2.44 m) (8 feet)

	Test	Stiffness	
		<i>kN/mm</i>	<i>lbf/in</i>
Connection Tests	Sidewall Connection	1.40	8000
	Shifted Configuration	4.94	28,234
	Reinforced Sidewall	2.08	11,889
	Reinforced Shifted Configuration	4.70	26,826
Salenikovich (2000)	Full Anchorage	1.62	9252
	Intermediate Anchorage	1.78	10,171
	No Anchorage	0.69	3953
Langlois (2002)	Full Anchorage	1.97	11,249

Displacement measurements were taken to investigate rotation from cross-grain bending, as occurs in traditional sill plate behavior. Cross-grain bending, coupled with beam bending has been observed to be the main factor in splitting sill plates. By transferring uplift forces through dowels centered on the reaction, the eccentricity causing splitting was eliminated. In addition to

eliminating cross-grain bending, locating anchor bolts closer to maximum uplift forces reduced cantilever behavior and resulting wall deflection. This suggests ideal anchorage conditions would be continuous along the length of sill plates—reducing upward deflection and essentially reducing flexural splitting.

3.3 Connection and Component Test Summary

WPC sections are durable and have the ability to be extruded in unique shapes and machined for specific applications. For the sill plate application, the following conclusions have been made resulting from preliminary section investigation:

- Fasteners between end studs and sills should provide the maximum edge distance, minimum number of penetrations, and distribution of load to the entire sill cross section to provide the optimal load and deflection capacities.
- Altering the traditional end stud-to-sill connection configuration provides substantial improved uplift capacity, decreased beam bending of sill ends, and eliminates cross-grain bending inherent in traditional sill plates. This shift in configuration includes moving the end stud in from the sill end, anchoring the sill 32-mm (1-1/4-in) from the end, and installing dowels through PP10 hollow cavities and through end studs.
- Stranding during processing creates weaknesses in the transverse direction. Methods of bonding reinforcement to the surface perpendicular to the failure plane, or installing screws into the thickness, perpendicular and through the failure plane, are efficient ways of improving the performance by avoiding early failure between strands.

CHAPTER 4 SHEAR WALL PERFORMANCE

4.1 Test Parameters

Test analysis was based on performance parameters outlined in ASTM E2126-02a, and detailed monotonic and cyclic test results can be found in Appendix B. Monotonic test response curves consist of load versus wall racking deflection, from zero deflection up until load drops to 20% of peak capacity. Cyclic test results are reported in the form of envelope response curves, developed by drawing a line through points of maximum loads in each cycle of the hysteresis curves. Wall deflections were measured along the top plate, in line with the center stud, in order to allow the actual horizontal displacement to be obtained without including displacements caused by uplift at walls' ends. Deflections for all response curves have also been adjusted to account for fixture slip. Due to reversed loading, positive and negative envelopes were developed for each test, and then the absolute values of the curves were averaged to develop a single quadrant envelope for each wall test, from which performance parameters were computed. For multiple tests within a test group, average group values were computed from average individual test parameters. Both monotonic response curves and calculations based on hysteresis loops included cycles up to failure loads based on average response curve parameters.

In developing complete hysteresis curves, data collected from wall displacement and load channels was edited. Positive hysteresis loops represent the response of the wall corresponding to the first peak of the primary cycle; negative hysteresis loops correspond to the second peak of the primary cycle. This becomes important as damage accumulation of the wall from the 1st primary peak affects performance in the reverse direction primary peak. Due to difficulties with digital control of the MTS 407 controller, actuator direction in the displacement-time history reversed during testing. Beginning loading sequences had first primary cycles in the positive

actuator direction, and shifted partway to be in the negative direction. To account for this switch, load-deflection data was multiplied by a negative one from the actuator reversal point to keep the positive and negative hysteresis loops consistent with the defined sign convention. Detailed time histories can be found in Appendix B.

Shear strength, v , is defined as the peak load, P_{peak} , divided by the wall length, L , and is expressed mathematically as:

$$v = P_{peak} / L \quad (4.1)$$

where P_{peak} is taken as the absolute maximum load. Failure loads and displacements (ultimate capacities) are by definition 80% of the peak load and occur on the post-peak portion of the response curve. Loads and displacements at 40% peak capacity are calculated and used in determining the elastic shear stiffness, k_e (ASTM 2126-02a).

$$k_e = 0.40P_{peak} / \Delta_{0.40P_{peak}} \quad (4.2)$$

Cyclic elastic shear stiffness is equal to the slope of the elastic portion of EEEP curves and provides an estimate of wall stiffness when subjected to multiple loading cycles at low to moderate amplitudes (Salenikovich, 2000).

Secant shear moduli may be determined at either 40% peak load or at peak load by taking the quotient of the load, P , and displacement, Δ , and multiplying by the wall's height-to-width ratio, H/L (ASTM 2126-02a). The secant shear moduli, G' , is represented as:

$$G' = (P / \Delta) * (H / L) \quad (4.3)$$

where, P is the load of interest, Δ is the corresponding displacement, H is wall height, and L is wall length. Height-to-width ratios for tests in this study were all 1:1.

Further performance characterization may be completed after constructing a curve representing an ideal perfectly elastic-plastic wall behavior—an equivalent energy elastic-plastic curve (EEEP). The curve is plotted such that the area enclosed equals the area under the envelope response curve. For monotonic test results, EEEP curves allow direct comparison of wall performance on an energy basis. For cyclic tests, the comparison is relative as the EEEP curve represents area under envelope curves, rather than total energy dissipated when summing the area under each overlapping cycle loop. Area enclosed under cyclic hysteresis curves must be calculated separately to truly compare energy dissipation.

EEEP curves consist of an elastic region that proceeds at a constant slope until yielding occurs, that is followed by a horizontal plastic region that is maintained until failure. The elastic portion goes through the origin and point of 40% peak load, at a slope equal to the elastic shear stiffness. The intersection point between elastic and plastic portions of curves is the point of yield and is positioned where the area under the EEEP curve is equal to the area under the response curve up to failure. The yield load is expressed as (Heine, 1997):

$$P_{yield} = \frac{-\Delta_{failure} \pm \sqrt{\Delta_{failure}^2 - 2A/k_e}}{-1/k_e} \quad (4.4)$$

where A is area under response curve up to the point of failure.

Ductility calculations provide a measure of walls' ability to withstand inelastic deflection during earthquake loading. In design, more ductile performance is credited with lower seismic forces to resist, as deformation in the inelastic region provides significantly more energy dissipation (Breyer et al, 1999). This reduction in base shear forces is accounted for in the IBC response modification factor, R (ICBO, 2000b).

In order to fully characterize a wall's inelastic response over the entire load range, three ductility ratios will be calculated for each wall type. The displacement measures to calculate these parameters are taken from the EEEP curve as light-frame shear walls are not perfectly-plastic in their behavior. These parameters must be considered in addition to maximum and ultimate displacements achieved, as the yield load and displacement affects ductility. The ductility ratio, D , is expressed:

$$D = \Delta_{peak} / \Delta_{yield} \quad (4.5)$$

The ultimate ductility ratio, D_u , provides a measure for comparison in the response of a wall between yield and failure. This value illustrates the amount of displacement available after yielding for load transfer to adjacent structural components (Salenikovich, 2000):

$$D_u = \Delta_{failure} / \Delta_{yield} \quad (4.6)$$

Lastly, the toughness index is calculated as a measure of displacement capacity remaining after reaching peak capacity:

$$D_f = \Delta_{failure} / \Delta_{peak} \quad (4.7)$$

4.2 Monotonic Test Results

Four monotonic walls, representing each wall type presented in Figure 4.1, were tested to develop reference displacements for cyclic tests. Racking displacement readings were taken at the top of wall, opposite load application. Detailed test photos and a summary of performance parameters are located in Appendix B. Performance parameters, such as maximum absolute load, failure load, 40% peak load, yield load, associated displacements, and energy dissipation, are reported. Knowing these factors, an equivalent energy elastic-plastic (EEEP) curve was

developed for each test. Due to the number of variables for each wall test, the following discussion is organized by addressing various performance aspects in each test type, making comparisons to previous wall configurations as required. Trends in the data will be summarized in monotonic test conclusions.

4.1.1 Test WOOD4-M

The response curve for Test WOOD4-M, having the traditional treated-lumber sill plate, is shown in Figure 4.1, along with the derived EEEP curve. Walls with wood sill plates reached a maximum absolute load of 12.7-kN (2849-lbf) with a corresponding displacement of 32-mm (1.26-in). This resulted in an ultimate shear capacity of 5.2 kN/m (356 lbf/ft). Failure occurred at a displacement of 63-mm (2.47-in), dissipating 643 kN-mm (5693 lbf-in) of energy. The elastic shear stiffness, k_e , equaled 1.1 kN/mm (6094 lbf/in).

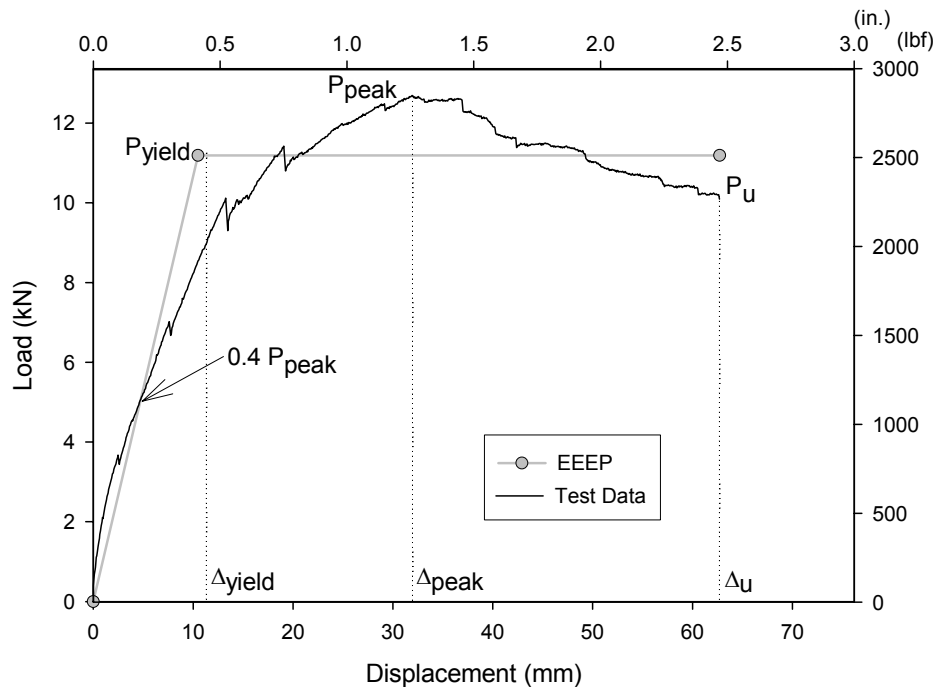


Figure 4.1 Response curve of monotonic wall test with traditional pressure-treated sill plate (WOOD4-M)

When loaded to failure, the wall exhibited rigid body rotation around the corner opposite load application, a typical response for walls without hold-down restraint. Sheathing and studs “unzipped” from the sill, beginning at the loaded end. Bottom sheathing nails bent and slightly withdrew from the sill. Failure occurred in the sill plate, splitting the entire length, down the line of plate washer edges, illustrated in Figure 4.2.



(a)



(b)

Figure 4.2 Monotonic test failures in sill: (a) Sill plate splitting along edge of plate washer and studs unzipping on loaded end of wall, (b) Split sill plate (end view)

Load cell washers (LW) were installed at three of the four anchor bolts, as illustrated in Figure 4.3. Data shown in Figure 4.4 from load cell washers illustrates the distribution of forces throughout the test. Test 1-M results were predictable, with the load distribution attenuated from the load application to LW3, to LW2, and to LW1, where LW3 is located 12-inches from the loaded end, LW2 is 24-inches from the end and LW1 is 12-inches from the compression end. As load drops occur in the wall response, the percentage of load that LW3 carries is shifted to LW2. It is not until post-peak when the sill has split along the length that LW1 carries any load.

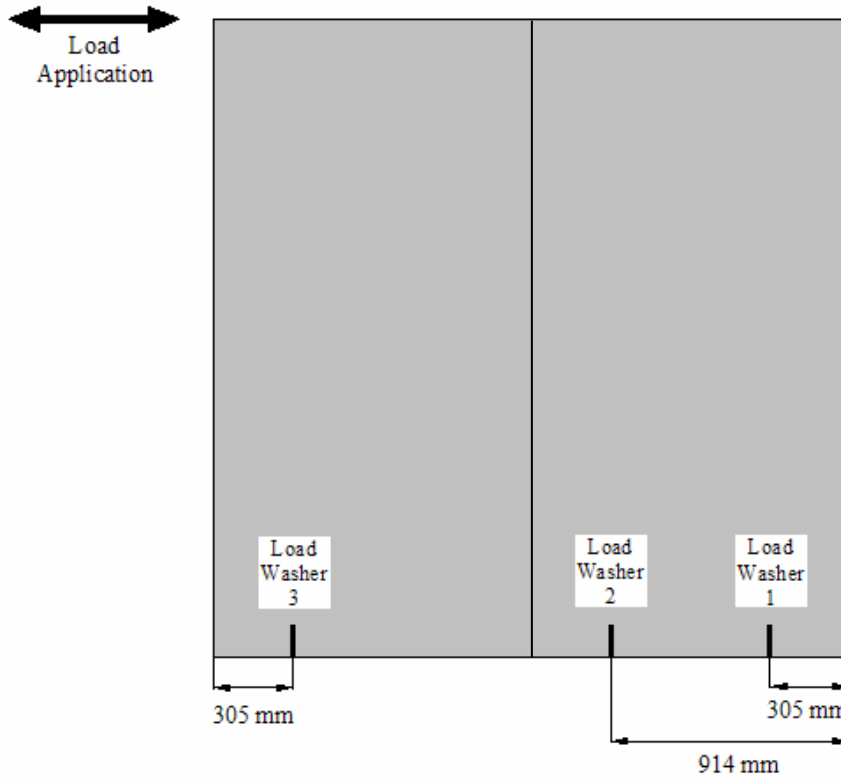


Figure 4.3 Load washer placement for WOOD4, PE3, and PP5

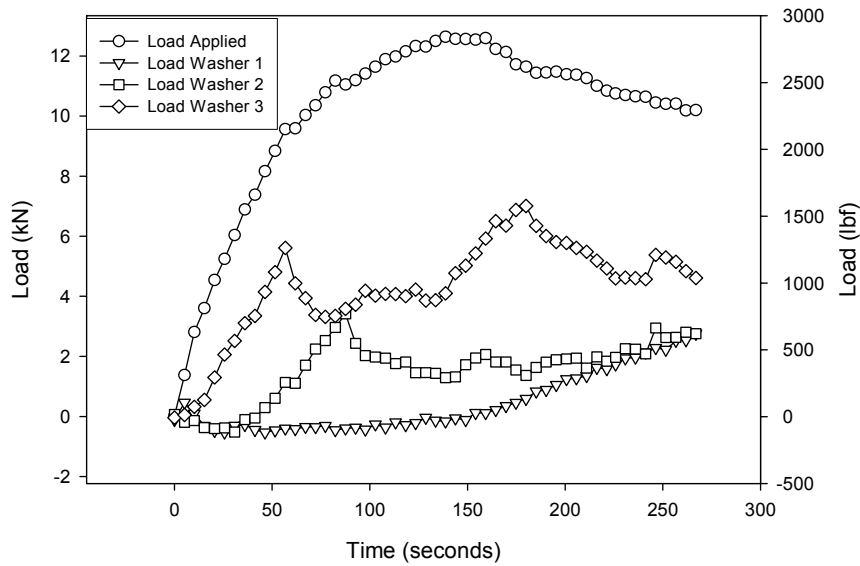


Figure 4.4 Test WOOD4-M Load washer readings over time

4.2.2 Test PE3-M

The response curve for Test PE3-M, having the solid polyethylene sill plate, is shown in Figure 4.5, along with the derived EEEP curve. Walls with solid polyethylene composite sill plates reached a maximum absolute load of 11.7-kN (2632-lbf) with a corresponding displacement of 21-mm (0.84-in). This resulted in a shear capacity of 4.8 kN/m (329 lbf/ft). Failure occurred at a displacement of 56-mm (2.20-in), dissipating 548 kN-mm (4853 lbf-in) of energy. The elastic shear stiffness, k_e , equaled 1.6 kN/mm (8939 lbf/in).

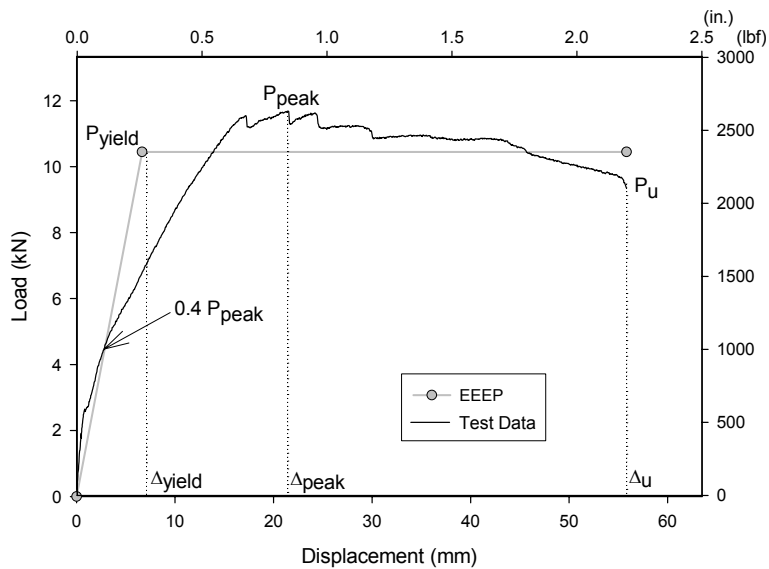


Figure 4.5 Response curve of monotonic wall test with solid polyethylene sill plate (PE3-M)

When loaded to failure, the wall exhibited rigid body rotation around the corner opposite load application. Sheathing and studs “unzipped” from the sill, having larger stud-sill separation at interior studs versus end studs. Loading caused the sill to bend upward at stud locations. Deflections became large enough to cause flexural cracking across the sill section at the two anchor bolts on the side being loaded, along with cracking at the locations of greatest deflections— between the two anchor bolts on the loaded end, and also near the center stud. Bent nails and nails torn through the side of the sheathing and the sill plate occurred at anchor

bolt locations as the sill was unable to displace with the sheathing. Figures 4.6a and 4.7 illustrate the failures at locations of maximum curvature and stress. Slight indentation into sill material from plate washers and elongated holes from bearing forces of anchor bolts is shown in Figure 5.5b. The different displacement pattern of the sill plate (when compared to the traditional wood sill plate) can be attributed to the lower bending stiffness of the wood-plastic member and the higher nail holding power of the material. This caused the uplift to be distributed along the length of the wall more than was observed in the traditional wall.



Figure 4.6 Sill failures: (a) Sill bending and flexural cracking at anchor bolt nearest loaded end stud, and (b) Plate washer indentation and anchor bolt hole size increase from bearing



Figure 4.7 Nail bending and tear-out from sheathing and sill plate at loaded end of wall

Anchor bolt load readings show load acquiring more quickly for LW2 instead of LW3 in Figure 4.8. It is not until the wall reaches peak capacity, that LW3 and LW1 increase load significantly. The reason for LW2 carrying more load initially is because it was tightened more than other washers before testing.

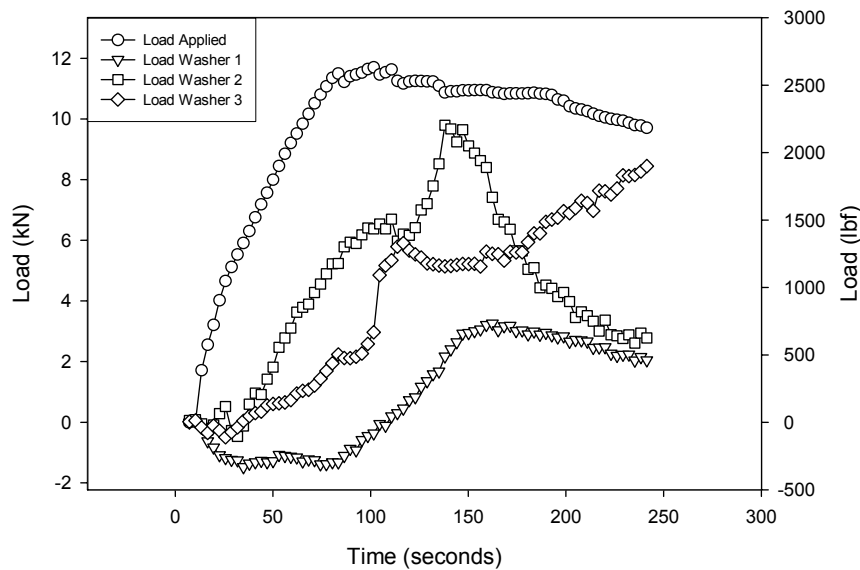


Figure 4.8 Test PE3-M Load washer readings over time

4.2.3 Test PP5-M

The response curve for Test PP5-M, having the hollow three-box polypropylene composite sill plate, is shown in Figure 4.9, along with the derived EEEP curve. Walls with polypropylene composite sills constructed using traditional methods reached a maximum absolute load of 15.8-kN (3561-lbf) with a corresponding displacement of 17-mm (0.68-in). This resulted in a shear capacity of 6.5 kN/m (445 lbf/ft). Failure occurred at a displacement of 24-mm (0.960-in), dissipating 268 kN-mm (2375 lbf-in) of energy. The elastic shear stiffness, k_e , equaled 1.6 kN/mm (9075 lbf/in).

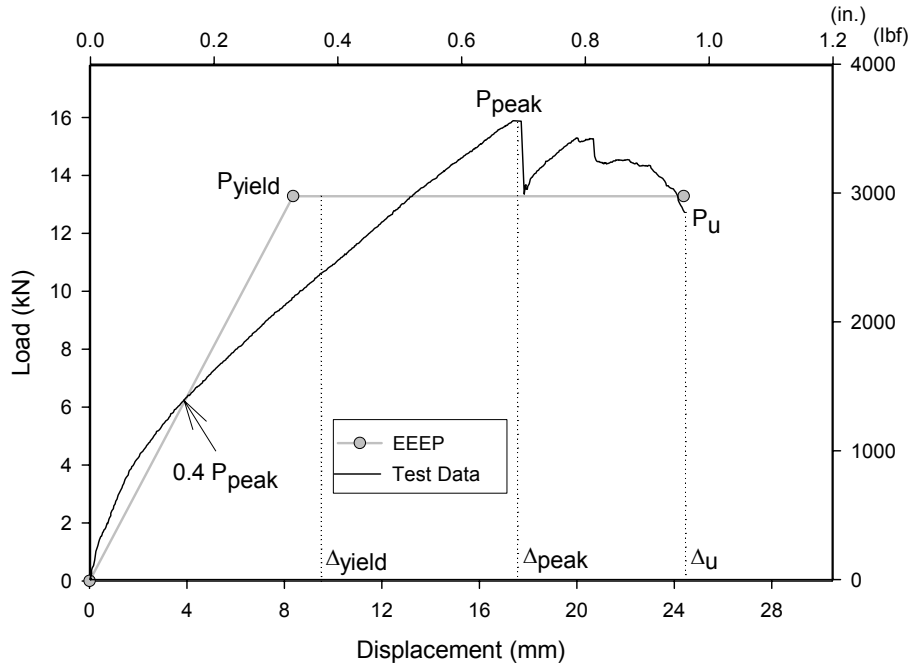


Figure 4.9 Response curve of monotonic wall test with hollow polypropylene three-box sill plate (PP5-M)

When loaded to failure, the wall exhibited rigid body rotation around the corner opposite load application. Sheathing and studs “unzipped” from the sill, and the sill rotated in the perpendicular-to-extrusion direction—this behavior is illustrated in Figure 4.10a. Failure was brittle, occurring in flexure at the location of the anchor bolt. The brittle failure occurred when the outside box, resisting the largest load, split along strands formed during processing. The split on the top surface paralleled the plate washer edges, and the side split occurred at the intersection of the side web and bottom flange, as shown in Figures 4.10b and 4.11. The failure was due to the inherent weakness of this material in the perpendicular-to-extrusion direction. Sheathing nails appeared to have withdrawn along the bottom edge at locations of greatest flexure—at the anchor bolt on the loaded end. Indentation from plate bearing, as occurred in the polyethylene composite, was not apparent for this polypropylene section.

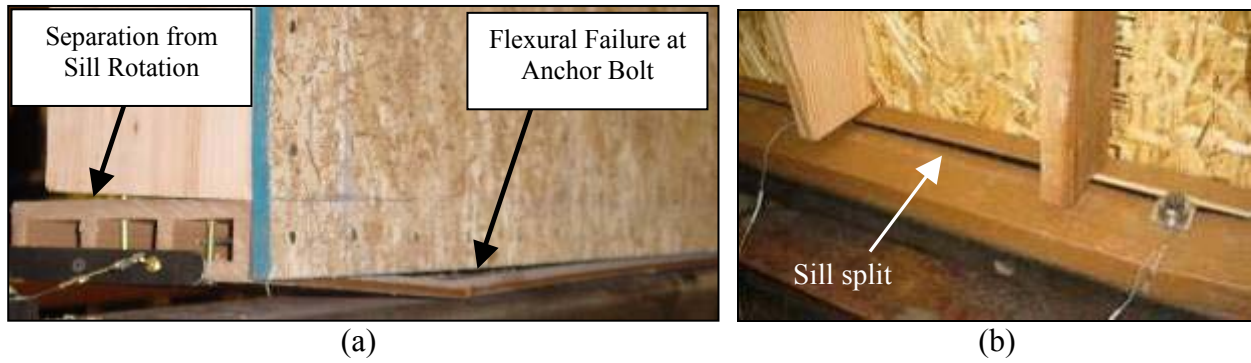


Figure 4.10 View of sill bending and splitting: (a) Overall behavior of sill end, (b) View from top of split along strand

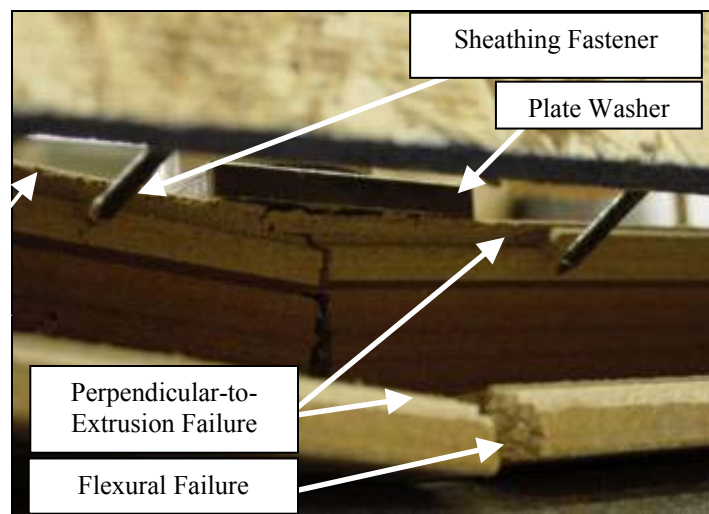


Figure 4.11 View of failure at anchor bolt location, shown from outside bottom edge

Anchor bolt readings for the three box section are presented in Figure 4.12. The plots show that rate of loading increases similarly for LW2 and LW3, with LW2 being attenuated in its load gain. Load carried by LW1 increased early in the test and then showed no further increases, suggesting the tension load was created from lateral forces in the wall.

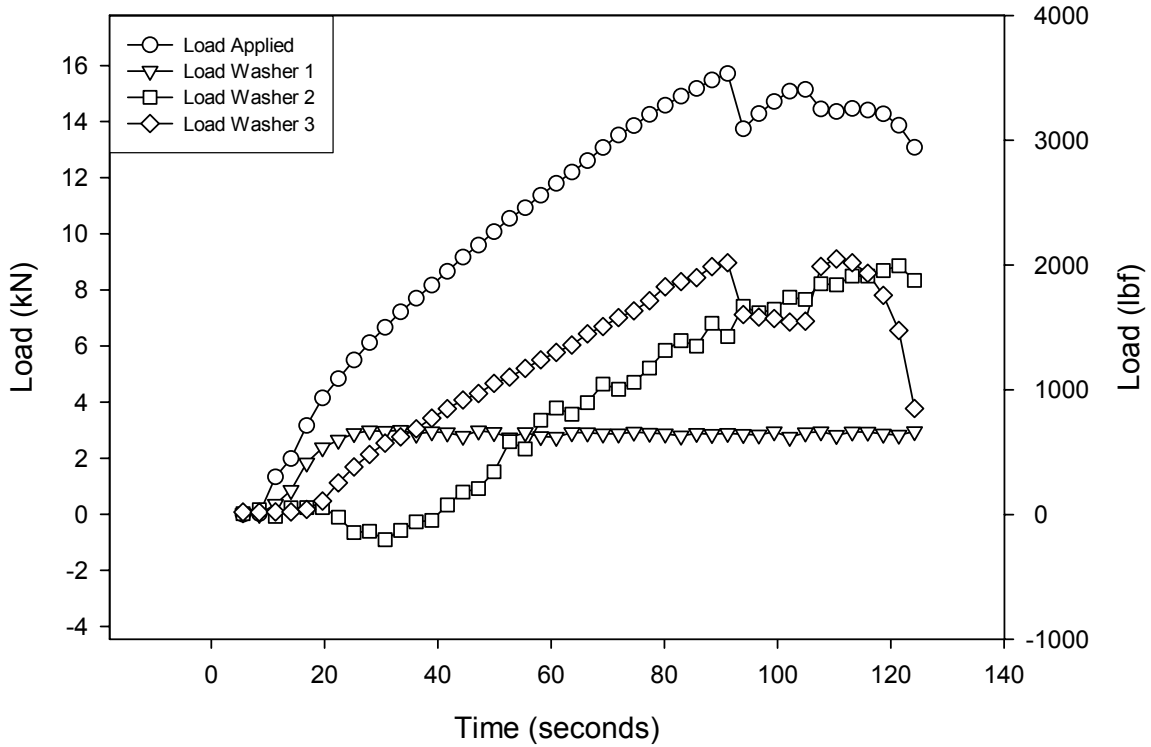


Figure 4.12 Test PP5-M Load washer readings over time

4.2.4 Test PP10-M

The response curve for Test PP10-M, having the hollow polypropylene 4x6 sill plate, is shown in Figure 4.13 along with the derived EEEP curve. Walls with machined polypropylene 4x6 sill plates reached a maximum absolute load of 23.5-kN (5293-lbf) with a corresponding displacement of 54-mm (2.14-in), resulting in a shear capacity of 9.7 kN/m (662 lbf/ft). Failure occurred at a displacement of 55-mm (2.17-in), dissipating 924 kN-mm (8175 lbf-in) of energy. The elastic shear stiffness, k_e , equaled 0.9 kN/mm (5285 lbf/in).

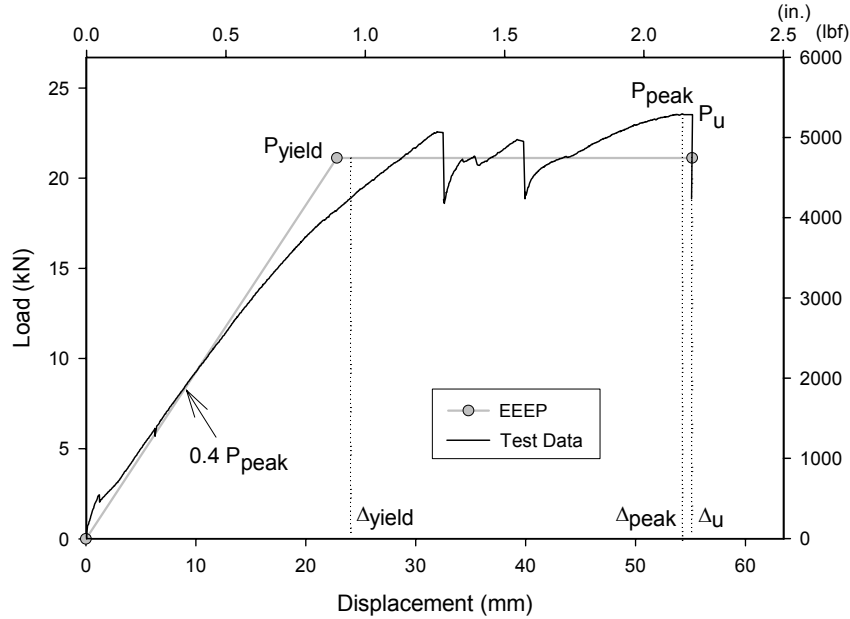


Figure 4.13 Response curve of monotonic wall test with polypropylene 100 mm x 152 mm hollow sill plate (PP10)

When loaded to failure, the wall exhibited limited rigid body rotation around the corner opposite load application. Rather, Test PP10-M exhibited racking behavior, or shear deformation of the wall into a parallelogram type shape for the framing and relative rotation of the sheathing with respect to the framing. Deflection occurred in the sill between the two anchor bolts on the loaded end, being greatest closest to the end anchor bolt, where tension forces concentrate in the end stud. The overall behavior is illustrated in Figure 4.14. Flexural cracking first occurred at the end stud slot, at the same location where failure frequently occurred in member tests. The second significant drop in load came when the sill plate cracked all the way through at the end stud slot, at which point dowel yielding was apparent. At the test end, dowels were completely yielded as shown in Figure 4.15b. The flexural failures would probably be minimized if the WPC section were extruded with a fin on the bottom that would be placed into the concrete foundation, resulting in a continuous hold-down effect along the length of the sill plate. Deflection was also significant at the location of the middle stud, as racking load from

both sheathing panels was transferred to the sill plate. Splitting occurred in interior studs from the screw fasteners. Both interior stud failures are depicted in Figures B.3 in Appendix B. Indentation from plate bearing was not apparent for this polypropylene section. Resulting failure modes of PP10-M began resembling those of traditional construction using hold-down anchors, as nail tear out was apparent in sheathing edges. Nails were bent and sheathing was bearing on the sill top edge near the compression chord, displacing 13-19 mm (0.5-0.75 in) past the sill edge. Though, not all failure modes indicative of fully-restrained walls were present (Heine, 1997).



Figure 4.14 Overall PP10 hollow sill plate behavior (load being applied from right side)

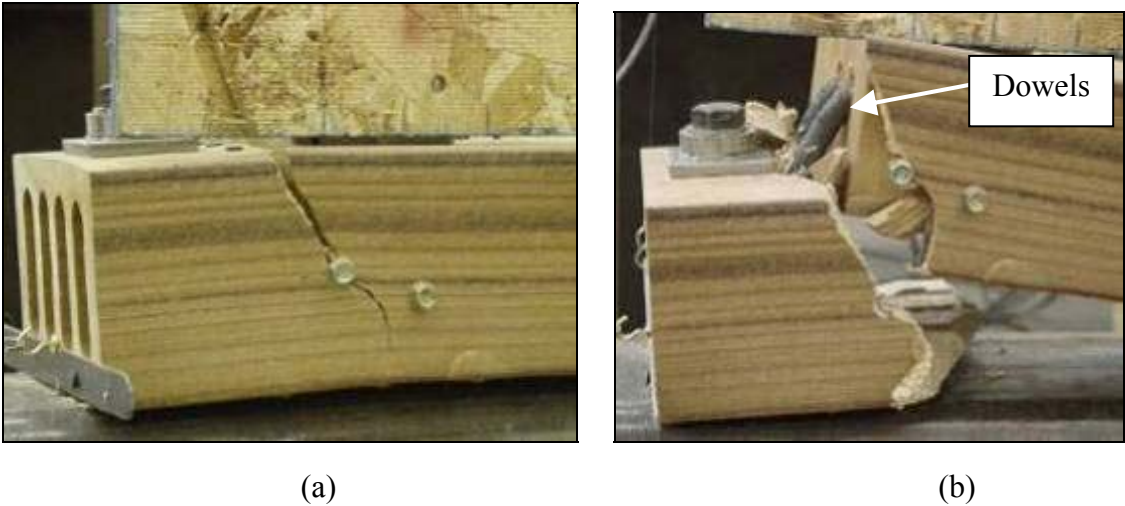


Figure 4.15 Sill failure at end stud: (a) First flexural failure, (b) Failure through section and dowels crushing upper flange and yielding

Load washer data in Figure 4.16 for PP10-M showed practically zero load carried in Load Washer 1. Load Washers 2 and 3 had similar responses to each other. Load Washer 2 gained load sooner from resisting uplift from the end stud as well as from the center stud, but its rate of increase reduced as the test progressed. Load Washer 3 gained load at a rate similar to the rate of load application, though, as wall load drops from sill failure, load shifted from Load Washer 3 to Load Washer 2.

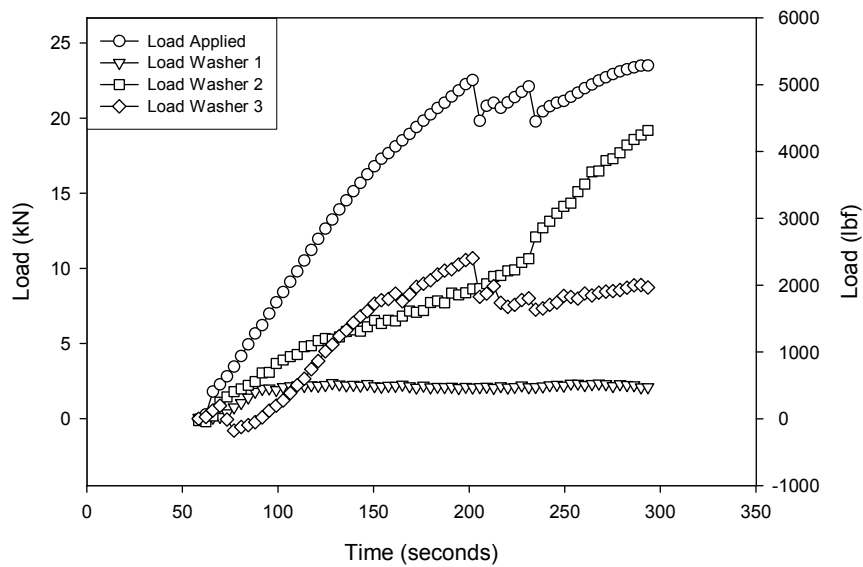


Figure 4.16 Test PP10-M Load washer readings over time

4.3 Monotonic Test Conclusions

Based on the monotonic performance parameters summarized in Table 4.1, composite sill plates prove to be competitive with traditional treated-wood sill plate behavior. Graphical comparisons of monotonic tests are located in Figures 4.17 and 4.18. Compared to traditional wood walls, load capacities at peak and failure increased for Tests PP5-M and PP10-M. Consequently, peak shear capacities increase. Test PP10-M reaches an ultimate shear capacity of 9.7 kN/m (662 lbf/ft), while a traditional wood wall without hold-down restraint reaches only 5.2 kN/m (356 lbf/ft). This equates to an ASD design capacity of 3.2 kN/m (220 lbf/ft) when assuming a factor

of safety of three between ultimate and design. This would place the performance on the lower end of engineered wall unit shear capacities from the NDS, but it also is almost double the value observed for the prescriptive configuration for light-frame construction. Comparing to previous shear wall testing using the information in Table 4.2, the capacity attained in wall PP10-M is close in value to those walls with full anchorage tested by Salenikovich (2000), with reduced deflection capacity and stiffness.

Table 4.1 Monotonic test summary of performance parameters

Test ID	Load (kN)			Deflection (mm)			D_u (mm/mm)	k_e (kN/mm)	E (kN-mm)	V_{peak} (kN/m)	Δ_{re} (mm)
	Yield	Peak	Failure	Yield	Peak	Failure					
WOOD4-M	11.2	12.7	10.1	11	32	63	5.98	1.07	643.2	5.2	41
PE3-M	10.4	11.7	9.4	7	21	56	8.39	1.57	548.4	4.8	35
PP5-M	13.3	15.8	12.7	8	17	24	2.92	1.59	268.4	6.5	18
PP10-M	21.1	23.5	18.8	23	54	55	2.42	0.93	923.7	9.7	36

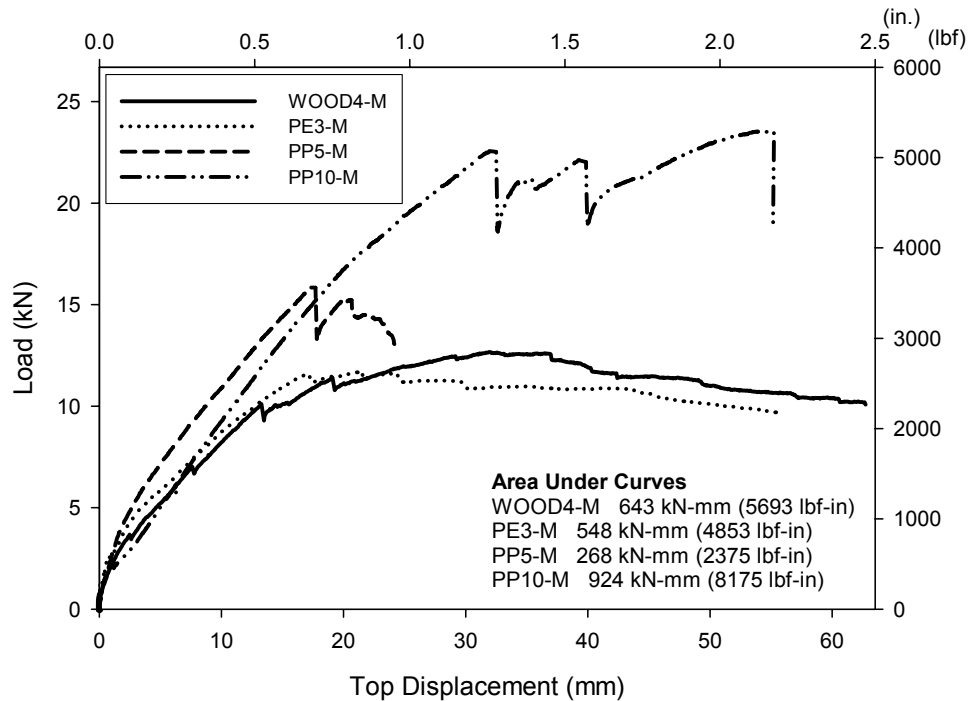


Figure 4.17 Load-displacement curves for monotonic tests

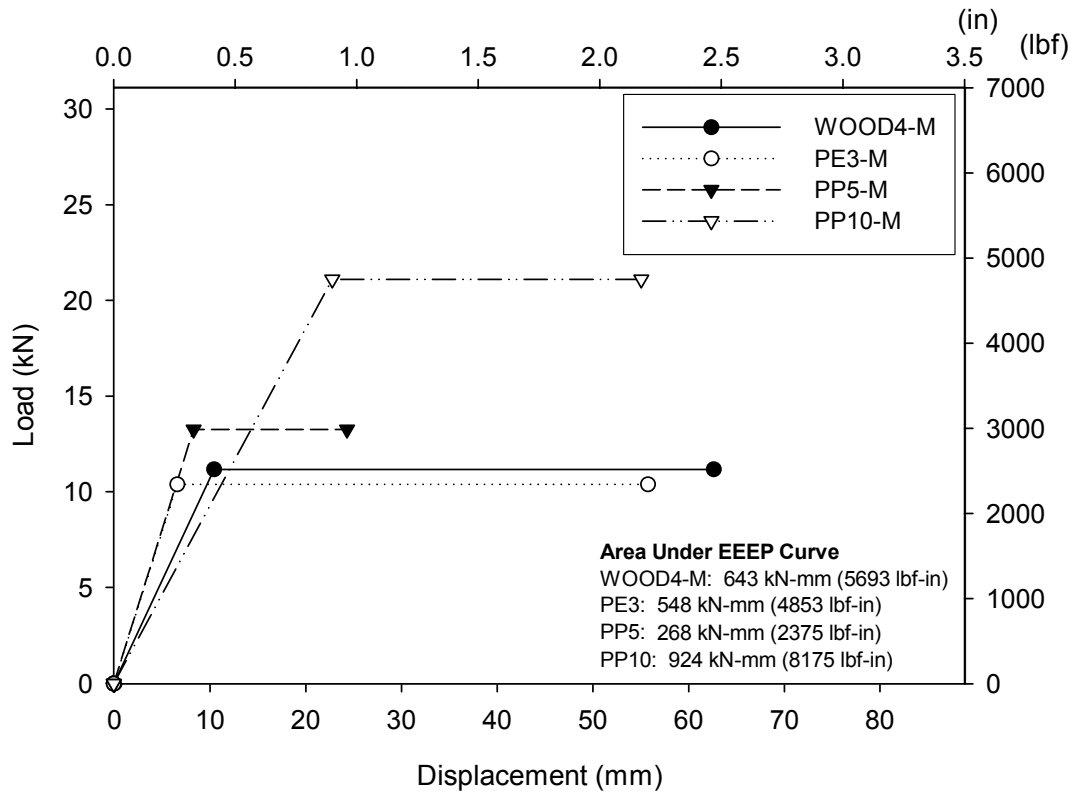


Figure 4.18 EEEP curves from monotonic test results

Table 4.2 Comparison of monotonic test parameters

Test	Anchorage Conditions	Peak Load, kN	Deflection, mm		k_e , kN/mm
			@ Peak Load	@ Failure	
WOOD4-M	Intermediate	12.7	32	63	1.1
PE3-M	Intermediate	11.7	21	56	1.6
PP5-M	Intermediate	15.8	17	24	1.6
PP10-M	Intermediate	23.5	54	55	0.9
Salenikovich (2000)	Full	24.2	73	107	1.6
	Intermediate	12.1	28	45	1.8
	None	8.2	20	28	0.7

Top wall displacement measures account for lateral displacement due to uplift and lateral displacement due to racking. The latter may be estimated by subtracting the tension chord uplift measure from total wall top displacement to remove the rigid body motion deflection. Comparing this measure versus wall displacement in Figure 4.19, it can be concluded that Test

PP10-M exhibits substantially more racking movement, which increases at a linear rate. This is consistent with damage observations unique to Test PP10-M, having more sheathing fasteners yielded and visible sheathing movement relative to studs. The majority of top wall displacement for Tests WOOD4-M, PE3-M, and PP5-M are contributed to uplift of wall ends from rigid body rotation. The deformation pattern of Specimen PP10-M is more desirable as it results in a more distributed damage pattern by activating more of the structure and increases the damping effects of the system.

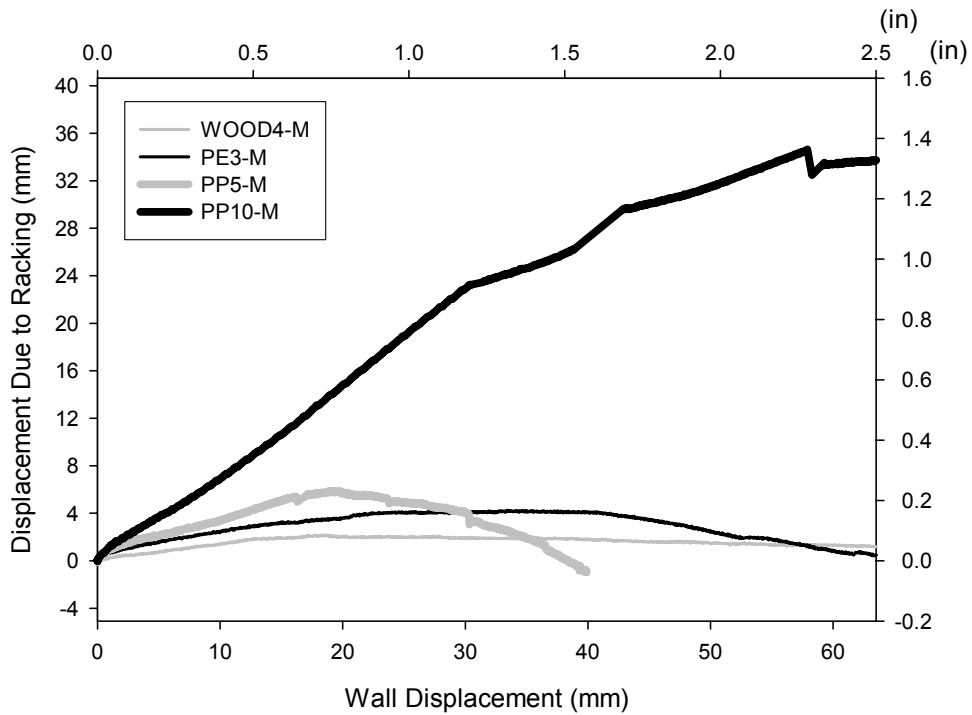


Figure 4.19 Racking displacement of walls in monotonic tests

After analyzing the data provided in Table 4.1 and the failure modes observed, the following conclusions can be inferred:

- The 1x solid polyethylene sill plate (PE3) proved feasible as an equal replacement for traditional wood sill plate, achieving the highest ductility of all wall configurations. Loads were comparable, with energy dissipation decreasing by 17%, and deflection is

limited, thus reducing overall story drift, when compared to traditional prescriptive construction.

- The hollow polypropylene three-box achieved higher loads and stiffness than Tests WOOD4-M and PE3-M, though it exhibited brittle and catastrophic failure (having lowest energy dissipation of all specimens), indicating the need to improve material properties in the perpendicular-to-extrusion direction if it is to be used for this application.
- The 100 mm x 152 mm hollow polypropylene section (PP10) was able to achieve racking behavior rather than rigid body overturning, dramatically affecting performance parameters of the wall system compared to traditional construction methods. The more efficient utilization of all system components results in higher loads and displacements, as well as a 44% increase in energy dissipation. Test PP10-M achieved an estimated design shear capacity of 3.2 kN/m (220 lbf/ft), which makes the load capacity equal to the lower strength walls designed according to the NDS. This load capacity essentially doubles the strength of prescriptive construction. Energy dissipation was distributed throughout the wall and not concentrated at the stud and sill as other walls demonstrated. Ductility did decrease as the yield load increased and stiffness decreased, as compared to other walls' performance.

4.4 Cyclic Test Results

The complete set of cyclic test parameters for individual wall tests, including positive and negative response, is located in Appendix B. A summary of average values is presented in Table 4.3.

Table 4.3 Performance parameters

<i>Average Values for Wall Type</i>	<i>WOOD4</i>	<i>PE3</i>	<i>PP5</i>	<i>PP10</i>	
Area Under Curve	416	346	303	1748	<i>kN-mm</i>
Area Enclosed by Hysteresis	2420	1602	1532	6398	<i>kN-mm</i>
Maximum absolute load, P_{peak}	10.8	11.9	16.9	28.6	<i>kN</i>
Maximum absolute displacement, Δ_{peak}	29	20	20	44	<i>mm</i>
Failure Load, $0.80 \cdot P_{peak}$	8.6	9.5	13.5	22.9	<i>kN</i>
Ultimate Displacement, cyclic, Δ_u	45	35	25	77	<i>mm</i>
$0.40 \cdot P_{peak}$	4.3	4.7	6.8	11.4	<i>kN</i>
Displacement, $\Delta_{0.4peak}$	2	3	4	9	<i>mm</i>
P_{yield}	10.0	10.9	14.7	26.2	<i>kN</i>
Yield Displacement, cyclic, Δ_{yield}	5	7	10	21	<i>mm</i>
Shear Strength, v_{peak}	4.4	4.9	6.9	11.7	<i>kN/m</i>
Secant Shear Modulus, $G' @ 0.4P_{peak}$	1.8	1.5	1.5	1.2	<i>kN/mm</i>
Secant Shear Modulus, $G' @ P_{peak}$	0.4	0.6	0.9	0.6	<i>kN/mm</i>
Elastic Shear Stiffness, K_e	1.8	1.5	1.5	1.2	<i>kN/mm</i>
$D, \Delta_{peak}/\Delta_{yield}$	5.3	2.7	2.0	2.1	<i>mm/mm</i>
$D_u, \Delta_{failure}/\Delta_{yield}$	8.1	4.7	2.6	3.6	<i>mm/mm</i>
$D_f, \Delta_{failure}/\Delta_{peak}$	1.5	1.8	1.3	1.7	<i>mm/mm</i>

4.4.1 WOOD4

Two walls with traditional treated sill plates were tested cyclically. Envelope curves for each test are plotted in Figure 4.20, along with the corresponding monotonic response curve for Specimen WOOD4-M. Cyclic results achieved lower load and displacement capacities than the monotonic results with the CUREE protocol, as elastic stiffness increased and the yield point lowered. This type of change in performance was observed in other cyclic tests of walls and is expected (Heine, 1997).

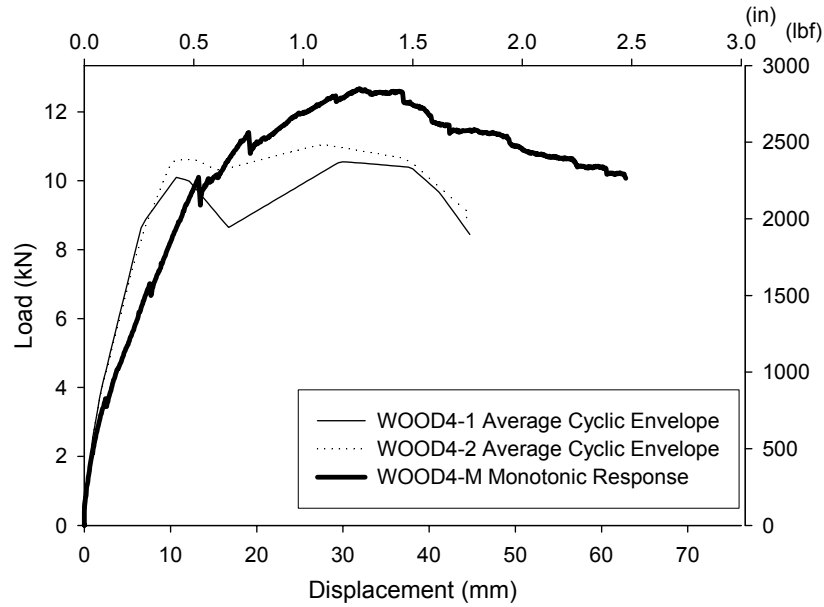


Figure 4.20 WOOD4 response curves

The cyclic shear strength averaged 4.4 kN/m (303 lbf/ft), with peak displacements averaging 29-mm (1.14-inches). Failure occurred after the 7th sequence completed (primary cycle at 1.0 Δ_{ref} and two trailing cycles) for Test WOOD4-1 and after the 8th sequence (1.5 Δ_{ref}) completed for Test 1-2, resulting in an average failure load of 8.6-kN (1942-lbf) and ultimate displacement of 4.6-mm (1.75-inches). An average ultimate ductility ratio of 8.1 was achieved, with 2420 kN-mm (21,422 lbf-in) of energy dissipated over all cycles up until failure.

Walls rotated in rigid body motion about the bottom corners. Sill splitting began at around 12-mm (0.5-inch) displacement (0.3 Δ_{ref}), initiating from the loaded end and propagating along the grain down the entire length of sill, as seen in Figures 4.21a and 4.21b. Because of rigid body motion, sheathing connectors were not taxed as would be in walls with hold-down hardware. Nail pull-out only occurred along the bottom edge of sheathing, nearest wall corners, as shown in Figure 4.21c. Sheathing remained well in contact with stud and sill edges.

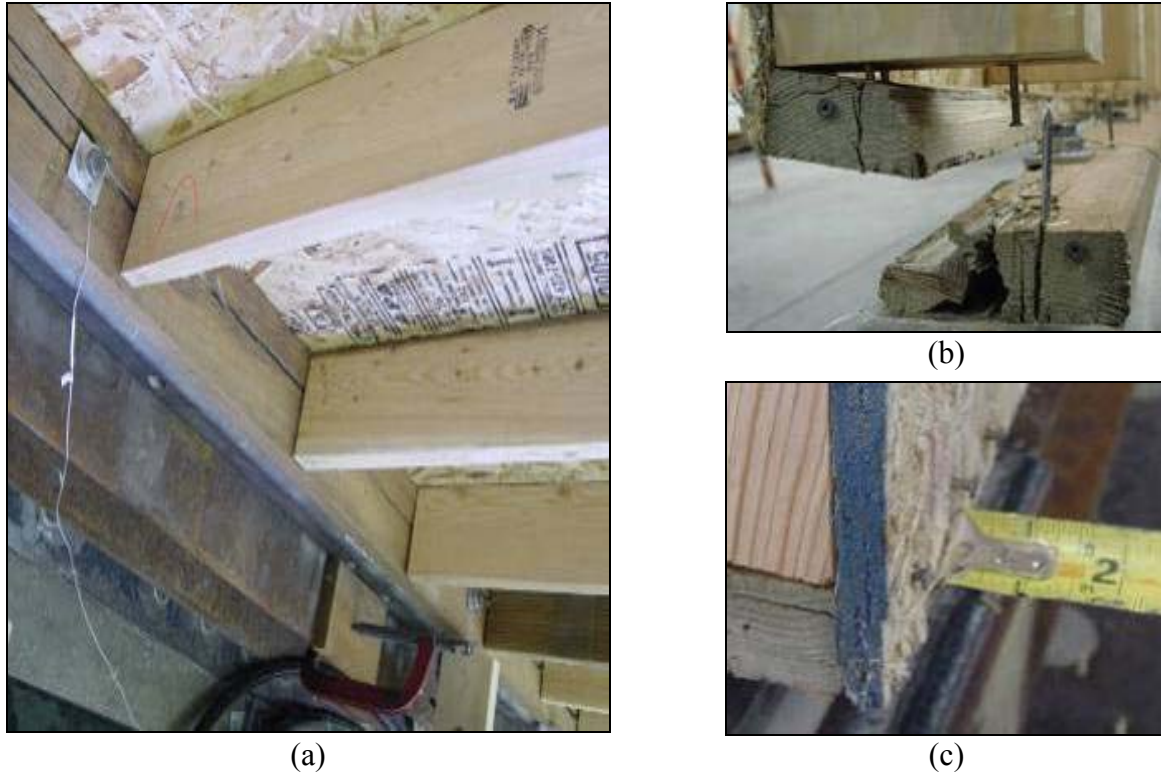


Figure 4.21 WOOD4 failures: (a) Typical sill splitting full length (Test WOOD4-1), (b) Sill end split (Test WOOD4-2), and (c) Sheathing nail pull-out at wall end (Test WOOD4-1)

4.4.2 PE3

Two walls having solid polyethylene composite sill plates produced response curves shown in Figure 4.22. Load capacities were comparable to monotonic test results, though with reduced displacement capacities as more energy was dissipated with reversed cycles.

Cyclic shear strength averaged 4.9 kN/m (333 lbf/ft) at peak, with a corresponding average displacement of 20-mm (0.78-in). Load resistance dropped 20% after the 7th loading sequence ($1.0 \Delta_{ref}$) for PE3, reaching an average failure load of 9.5-kN (2134-lbf) and ultimate displacement of 5-mm (1.75-in). A ductility factor of 4.7 was achieved and 1602 kN-mm (14,176 lbf-in) of energy was dissipated.

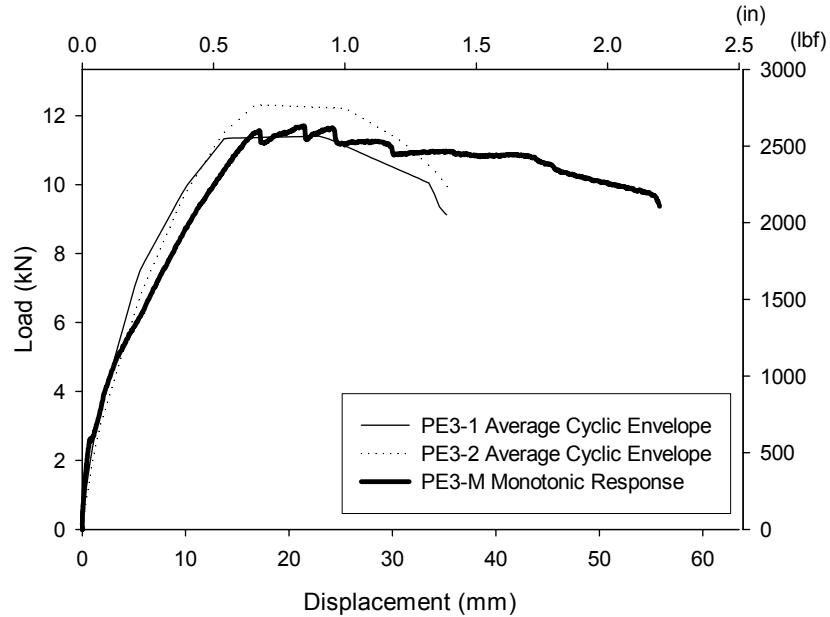
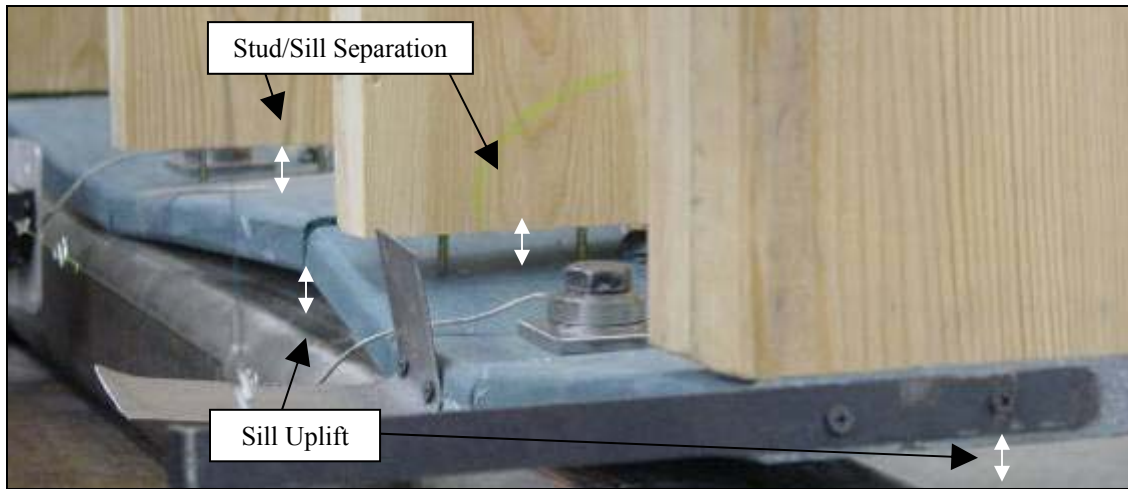
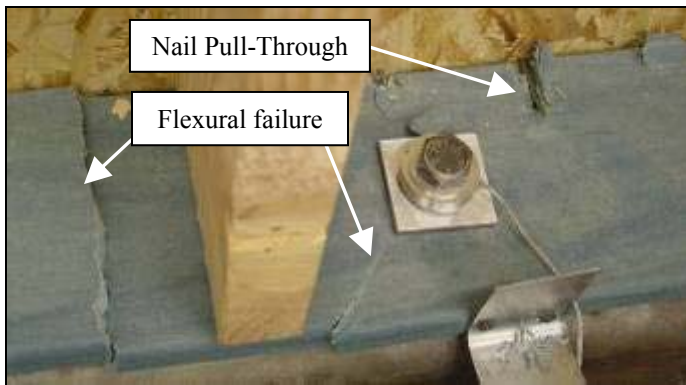


Figure 4.22 PE3 response curves

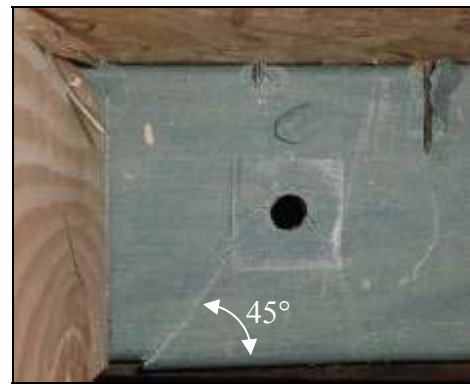
Walls rotated as a rigid body about bottom corners. Sill behavior was characterized by upward bending at stud locations as shown in Figure 4.23a, creating noticeable curvature between anchor bolts when wall displacements reached $0.7 \Delta_{ref}$. At $1.0 \Delta_{ref}$, nails began tearing through sill top edges at end anchor bolt locations, and “popping” was audible. At this same time, interior stud separation from the sill was apparent. Flexure failure occurred inside the 1st interior stud on both ends at $1.5 \Delta_{ref}$, and propagated from the anchor bolt, out to the edge at a 45 degree angle, at the next primary cycle. These failure modes are depicted in Figures 4.23b and 4.23c. Because of rigid body rotation, nails were only pulled out along the bottom sheathing edge. Of the nails that pulled out, one pulled out greater than 25-mm (1-inch). Significantly more nail pull-through occurred in the sheathing and the sill plate in PE3 versus WOOD4, as the clamping force on fasteners is greater, and the sill resisted longitudinal splitting and continued to transfer sheathing forces to the foundation. Unique to this test group behavior, only interior studs unzipped from sills, whereas both end studs remained in contact.



(a)



(b)



(c)

Figure 4.23 PE3 failures: (a) Overall bending during test (Test PE3-2), (b) Failures near end anchor bolt (Test PE3-1), and (c) End anchor bolt plate washer indentation and 45 degree failure (Test PE3-1)

4.4.3 PP5

Load deflection response curves for walls with polypropylene composite three-box sills are shown, along with monotonic response curves, in Figure 4.24. Compared to monotonic tests, cyclic load capacity improved slightly (within 10%), as did both maximum and ultimate displacements. Stiffness of walls remained relatively independent of loading method.

PP5 averaged shear strengths of 6.9 kN/m (475 lbf/ft) at maximum displacement of 20-mm (0.78-in). Resistance dropped 20% from peak capacities after the 8th and 9th sequences for

Test 3-1 and 3-2, respectively. At these points of failure, average load and displacement reached 13.5-kN (3038-lbf) and 25-mm (0.99-in). A ductility factor of 2.6 was achieved at failure, along with 1532 kN-mm (13,562 lbf-in) of energy dissipation.

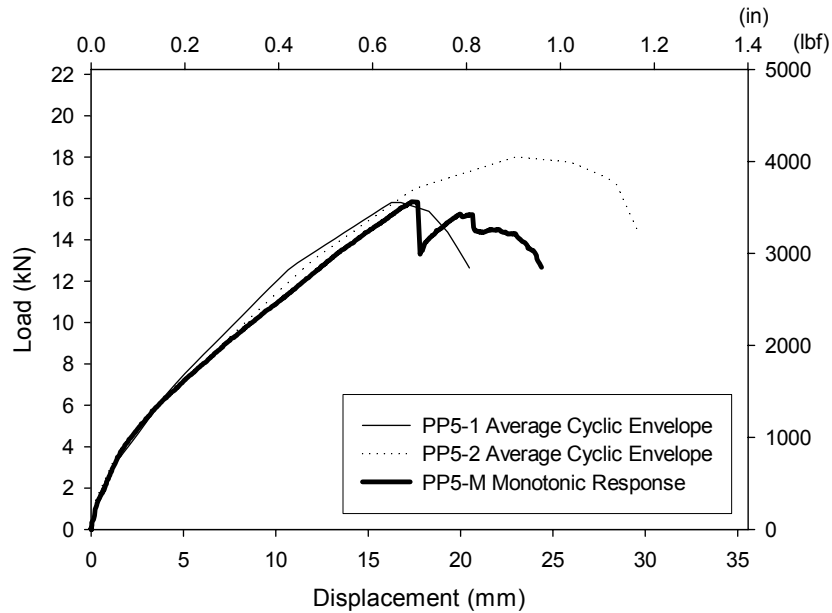


Figure 4.24 PP5 response curves

Behavior for PP5 was rigid body motion, with studs separating from the sill plate, along with sill plate rotation. Audible signs of failure did not occur until reaching $1.0 \Delta_{ref}$ —probable failure between the web and flange in the outside box of sections. By $1.5 \Delta_{ref}$, catastrophic failure occurred, splitting down the entire section along strands. Flexural failure also occurred at end anchor bolts, along with complete blow-out of part of the top flange near the anchor bolt. The splitting along the sill and between strands is illustrated in Figure 4.25. Nail tear-out of sheathing was not nearly as frequent as in PE3, and nail pull-out occurred only at the bottom row, near sill ends. Sheathing remained flush to stud edges.

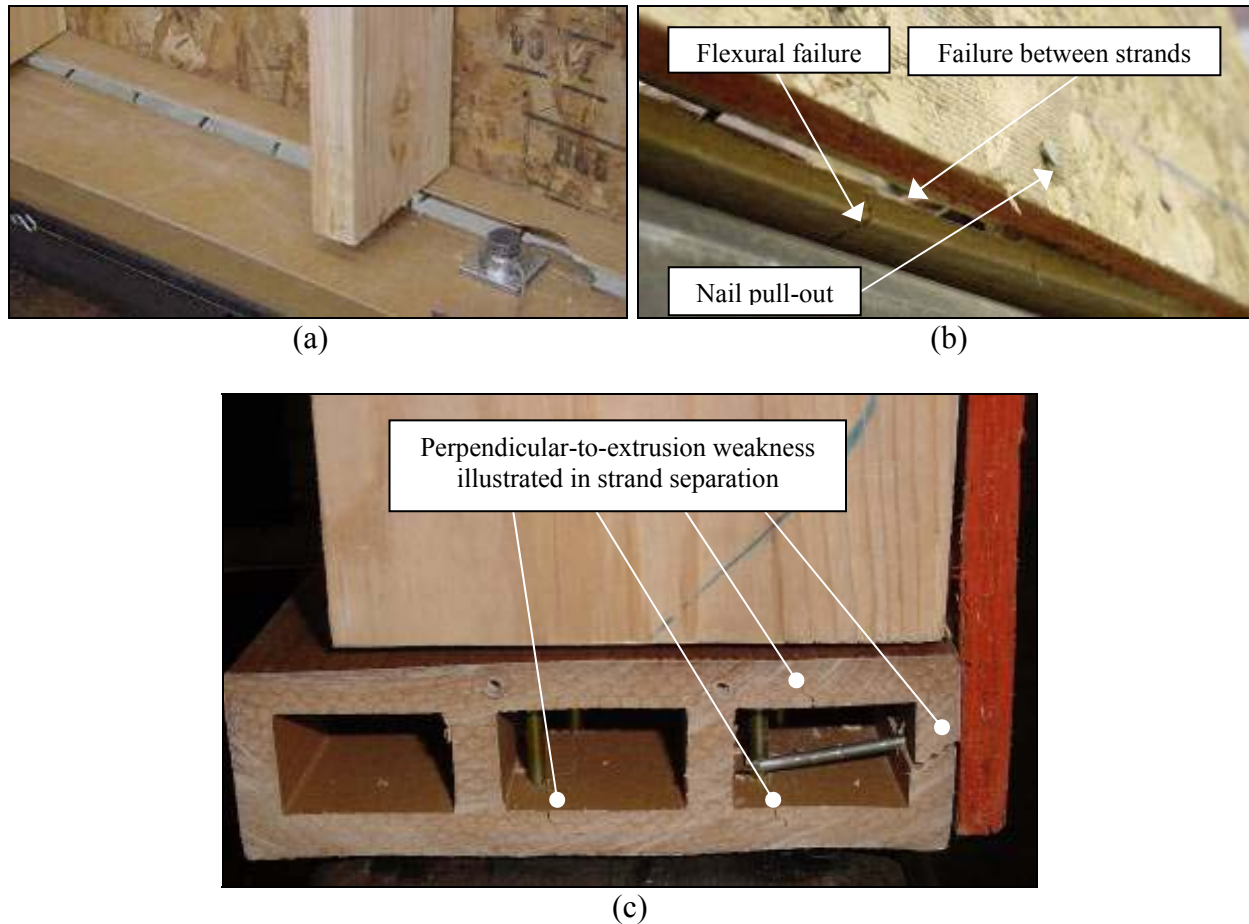


Figure 4.25 PP5 failures: (a) Side box split down length of sill, (b) Bottom view of split box between outside web and flange and flexural failure, and (c) End view of split showing separation between strands

4.4.4 PP10

The response curves for both walls in PP10 and for the monotonic test are shown in Figure 4.26. More so than previous wall configurations, cyclic response curves exceeded monotonic results. This is consistent with similar findings by Heine, showing increased differences between monotonic tests and cyclic tests (SPD protocol) with increased overturning restraint (Heine, 1997). With increased anchorage provided in PP10, load distributed more uniformly throughout the wall, as walls are able to deform by racking. Displacement at failure increased from the ability to accumulate more damage when racking. Stiffness increased by

33% for cyclic tests, most likely due to difference in load rate and amount of friction being created at stud-to-sill connections in reverse cycling.

Shear strength reached an average 11.7 kN/m (803 lbf/ft) at a maximum displacement of 44-mm (1.75-in). PP10 was able to undergo 9 and 10 loading sequences before load carrying capacity dropped to 80% of peak loads, for Test PP10-1 and PP10-2, respectively. Test 4-2 required terminating before load resistance clearly showed a 20% drop, due to actuator stroke limitations. Ultimate load and displacement averaged 22.9-kN (5140-lbf) and 77-mm (3.04-in). A ductility factor of 3.6 was achieved and energy dissipation totaled 6398 kN-mm (56,630 lbf-in) from all cycles until failure.

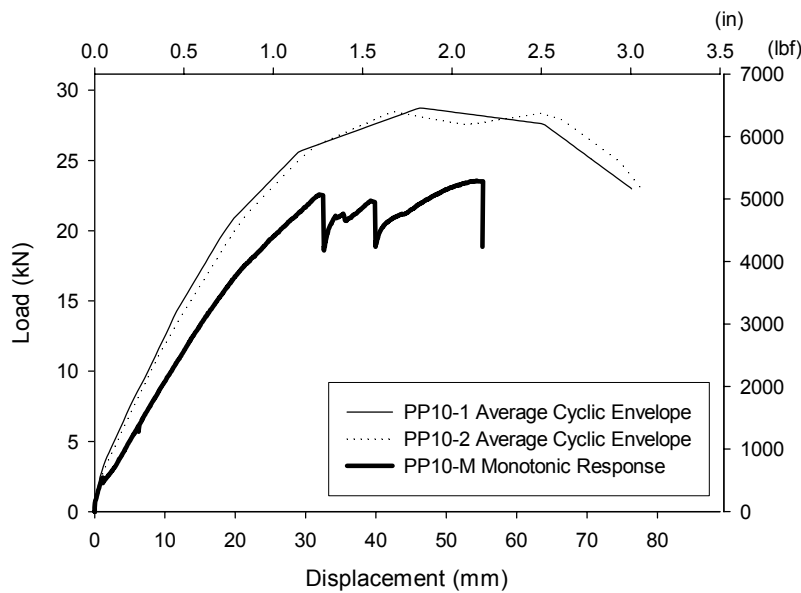


Figure 4.26 PP10 response curves

Behavior in PP10 dramatically changed as racking occurred, utilizing the sheathing connectors in dissipating energy. When racking displacements equaled reference displacement, audible popping occurred near the end stud slot, though failure was not visible. Flexural splitting at the end stud location happened at $1.5 \Delta_{ref}$. At this point, nail fatigue in sheathing connectors was apparent. By $2.0 \Delta_{ref}$, sheathing nails into the center stud pulled out. The dowel connection

yielded, in a ductile Mode III, and, at extreme displacements for Test PP10-2 ($2.5 \Delta_{ref}$), the top flange portion of the sill crushed above the dowels. Dowel yielding dissipated energy which reduced the amount of inelastic deformation to undergo by sheathing fasteners. Similar conclusions were made by Jones (1996) for traditional framed walls with overturning anchorage. Evaluation after testing shows additional flexural failures occurring at interior stud slots, along with splitting of studs from screw fasteners. Due to the racking behavior, nail pull-out was frequent and extended up edges of sheathing approximately two feet. Sheathing separated from stud edges dramatically and nail fatigue and fracture were apparent. The variety of failures occurring in PP10 can be seen in Figure 4.27.

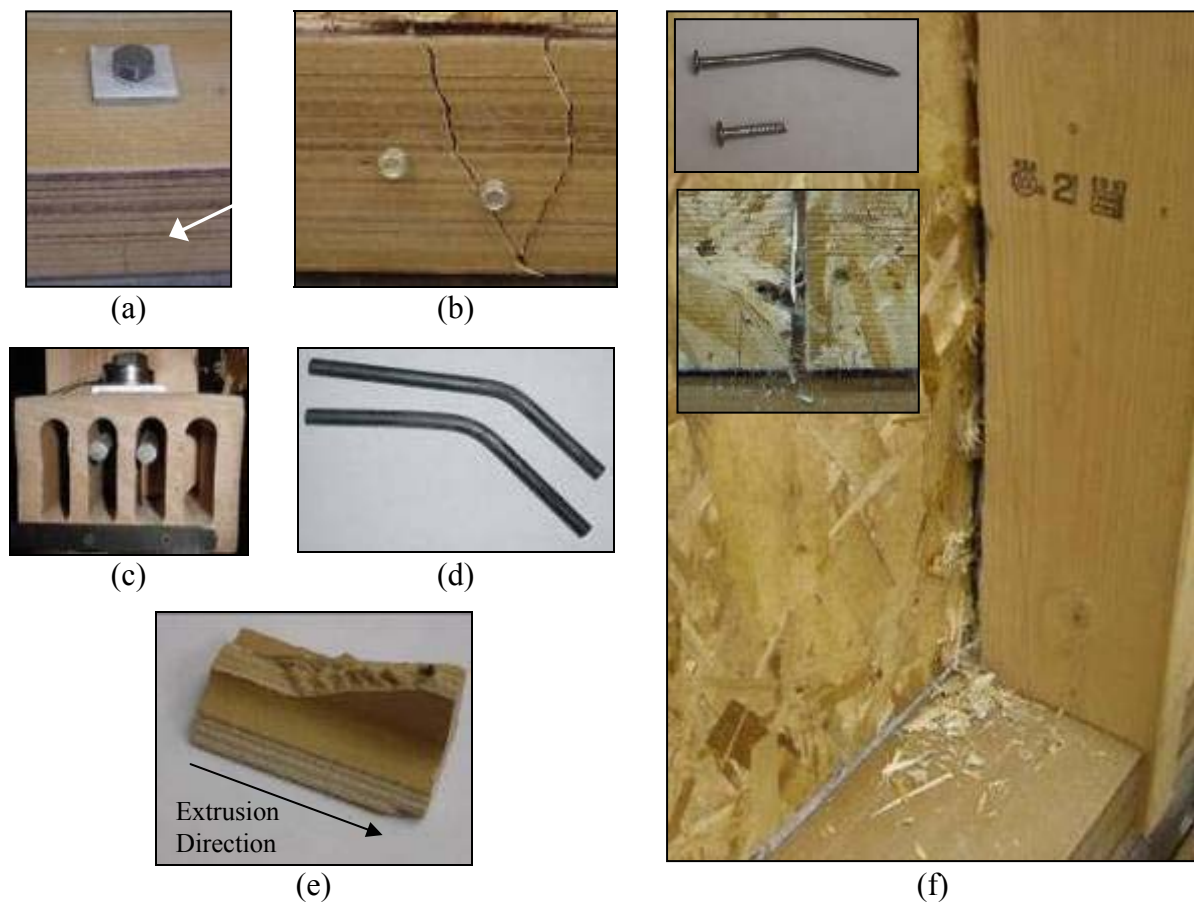


Figure 4.27 PP10 failures: (a) Flexural failure at interior anchor bolt, (b) Flexural failure at end stud connection, (c) End view of dowels yielding, (d) Yielded dowels from Test PP10-2, (e) Failure plane along section strands, and (f) Nail pull-through at panel joint (inset photos of yielded fasteners and view of panel joint from outside)

4.5 Cyclic Test Discussion

4.5.1 Test Group Comparison

Use of a WPC material as a sill plate can improve the shear wall performance under lateral loads. The following discussion compares the performance of various wall configurations based upon observed failure mechanisms and calculated performance parameters. For a visual comparison, each test group had a best fit line through average envelopes for individual tests, and the resulting average curves are shown in Figure 4.28. Wall capacities were conservative as applied dead load in service and adjacent corner elements would improve capacity, along with the ability of top and bottom panel edges to bear on adjacent walls. Similar conclusions were reached by Heine (1997) and Rose (1998), respectively, when they reviewed test results for traditionally framed walls.

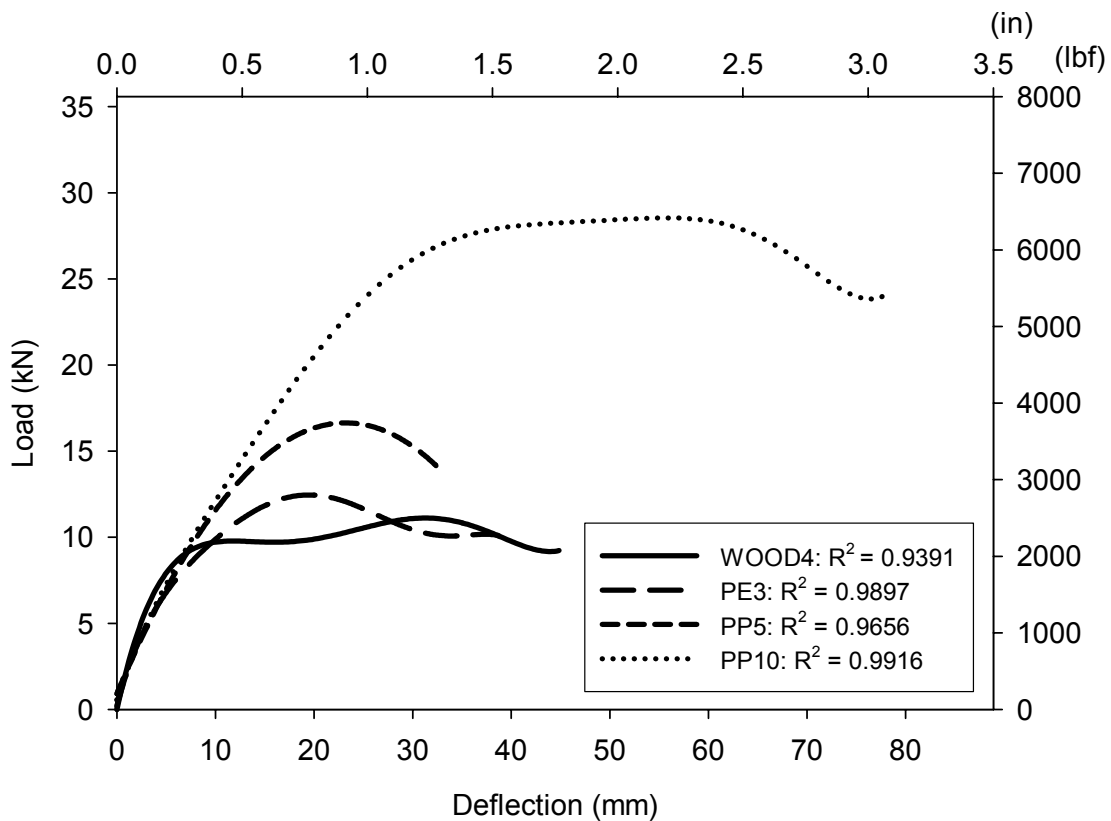


Figure 4.28 Best fit lines for each test group

Cyclic test results of walls with a solid polyethylene sill may be compared to that of traditional walls with treated-wood sill plates in WOOD4. Similar loads, and therefore shear strengths (10% increase), were achieved. Though with an increased yield displacement (40%) and decreased maximum and ultimate displacements, and elastic shear stiffness decreased resulting in reduced wall ductility. Attributable to lowered displacement capacities, energy dissipation from cycles up to failure decreased by almost 40% for walls with a polyethylene WPC sill. This section, if having equivalent thickness to 38-mm (nominal 2x) wood sill plates could potentially have a larger improvement in performance, due to increased flexural resistance of the sill plate.

PP5 test results show improved load capacities, 50% over that of WOOD4. Similar to PE3 improvements, yield displacements of PP5 increased by at least 50%, consequently lowering elastic stiffness. With a decrease in maximum and ultimate displacements due to brittle failure, the ductility was reduced tremendously. As expected from such brittle failure, energy dissipation decreased by 40%. Despite these disadvantages on earthquake performance, walls with the three-box polypropylene section were able to provide over 50% more shear strength than the traditional wood sill plate. To capitalize on this wall configuration's improved shear strength, weaknesses in the perpendicular-to-extrusion direction in the section must be addressed to provide desirable earthquake performance. Surface reinforcement, section profile changes, or elimination of die stranding could be viable options to improve upon sill plate behavior.

Comparing WPC sill plates intended for direct substitution (PE3 and PP5), negligible difference is found in energy dissipation abilities, as well as in elastic shear stiffness. Though, due to the brittle behavior of PP5, ductility decreased by almost 45% compared to PE3. Weaknesses between strands of PP5's section created brittle failure mechanisms and catastrophic

failure. The advantage of this particular polypropylene section exists in its improved load capacities compared to a solid polyethylene or wood sill.

4.5.2 Shear Deformation Contributions

PP10 developed different load-deflection behavior, due to deformations from overturning, shifting to deformations from shear. Deformations due to overturning were measured by end chord uplifting, whereas shear deformation was measured as the difference between top wall displacement and uplift displacements. Comparing the percentage of wall displacement contributed by shear deformations in Table 4.4, there is a clear trend for PP10, having approximately doubled the amount of shear deformation than all other wall configurations.

Table 4.4 Amount of wall displacement from shear deformations at point of maximum load

Test Group	Total Wall Displacement (mm)	Displacement Contributed by Uplift (mm)	Displacement Contributed by Shear (mm)	Percentage of Wall Displacement Contributed by Shear Deformation (Racking)
WOOD4	22	14	8	37%
PE3	20	12	8	39%
PP5	21	11	9	46%
PP10	54	10	44	82%

By being able to minimize the uplift in end chords from overturning (or hold-down slip when applicable), forces on fasteners in corners are reduced—at locations furthest from center of rotations. In fully anchored walls with treated wood sill plates, added percentages of uplift displacements were found to reduce wall capacity by causing splitting of plates and premature fastener fatigue (Rose, 1998). Although splitting from cross-grain bending is not a concern for PP10’s sill configuration, the amount of force imparted on sheathing fasteners from wall uplift affects energy dissipation and ultimate capacity.

4.5.3 Earthquake Performance Evaluation of PP10

The most significant improvement in PP10 performance over conventional wood sill wall configurations existed in the 155% increase in energy dissipation for all cycles up until failure. This is attributable to the racking behavior of the system, distributing load to all components and allowing greater than 160% more load than conventional wood sill configurations (at peak capacity) to be carried, and having improved displacement capacity. It can be inferred that these increases would be even more substantial had there been a bottom row of sheathing nails attaching the sheathing to the sill member. For future improvements, the section could be redesigned to provide an extended ledge into which to fasten the sheathing, similar to blocking.

PP10 had improved results for all parameters except for elastic stiffness and ductility. Yield displacements increased due to yield load increasing by over 100%. Yield displacements showed additional increases due to a decrease in stiffness of approximately 30%. Ductility decreases for PP10 as compared to ductility ratios for previous tests. However, due to the significant changes that occurred in load capacity and displacement capacity, the entire load-deflection behavior is dramatically different for PP10. Ductility may not fully describe the changes in behavior in comparison to WOOD4, PE3, and PP5.

In order to predict successful earthquake behavior, ultimate displacements, stiffness, and energy dissipation must be considered in addition to ductility. For design purposes, peak loads will also be considered. The data in this study is compared to results by Salenikovich (2000) and Langlois (2002), testing similar wall configurations with and without full anchorage (Table 4.5). The tests with overturning anchorage, having larger load capacities and displacement capacities, will be closer in their load-deflection behavior to PP10 to provide comparisons. It should be noted that results from walls tested using the Sequential Phased Displacement (SPD) protocol

have 20% less load capacity and decreases in deflections when compared to walls tested under the CUREE protocol. On the contrary, energy dissipation will be greater for walls tested using SPD, as cycles are more frequent and reach higher displacements. There have been no trends found between loading protocol and stiffness (Gatto and Uang, 2002).

Table 4.5 Capacities of walls with overturning anchorage

	Stiffness	Ultimate Displacement	Peak Load	Ductility	Energy Dissipation
	<i>kN/mm</i>	<i>mm</i>	<i>kN</i>		<i>kN-mm</i>
PP10	1.2	77	28.6	3.6	6398
Salenikovich (2000) ^a Full Anchorage	1.9	72	19.6	7.6	14,955
	1.8	73	19.2	7.5	15,203
Salenikovich ^a Intermediate Anchorage	0.7	39	10.2	3.1	3428
	1.4	30	11.1	4.3	1690
Salenikovich ^a No Anchorage	1.4	36	10.8	5.4	3584
Langlois (2002) ^b Full Anchorage	2.1	62	36.7	NA	11,076

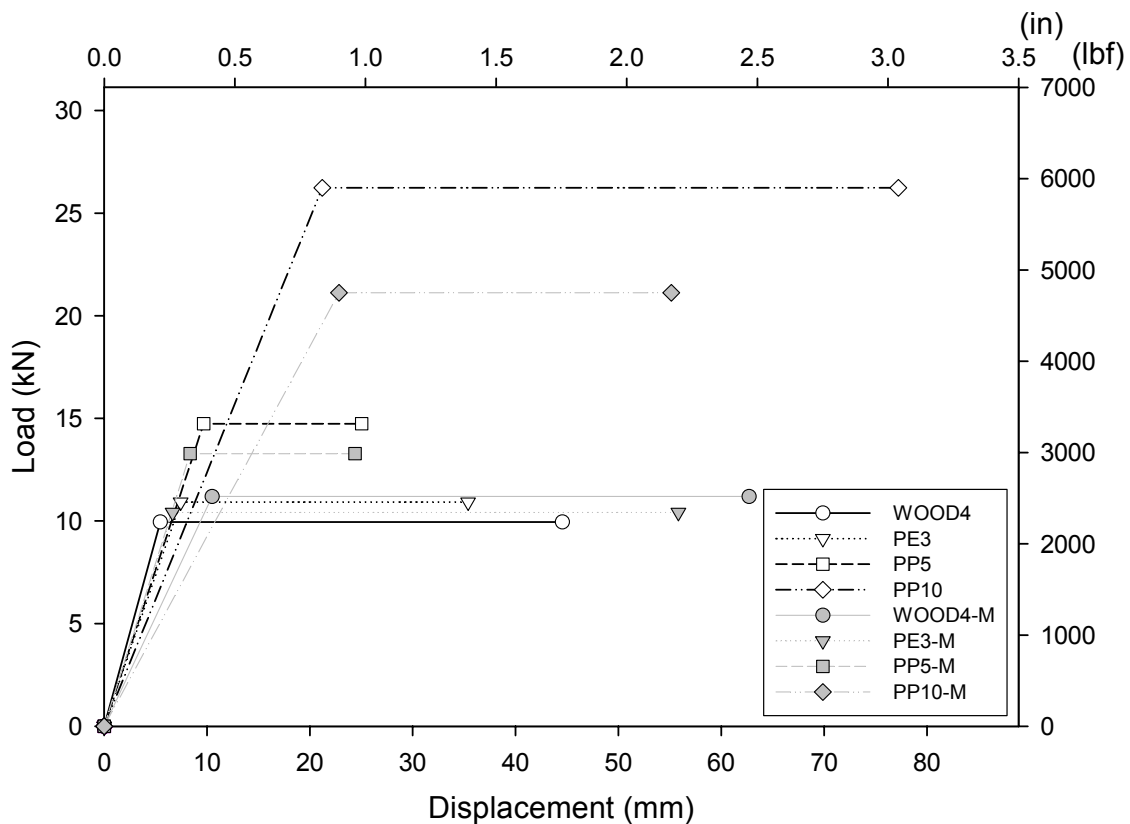
^a 2x4 lumber, 7/16" OSB, 6/12" nail spacing; values based on initial response for SPD protocol

^b 2x4 lumber, 15/32" OSB, 4/12" nail spacing; values reported are average of 8 tests with varying reference displacements; CUREE protocol

Compared to fully anchored walls, PP10 wall configurations are less stiff, and therefore will not attract additional load in the structure than an engineered wall would. Additionally, it will require higher displacements to achieve a plastic response in these walls. This could be expected due to not having stiff hold-down connectors at wall ends. Load capacity of PP10 is more comparable to results found by Langlois (2002), also using the CUREE protocol. In comparison to Langlois, PP10 energy dissipation is lower than fully anchored walls; the amount of energy dissipated could be increased if a greater percentage of sheathing fasteners were worked in shear resistance. This improvement could be achieved by adding a bottom row of fasteners on sheathing panels to distribute the load more uniformly. As well, if a fin were added to the bottom of the WPC sill to be embedded in the concrete foundation, the continuous anchorage

would eliminate the flexural failures that occurred in the tests of the current configuration and stiffen the overall wall.

A presentation of EEEP curves for both cyclic and monotonic tests is shown in Figure 4.29. There is a clear illustration of energy dissipation differences as well as ductility in ultimate displacement capacities between the different wall configurations. Energy dissipation for cyclic data is based on the area under the average response curves for a relative comparison (actual energy dissipation was calculated separately for all cycles).



MONOTONIC

Area Under EEEP Curve
 WOOD4-M: 643 kN-mm (5693 lbf-in)
 PE3-M: 548 kN-mm (4853 lbf-in)
 PP5-M: 268 kN-mm (2375 lbf-in)
 PP10-M: 924 kN-mm (8175 lbf-in)

CYCLIC

Area Under EEEP Curve
 WOOD4: 416 kN-mm (3683 lbf-in)
 PE3: 346 kN-mm (3059 lbf-in)
 PP5: 303 kN-mm (2678 lbf-in)
 PP10: 1748 kN-mm (15,470 lbf-in)

Figure 4.29 Average EEEP curves for wall configurations under monotonic and cyclic loading

The ductility of PP10 compares closely with the full anchorage walls tested by Salenikovich (2000), though loads are still quite different. Ductility ratios provided by Salenikovich are double PP10. Also considering damage, it can be inferred the PP10 configurations provide a better solution that will have more integrity remaining after wall damage has occurred. Unlike wood walls, PP10 walls do not split longitudinally down the plate and still retain lateral sliding capacity.

4.5.4 Comparison of Monotonic and Cyclic Results

Response of walls under cyclic and monotonic tests was not found to be significantly different in previous shear wall testing. The CUREE protocol produces peak loads fairly close to monotonic loads (Gatto and Uang, 2002). If differences occur, studies have shown monotonic tests to result in slightly higher response than cyclic tests. Studies by Langlois (2002), using the CUREE protocol, and Heine (1997), using the SPD cyclic method, found this to be true for the majority of their tests. Because monotonic capacities were often higher than cyclic shear wall capacities, the City of Los Angeles Department of Building and Safety required a 25% reduction in design shear load for seismic design after the Northridge earthquake to avoid non-conservative designs. (Rose, 1998). Langlois (2002) found monotonic response was slightly lower than cyclic only for walls without uplift anchorage. It was rationalized that for walls without full anchorage, it is common for cyclic results to exceed monotonic results as more energy is dissipated in unzipping of studs in reversed cycles.

The ratios of maximum loads for cyclic tests compared to monotonic tests completed in this study are included in Table 4.6. Tests performed in this study show that monotonic results for PE3, PP5, and PP10 under-performed cyclic tests at maximum load, while WOOD4 monotonic results exceeded cyclic results. Walls PE3, PP5, and PP10 have as much as a 20%

increase in capacity when loaded cyclically. This increase could potentially be an advantage to utilizing WPC material for cyclic loading applications. The reason for this reverse trend may be in the material behavior of the thermoplastic sill plates, resulting in a change in distribution of load demand on the sheathing fasteners. In particular, the higher resistance for WPC sill plates in bearing/clamping of fasteners may reduce the amount of localized crushing at connections in cyclic loading. As well, the increased load rate for cyclic tests, as compared to monotonic tests, may contribute to higher resistance in connections. The limited number of samples and wide amount of variables makes this inconclusive and requires further study.

Table 4.6 Comparison of monotonic and cyclic wall capacities

Test Group	$P_{\text{peak cyclic}} / P_{\text{peak monotonic}}$
WOOD4	0.85
PE3	1.01
PP5	1.07
PP10	1.21

4.5.5 Cyclic Stiffness

The stiffness of systems is important in predicting how loads distribute through a structure. In the case of lateral force resisting systems, stiffness of shear walls (and rigidity of diaphragms) determine the amount of lateral forces attracted (Paevere et al, 2003). The elastic stiffness of cyclic tests progressively decreased from WOOD4 to PP10 (as much as 32%). According to Heine (1997), anchorage does not influence cyclic stiffness. Therefore, one may conclude that the difference in stiffness is more of a system effect, resulting from connection slack, and load distribution among sheathing fasteners and stud connections. Because of this decrease in stiffness and higher yield loads, PP10 walls theoretically did not achieve plastic behavior until 21-mm (0.84-inches) of lateral deflection. This deflection is approaching 1/3 of the maximum story drift limit (2.5%) when structural damage may occur (ICBO, 2000b). The

majority of this wall displacement is due to racking, as stud uplift only accounts for a maximum of 3-mm (0.125-inches). The elastic stiffness must increase to provide a wall that has better ability to control deflections in the elastic range in normal service conditions. By stiffening the wall, smaller forces will not cause large amounts of damage in adjacent systems, and yielding will occur at smaller displacements, beginning greater energy dissipation from plastic deformation. Because large displacements are in shear deflections, a change to the design that could provide increased stiffness is installing fasteners along the bottom edge of the wall sheathing. This would allow force to transfer to interior studs rather than remaining concentrated at the center and end studs where dense nailing results in additional stiffness. Another solution to reduce the amount of stud movement from its vertical position would be to eliminate connection slack in dowels and extra space within end slots that allow stud rotation within the plane of the wall with shims or other means.

Taking a further look at stiffness performance, and how it degrades with each subsequent cycle, a better estimate of design success may be made. Figure 4.30 plots stiffness with increasing displacement—at the peak of each cycle for both positive and negative envelopes. Because of the non-linearity of shear wall behavior, stiffness is not constant during one loading cycle. Therefore, the stiffness was estimated by passing a line through the origin and point of maximum load and corresponding displacement. A full list of stiffness values for each cycle can be found in Table B.17 in Appendix B. WOOD4 has the fastest degradation in stiffness as cycles proceed, resulting from the brittle splitting of wood sill plates in early cycles. PE3 mimics this stiffness degradation, though having a quicker drop in stiffness at wall deflections of 12-mm (0.5-in), resulting from flexural failures of the sill plate. PP5 has low stiffness degradation in beginning cycles, but then drops suddenly from brittle and complete splitting in the outside box

of the section. Throughout all cycles, PP10 has the best performance in retaining wall stiffness. The rate of degradation is slower than all other wall configurations, and it lacks any sudden drops. Studs were unable to displace large distances from the sill, having stiff fasteners connecting studs to sills. This eliminates some of the stiffness degradation found in walls where sheathing and studs unzip from sills.

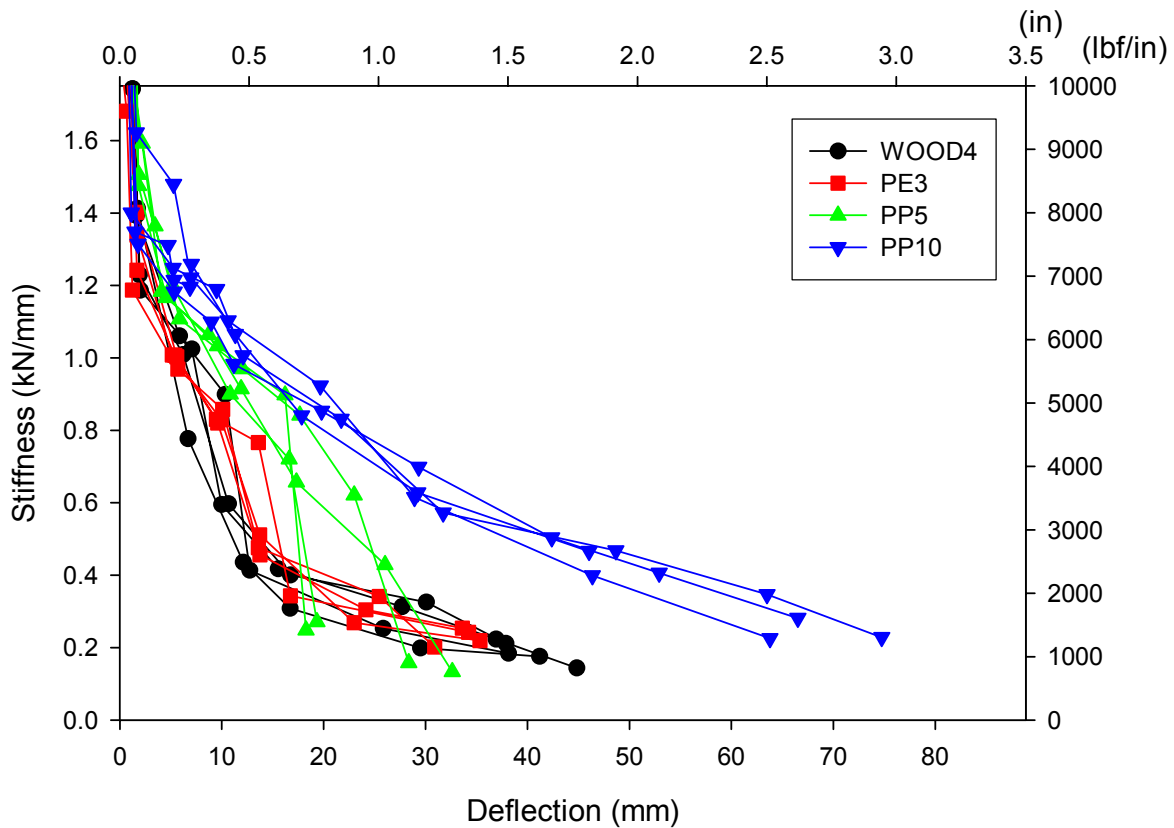


Figure 4.30 Stiffness degradation from cyclic loading

The ability to minimize stiffness degradation after repeated cycling becomes an advantage over traditionally constructed sill plate connections in WOOD4, PE3, and PP5. This becomes important in a wall's ability to continuously resist deflections and failure in earthquake loading. An example of brittle behavior is exhibited in PP5's abrupt stiffness degradation from less than ideal splitting of the section at wall deflections approximately 20 mm. WOOD4, PE3,

and PP10 had similar shapes to their degradation curves, however Groups 1 and 2 had increased stiffness degradation. This has been found in previous studies to approximate an exponential decrease (Heine, 1997). Also a benefit from slower loss of stiffness is the continued ability of the wall to dissipate energy, another reason for WOOD4 wall configuration having superior performance.

4.5.6 Cyclic Test Results

Cyclic shear wall tests exhibit successful performance for WPC sill plates when subjected to reversed loading.

- Cyclic test behavior exceeded monotonic test response for walls with WPC sill plates, most dramatically for PP10, having an increase of 20% in peak performance. Due to changed load distribution throughout sheathing fasteners (possibly from improved bearing/clamping forces in WPC sill plates), this better performance may be a motivating factor in utilizing composite material in cyclic load applications.
- PE3 wall configuration would be a suitable substitution for wood sill walls, however improvements in energy dissipation and ductility could be achieved by providing a section with a thickness equal to 38-mm (2x nominal) depth.
- PP5 exhibited brittle failure and weakness between strands, suggesting the need for section improvement before further utilization is possible. Improvements should be made in order to resist tension forces perpendicular-to-extrusion at the sheathing connection, as well as at the line of anchor bolts where bending occurs due to the eccentricity between sheathing uplift and anchor bolt resistance.
- PP10 exhibits significantly improved load and deflection capacities by enabling racking movements—achieving performance resembling fully anchored wall assemblies.

Deformations contributed by racking (shear deformations) were found to be double at maximum loads over that of all other wall configurations

- Despite PP10 having the lowest elastic stiffness values, cyclic stiffness degradation occurred at the slowest rate, demonstrating a significant improvement in energy dissipation and overall ductile performance.
- PP10's sill plate design should incorporate a ledge for a bottom row of sheathing fasteners to fasten into, similar to blocking.
- To avoid extensive structural damage and damage in brittle finishes, the initial stiffness of walls could be increased to control deflections in the elastic loading range. For PP10, this can be achieved by adding bottom fasteners and/or eliminating connection slack in stud-to-sill connections.
- Flexural failure of the sill plate could be eliminated by adding a fin for embedding the sill plate into the concrete foundation. This would provide continuous lateral and uplift resistance along the length of the sill plate. It would also be likely to increase the elastic stiffness by eliminating uplift of the ends of the member.
- For earthquake performance, the design must be stiff enough to resist displacements at small forces, but still provide for ductility at larger magnitude forces. A combination of racking ability, force distribution throughout sheathing fasteners, and ductile behavior of the stud-to-sill connections have allowed PP10 to achieve this level of performance, with significantly more energy dissipated than any other wall configuration.

CHAPTER 5 CONCLUSIONS AND RECOMMENDATIONS

Composite wall-to-foundation connection systems were first tested by isolating the end stud-to-sill connection. In order to develop an optimum fastener configuration to facilitate the most effective transfer of load, a total of 16 connections were tested, modifying and improving the design as needed. From these tests, four levels of performance were obtained, with the reinforced shifted configuration being selected for final full-scale member and shear wall design. Isolated connection tests provided supplemental information regarding necessary section improvement. In order to statistically characterize this design, multiple repetitions were performed on single members. These tests, closely resembling loading conditions inherent in shear wall behavior, estimated the capacity and performance. Conclusions obtained from preliminary isolated connection tests and member tests can be summarized below as:

5.1 Connection and Component Conclusions

- The polypropylene 102-mm x 152-mm (4-in x 6-in) section exhibits weakness in the perpendicular-to-extrusion direction due to strands formed by the die.
- Inherent weaknesses in the perpendicular-to-extrusion direction can be effectively reinforced by the use of polypropylene/glass fiber tape applied with the fiber direction perpendicular-to-extrusion, or by installing screws perpendicular-to-extrusion at the location of failure.
- By connecting the stud to the sill plate with dowels, cross-grain bending (which has caused splitting of sill plates currently in use) can effectively be eliminated.

- Substantial increases in load capacity of the end stud connection resulted from the shifted configuration (stud slot and dowel connection), exceeding traditional end nailed connections by 26.7-31.1-kN (6000-7000-lbf).
- The most effective anchorage for uplift is that positioned near the end of the sill, minimizing the moment arm created from the transferred uplift force.
- Wood plastic composites prove to be durable materials that have the capability of being extruded and machined into complex structural shapes.

5.2 Shear Wall Conclusions

Further tests demonstrated the effect of using durable wood plastic composites as a structural member in a full-scale wood shear wall. Failure modes and performance parameters were compared to identify effects on wall behavior from various sill plate configurations. By achieving results comparable to fully restrained walls, WPC material can be utilized effectively in structural applications. The following conclusions highlight each section's distinguishing behavior and performance implications.

- Solid polyethylene sill plates prove to be feasible as substitutes for walls with traditional wood sill plates without hold-downs. Section integrity relies on flexural strength and nail pull-through resistance.
- A polypropylene three-box section requires section improvement to avoid brittle behavior and widespread damage before being fully utilized as a sill plate in cyclic applications. Improvements can be made by eliminating strands, increasing wall dimensions, or applying exterior reinforcement.

- A polypropylene 102-mm x 152-mm (4x6) hollow section (PP10) engaged full wall elements, exhibiting racking behavior and achieving a design shear capacity of 3.2 kN/m (220 plf) from monotonic loading. Racking deformations doubled compared to all other WPC sill plate and wood sill plate walls. From this improved load distribution, loads and displacements increased (load capacity increased by 160% over current prescriptive construction)—having entirely different load-deflection behavior than previous wall configurations. This configuration resulted in load capacities in the lower range of engineered wood-framed walls. Consequently, energy dissipation more than doubled over traditional wood sill wall configurations. Section integrity relied on flexural resistance at end stud locations, as well as strength perpendicular-to-extrusion. The latter could be improved with reinforcement or processing without stranding.
- Walls having WPC sill plates show improved capacities when loaded under cyclic loading versus monotonic, contributable to different load distribution among sheathing fasteners as compared to walls with traditional wood sill plates (possibly due to load rate effects, or improved bearing/clamping forces on fasteners).
- Elastic stiffness decreased from stiffness values for wood sill wall configurations. To limit displacements in the elastic range, this stiffness should be increased by eliminating connection slack and adding a bottom row of sheathing fasteners. Stiffness may also be increased by the addition of a fin along the bottom of the section that would embed into the concrete, thus providing continuous anchorage and minimizing uplift.
- Stiffness degradation was distinctly different for polypropylene sections, having slower degradation for subsequent cycles. Only the deep polypropylene hollow section (PP10) was able to retain stiffness throughout cycles, avoiding sudden drops in stiffness from

brittle failure. This measure of stiffness throughout cycles is an important indicator for the wall's ability to continuously resist cyclic loading and control displacements, especially when behaving in a plastic manner.

- Stiffness, energy dissipation, ultimate loads, and resulting damage become more revealing measures of earthquake behavior than ductility ratios between the tested wall configurations due to differing load-deflection behavior.
- Compared to fully restrained walls completed in previous studies, the polypropylene section must be improved to force loads to distribute more uniformly throughout sheathing to efficiently utilize all components. This will provide more energy dissipation that would be comparable with energy values reported for fully restrained wall configurations.

5.3 Future Research

Results from this study are based on one monotonic test to determine reference displacements and two cyclic tests for each wall configuration. Further testing would be required to statistically conclude design loads and failure modes.

- Improvements in test methods would be to obtain more accurate cyclic load control hardware to obtain consistent loading directions as well as collecting data more frequently.
- Tests should be completed under monotonic versus cyclic loading to compare performance of walls having WPC sill plates, to verify that wall behavior under cyclic loading exceeds monotonic.
- Future research should focus on optimizing prototype sections tested in this study. Though member test damage resembled that seen in full wall systems, a shear wall test

program of optimized sections would provide more complete information useful to the designer and for making predictions about earthquake performance. Specific section improvements should be made for each wall configuration before testing additional shear walls.

- ✓ Initial work must be completed to successfully process reliable sections without stranding or apply reinforcement to weak areas of sections (at locations identified previously).
- ✓ Solid polyethylene sections should be extruded or built-up as 38 mm (2x nominal) thickness and tested in full-scale shear wall tests to verify the benefit of improved flexural properties.
- ✓ Polypropylene three-box sections should have changed dimensions of the outside box to increase properties, eliminate stranding, or provide reinforcing across the observed failure plane.
- ✓ Polypropylene 102-mm x 152-mm (4-in x 6-in) hollow sections (PP10) should have the following section changes:
 - Provide ledge into which to fasten sheathing, similar to blocking.
 - Design an extension along the entire bottom length to cast into concrete, providing continuous sill anchorage.
 - Investigate behavior of the section that is manufactured without stranding.
 - Investigate side-wall connectors that fit flush to the section.
- ✓ Redesign sections to 38-mm (2x nominal) dimension at stud locations, to match nominal dimensioned lumber currently used in low-rise construction.

- ✓ Provide a solution for installing nail fasteners into wood plastic composite material that will be economical and feasible for current construction methods.
- Tests should be performed on walls with different sheathing nail schedules, as well as different sheathing and finish materials (interior and exterior), to determine the range of design loads for the walls using this section.
- Further tests should investigate placement of anchor bolts in the 102-mm x 152-mm (4-in x 6-in) WPC wall configurations—to identify optimal locations, if bolted, and changed wall behavior, if continually anchored.

The data proving the feasibility of WPC structural members in shear wall systems can be strengthened by making the necessary improvements in sections and in testing methods. The information provided by this study sufficiently proved the structural capacities of these wood plastic sections to be comparable to conventional structural material in earthquake applications, and even demonstrate improved behavior and more ideal failure modes. In addition, this system avoids chemicals that have potential to leach, and it provides a conscious effort to contribute sustainable construction methods with durable materials.

REFERENCES

- Adcock, Timothy, Wolcott, Michael P., and Hermanson, John C. (2001a). "The Influence of Wood Plastic Composite Formulation: Studies on mechanical and physical properties." Project End Report. Engineered Wood Composites for Navy Waterfronts. Task 1D-1 Evaluate Extruded Materials. Washington State University. Pullman, Washington.
- American Forest and Paper Association (AF&PA). (2001). Special Design Provisions for Wind and Seismic Supplement. 2001 ed., AF&PA, Washington, DC.
- ASTM E564-00e1. (2000). "Standard Practice for Static Load Test for Shear Resistance of Framed Walls for Buildings." American Society of Testing Materials, Vol. 04.11.
- ASTM E2126-02a (2002). Standard Test Methods for Cyclic (Reversed) Load Test for Shear Resistance of Framed Walls for Buildings, Vol. 04.12.
- Bracci, Joseph M., Stromatt, R. F., and Pollock, D. G. (1996). "Seismic Performance of Confined Sill Plate Connections." *Journal of Structural Engineering*, American Society of Civil Engineers. 122(11), 1357-1363.
- Breyer, Donald E., Fridley, Kenneth J., Cobeen, Kelly, E. (1999). *Design of Wood Structures ASD*. 4th Ed. McGraw-Hill, New York, New York.
- Clemons, Craig. (2002). "Wood-Plastic Composites in the United States: The Interfacing of Two Industries." *Forest Products Journal*, Forest Products Society, 52(6), 10-18.
- Cox, Caroline. (1991). "Chromated Copper Arsenate." *Journal of Pesticide Reform*, 11(1), 2-6.
- CRD. (2003). "Conceptualized Reference Database for Building Envelope Research." Building Envelope Performance Laboratory. Centre for Building Studies. Department of Building, Civil and Environmental Engineering. Concordia University. Website: <http://alcor.concordia.ca/~raojw/crd/index.html>
- CWC. (2004). "Types of Preservatives." The Canadian Wood Council. Ottawa, Ontario.
- Day, Robert W. (1996). "Performance of Single Family House Foundations During Northridge Earthquake." *Practice Periodical on Structural Design and Construction*. 1(2). 85-88.
- Delli Quadri, Nicolino G. (2003). Los Angeles County. (personal correspondence).
- Gatto, Kip, and Uang, Chia-Ming. (2002). "Cyclic Response of Woodframe Shearwalls: Loading Protocol and Rate of Loading Effects (CUREE Publication No. W-13)," CUREE, Richmond, CA.
- Haiar, Kevin J. (2000). "Performance and Design of Prototype Wood-Plastic Composite Sections." Washington State University; Master Thesis.

- Hall, John F. (2002). "CUREE – Caltech Wood-frame Project – Overview." CUREE, Richmond, CA.
- Hamburger, Ronald O. (1994). "Lessons Learned in the Northridge Earthquake on Wood Frame Buildings." Spring Seminar, Structural Engineers Association of Northern California (SEAoNC), San Francisco.
- Heine, Christopher. (1997). "Effect of Overturning Restraint on the Performance of Fully Sheathed and Perforated Timber Framed Shear Walls." Virginia Tech; Master Thesis.
- ICBO. (1994). Suggested Revisions to the 1994 Editions of the Uniform Codes (Submittals for 1995). International Conference of Building Officials. Whittier, CA.
- ICBO (1996). 74th Annual Education and Code Development Conference. International Conference of Building Officials. St. Paul, MN.
- ICBO. (2000a). International Residential Building Code. International Conference of Building Officials. Whittier, CA.
- ICBO. (2000b). Uniform Building Code. International Conference of Building Officials, Whittier, CA.
- Jones, Donald A. (1996). "Performance of Bolted Wood-To-Concrete Connections and Bolted Connections in Plywood Shear Walls." Texas A&M University; Master Thesis.
- Kiefer, Stephan. (1998). "Chapter 4 Connections" in *Seismic Retrofit Training for Building Contractors & Inspectors*. Seminar Participant Handbook.
<http://www.abag.ca.gov/bayarea/eqmaps/fixit/manual>
- Kobbe, Ryan. (2005). "Creep Behavior of a Wood-Polypropylene Composite." Washington State University; Master Thesis.
- Krawinkler, Helmut, Parisi, Francisco, Ibarra, Luis, Ayoub, Ashraf, and Medina, Ricardo, (2001). "Development of a Testing Protocol for Wood Frame Structures (CUREE Publication No. W-02)," CUREE, Richmond, CA.
- Kubal, Michael T. (2000). Construction Waterproofing Handbook. McGraw-Hill. New York, NY.
- Langlois, Jeffrey. (2002). "Effects of Reference Displacement and Damage Accumulation in Wood Shear Walls Subjected to the CUREE Protocol." Oregon State University; Master Thesis.
- Laver, T. C. (1996). Extruded synthetic wood composition and method for making same. Patent number 5,516,472.

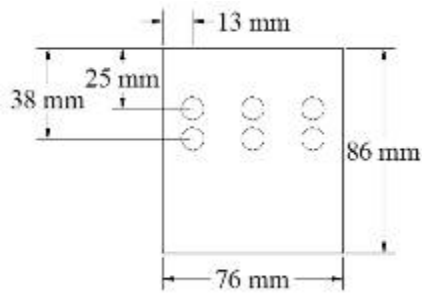
- Mahaney, James. A., and Kehoe, Brian. E. (2002). "Anchorage of Wood-frame Buildings: Laboratory Testing Report (CUREE Publication No. W-14)," CUREE, Richmond, CA.
- Martin, Zeno. (2003) APA—The Engineered Wood Association. (personal correspondence).
- Mapleston, P. (2001). "It's One Hot Market for Profile Extruders." *Modern Plastics*, June. Pp. 49-52.
- Meohle, Jack P. (1994). Preliminary report on the seismological and engineering aspects of the January 17, 1994 Northridge earthquake. Earthquake Engineering Research Center, University of California, Berkeley, CA, Report UCB/EERC-94/01.
- Morrison, Daniel S. (2004) "Pressure-Treated Wood: The Next Generation." *Fine Homebuilding*. No. 160. 82-85.
- National Design Specification (NDS). (2001). American Forest and Paper Association. AF&PA, Washington, D.C.
- Paevere, Phillip, J., Foliente, Greg C., Kasal, Bo. (2003). "Load-Sharing and Redistribution in a One-Story Woodframe Building." *Journal of Structural Engineering*, American Society of Civil Engineers, 129(9), 1275-1284.
- Pendleton, David, Hofford, Theresa.A., Adcock, Tim, Woodward, Bessie. and Wolcott, Michael P. (2002). "Durability of an Extruded HDPE/Wood Composite." *Forest Products Journal*, Forest Products Society, 52(6), 21-27.
- Rose, John D. (1998). Preliminary Testing of Wood Structural Panel Shear Walls Under Cyclic (Reversed) Loading. APA Research Report 158. APA The Engineered Wood Association, Tacoma, WA.
- Rosowsky, David., Elkins, Lori, and Carroll, Cameron. (2004). "Cyclic tests of engineered shearwalls considering different plate washer sizes." For American Forest & Paper Association.
- Salenikovich, Alexander. (2000). "The Racking Performance of Light-Frame Shear Walls." Virginia Tech; PhD Dissertation.
- Schierle, Goetz G. (2002). "Northridge Earthquake Field Investigations: Statistical Analysis of Wood-frame Damage (CUREE Publication No. W-09)," CUREE, Richmond, CA.
- Showalter, John, Glowinski, Robert, Woodson, George, and Price, Eddie W. (2003). "Framing the Future." *Forest Products Journal*, Forest Products Society, 53(3), 4-9.
- Slaughter, Andrew E. (2004). "Design and Fatigue of a Structural Wood-Plastic Composites." Washington State University; Master Thesis.

- Smart, Jason. (2002). "Capacity Resistance and Performance of Single-Shear Bolted and Nailed Connections: An Experimental Investigation." Virginia Tech; Master Thesis.
- Smith, Paul M. (2001). "U.S. Woodfiber-Plastic Composite Decking Market." In: Proc. Sixth International Conference on Woodfiber-Plastic Composites. Forest Products Society, Madison, WI. pp. 13-17.
- Smulski, Stephen. (1996). "Wood-Destroying Fungi in Residential Construction" Wood Science Specialists Inc. Shutesury, MA.
<http://alcor.concordia.ca/~raojw/crd/essay/essay000142.html>

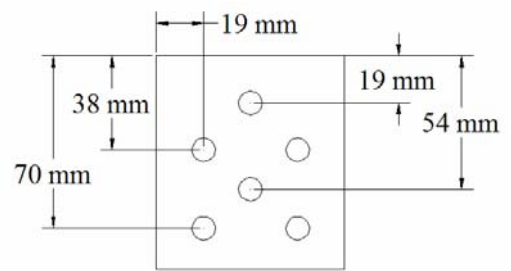
APPENDIX A: CONNECTION AND COMPONENT TEST RESULTS

A.1 Connection Test Fastener Configurations

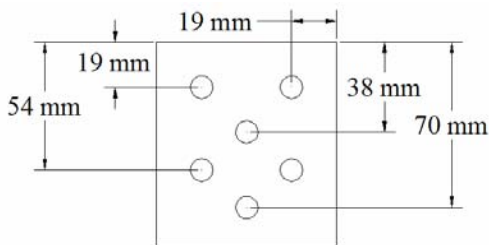
Fastener geometry for connections between the polypropylene (PP10) sill plate and end studs varied for each connection test. Tests 1-11 had end studs located at the end of the sill, as traditional wood-frame construction uses. Tests 12-16 shifted the end stud in from the end of the sill, as depicted by 108 mm end distances to the first fastener.



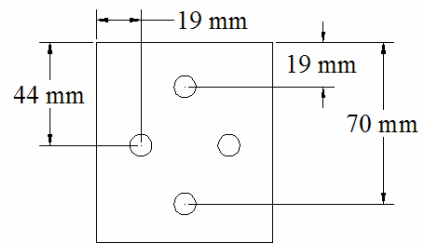
Connection Test 1



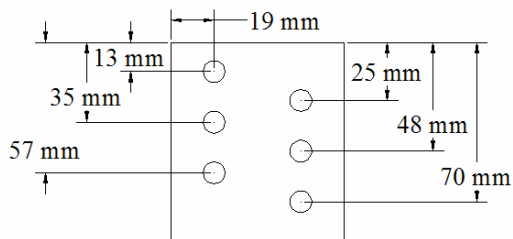
Connection Test 2



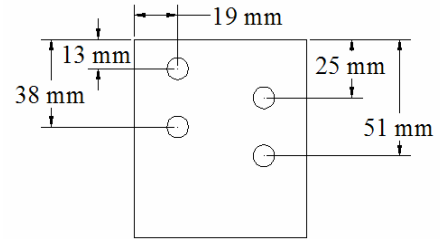
Connection Tests 3, 7^a



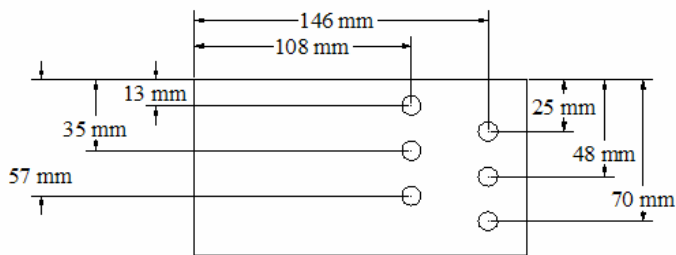
Connection Test 4



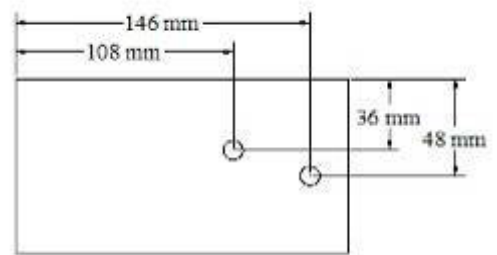
Connection Tests 5, 8^b, 9^a, 10^c, 11^d



Connection 6



Connection 12, 13^e



Connection 14^{e,f}, 15^{e,f,g}

Connection 16^{e,f,g}: Stud shifted and no screw fasteners into stud

Figure A.1 Connection configurations

- ^a Helical threaded nails
- ^b Includes toe-nailed screws
- ^c Reinforced perpendicular-to-extrusion: Drywall screws
- ^d Reinforced perpendicular-to-extrusion: Fiberglass/PP tape
- ^e 13mm (1/2 in) Steel dowels
- ^f 9.5 mm x 76 mm x 152 mm (3/8 in x 3 in x 6 in) Plate washer
- ^g Reinforced with drywall screws at perpendicular-to-extrusion failures

A.2 Connection Test Failure Photos



Connection 1



Connection 2



Connection 3



Connection 4



Connection 5



Connection 6



Connection 7



Connection 8*



Connection 9



Connection 10*



Connection 11*



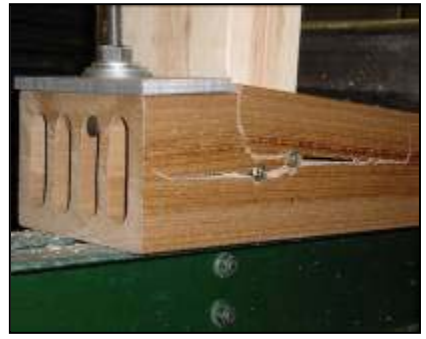
Connection 12

*Screws toe-nailed from top of WPC into stud side not depicted

Figure A.2 Connection Tests 1-12 failure photos



Connection 13



Connection 14



Connection 15



Connection 16

Figure A.3 Connection Tests 13-16 failure photos

A.3 Connection Test Detailed Test Data

Table A.1 Full connection test data

Test Group	Specimen Number	Stiffness (kN/mm)	Load (kN)		Deflection (mm)	
			@ Peak	@ Failure	@ Peak	@Failure
Sidewall Connection Only	1	1.0	5.8	4.7	5.5	6.7
	2	1.6	6.6	5.3	4.8	5.0
	3	1.8	9.5	7.6	5.6	6.0
	4	1.3	8.5	6.8	5.8	5.8
	5	1.5	9.4	7.5	6.1	6.1
	6	1.2	7.5	6.0	6.7	7.2
	7 ^c	1.3	6.8	5.5	6.7	6.7
	9 ^c	1.6	7.9	7.5	4.8	5.1
	8 ^d	1.4	9.3	6.3	4.9	5.2
Shifted ^a Configuration	12	NA	16.3	16.3	5.7	5.7
	13 ^e	6.1	22.7	18.2	3.9	4.2
	14 ^{e,f}	4.2	19.6	15.7	4.8	6.6
Reinforced ^b Sidewall Connection	10 ^d	2.1	16.4	13.1	8.0	8.2
	11 ^d	2.0	14.6	11.8	7.0	8.8
Reinforced ^b Shifted Configuration	15 ^{e,f}	5.3	30.8	24.7	6.4	12.4
	16 ^{e,f,g}	5.0	25.8	20.6	6.4	7.0

^a Stud shifted 5 inches from end of sill

^b Reinforcement for perpendicular-to-extrusion direction

^c Helical threaded nails

^d Includes toe-nailed screws

^e 1/2" Steel dowels

^f 3/8"x3"x6" Plate washer

^g No screw fasteners into stud

A.4 Component Test Detailed Test Data

Table A.2 Full component test data

Specimen ID	Crosshead Measures			String Pot Measures		
	Max Load	Max Deflection	Structural Stiffness	Inner Deflection	Outer Deflection	Rotation at Max Load
	<i>kN</i>	<i>mm</i>	<i>kN/mm</i>	<i>mm</i>	<i>mm</i>	<i>degrees</i>
1	19.8	6.8	2429	1.7	3.0	0.504
2	13.9	4.6	2193	1.2	2.1	0.350
3	22.2	7.2	2235	2.7	3.9	0.457
4	19.5	5.7	3123	2.5	2.1	0.146
5	21.9	6.9	2036	2.4	3.9	0.563
6	17.6	6.6	2391	2.0	1.8	0.078
7	16.3	5.6	2436	1.2	2.1	0.323
8	20.0	6.1	2741	2.6	2.0	0.253
9	16.9	6.2	2881	0.8	2.2	0.544
10	20.9	7.5	2210	2.8	3.0	0.088
11	21.9	8	1970	2.7	3.9	0.476
12	17.7	7.5	1966	2.1	4.9	1.078
13	18.7	5.6	2434	1.7	2.7	0.369
14	20.2	5.5	2255	2.7	3.0	0.146
15	15.7	4.9	2092	1.6	2.5	0.359
16	19.1	4.4	2452	2.1	2.0	0.049
17	16.4	5.4	2016	1.2	2.3	0.418
18	14.7	3.3	2330	1.9	1.8	0.039
19	19.5	5.3	2271	1.8	3.0	0.485
20	15.1	4.3	1864	1.8	2.5	0.282
21	19.3	6.3	1975	1.3	4.1	1.087
22	17.9	4.2	3010	1.5	2.2	0.233
23	20.5	6.3	2348	3.0	3.7	0.262
24	18.2	14.3	2135	5.6	8.3	1.030
25	19.8	4.4	2990	2.0	2.3	0.116
26	15.9	4.9	2581	2.1	1.3	0.282
27	17.7	4.1	2764	1.6	2.3	0.243
28	17.3	4.5	1672	2.1	2.0	0.019
Average	18.4	5.6	2350	2.0	2.7	0.305
Standard Deviation	2.2	1.3	368	0.6	0.9	0.359
COV	12.18%	21.63%	15.66%	29.10%	32.43%	117.55%

APPENDIX B: SHEAR WALL TEST RESULTS

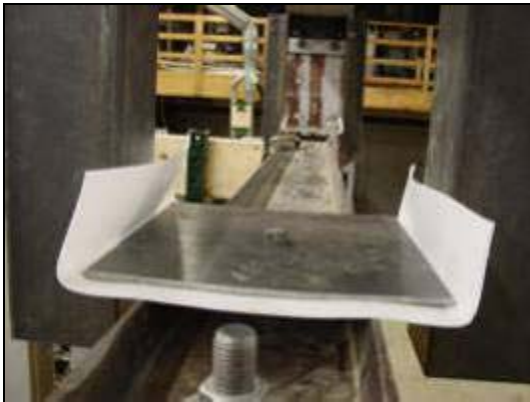
B.1 Test Setup



Actuator connection to top load beam



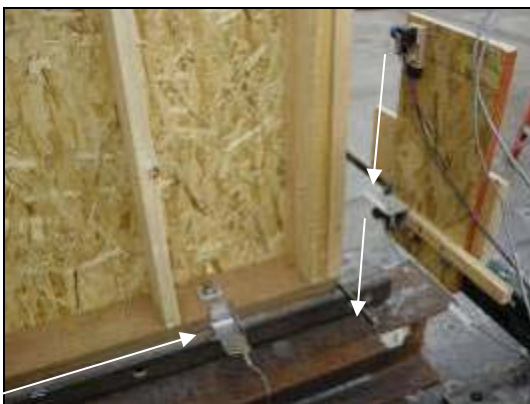
Lateral Bracing—North End



Lateral Bracing—Top view



Top Displacement Measures



Stud, Sill, and Bottom Slip Displacement Measures—South End



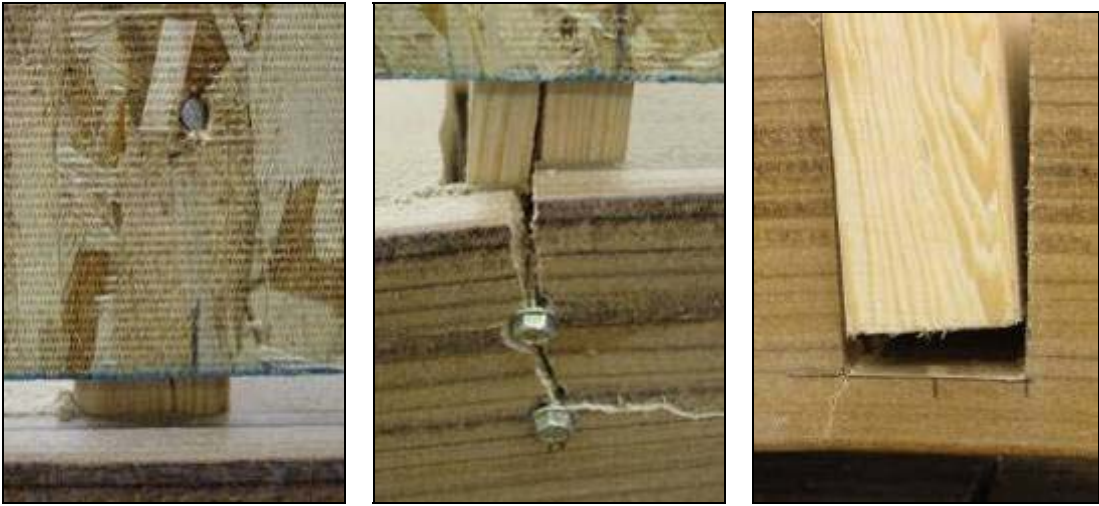
Stud and Sill Displacement Measures—North End

Figure B.1 Shear wall test setup photos

B.2 Supplement Test Photos: Test PP10-M Failures



Figure B.2 Test PP10-M sill failure and overall behavior



(a)

(b)

(c)

Figure B.3 Interior stud-to-sill connection behavior: (a) Nail bending with sheathing racking, (b) Stud splitting from screw connectors, and (c) Interior stud movement in slot and crack in bottom flange



(a)



(b)



(c)

Figure B.4 Illustration of sheathing racking: (a) Bearing on sill top, (b) Displacing 13-19 mm (0.5-0.75 inches) past end of sill, and (c) Racking at panel joint



Figure B.5 End stud failed connection (top view): dowels yielded, top flange crushed, sill cracked through

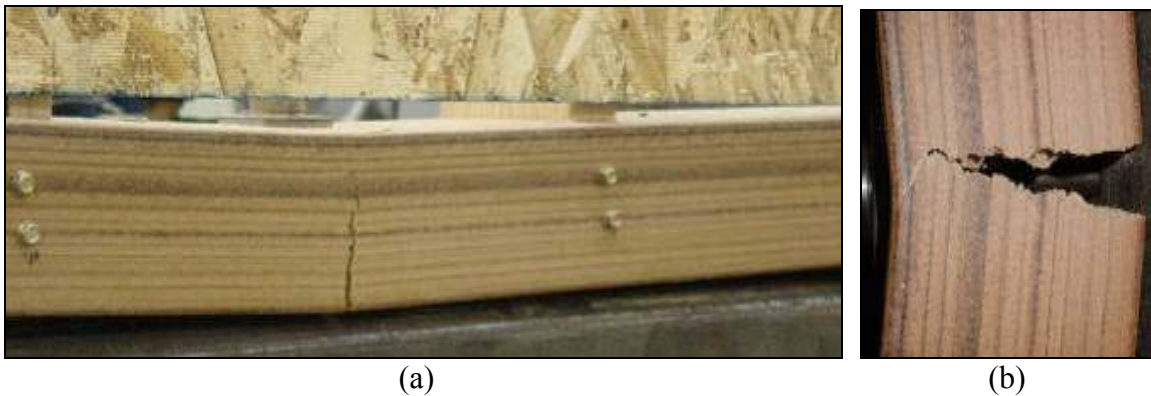


Figure B.6 Flexural failure at second anchor bolt: (a) Location along sill, (b) Failure exposes anchor bolt within

B.3 Cyclic Test Data

Presented for each cyclic test are summarized test parameters, hysteresis curves, time histories, and energy and damping calculations. Test parameters are summarized in Tables B.1, B.3, B.5, B.7, B.9, B.11, B.13, and B.15, based on averages from positive and negative response and EEEP parameters. Hysteresis curves include full data collected and overlaying response curves represent behavior up until failure (80% peak loads). Time histories are presented for each test, representing displacements induced by the hydraulic cylinder. Finally, damping ratios are calculated for each cycle (Tables B.2, B.4, B.6, B.8, B.10, B.12, B.14, B.16), based on the strain energy and work done per cycle. The sum of the work done approximates energy dissipation in cyclic loops up until the point of failure. Hysteresis and strain energy have negative values for some early cycles due to measurement accuracy at these small displacements. Contributions to area totals are negligible.

Test WOOD4-1

Table B.1 Test WOOD4-1 Summary

Specimen WOOD4-1
Sill Plate Type Pressure-treated wood
Date April 23, 2005

Area Under Envelope Curve	<i>kN-mm</i>	405
	<i>lbf-in</i>	3584
Area Enclosed by Hysteresis	<i>kN-mm</i>	2395
	<i>lbf-in</i>	21,195
Maximum absolute load, P_{peak}	<i>kN</i>	10.6
	<i>lbf</i>	2372
Maximum absolute displacement, Δ_{peak}	<i>mm</i>	30
	<i>in</i>	1.18
Failure Load, $0.80 \cdot P_{peak}$	<i>kN</i>	8.4
	<i>lbf</i>	1898
Ultimate Displacement, cyclic, Δ_u	<i>mm</i>	45
	<i>in</i>	1.76
$0.40 \cdot P_{peak}$	<i>kN</i>	4.2
	<i>lbf</i>	949
Displacement, $\Delta_{0.4peak}$	<i>mm</i>	2
	<i>in</i>	0.09
P_{yield}	<i>kN</i>	9.6
	<i>lbf</i>	2158
Yield Displacement, cyclic, Δ_{yield}	<i>mm</i>	5
	<i>in</i>	0.20
Shear Strength, v_{peak}	<i>kN/m</i>	4.3
	<i>lbf/ft</i>	296
Secant Shear Modulus, $G' @ 0.4P_{peak}$	<i>kN/mm</i>	1.9
	<i>lbf/in</i>	10737
Secant Shear Modulus, $G' @ P_{peak}$	<i>kN/mm</i>	0.4
	<i>lbf/in</i>	2010
Elastic Shear Stiffness, K_e	<i>kN/mm</i>	1.9
	<i>lbf/in</i>	10737

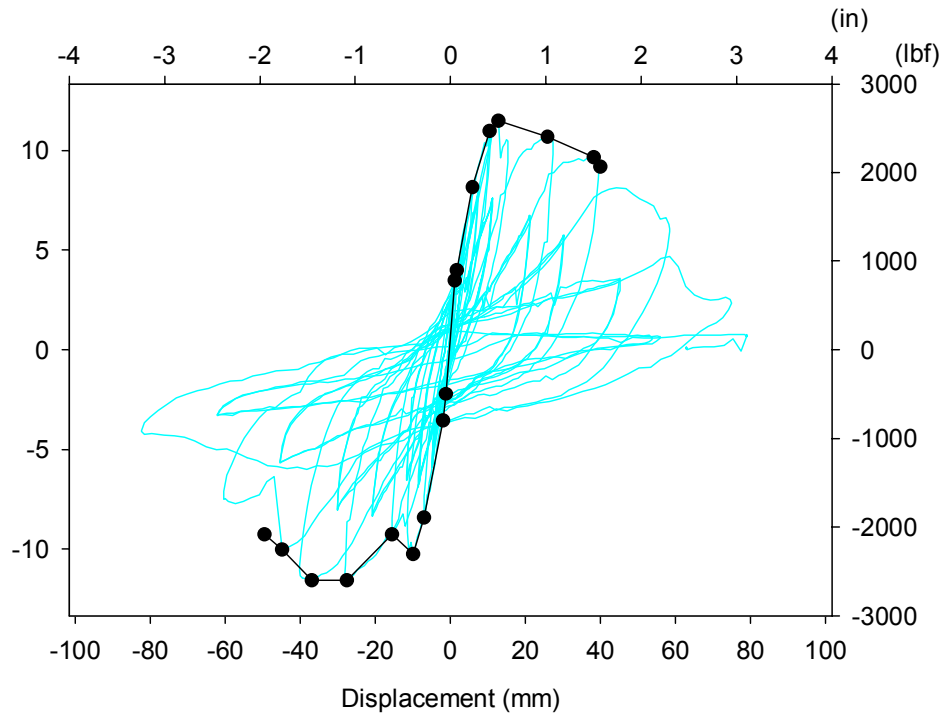


Figure B.7 Test WOOD4-1 Hysteresis: Reference Displacement = 41 mm (1.61 in)

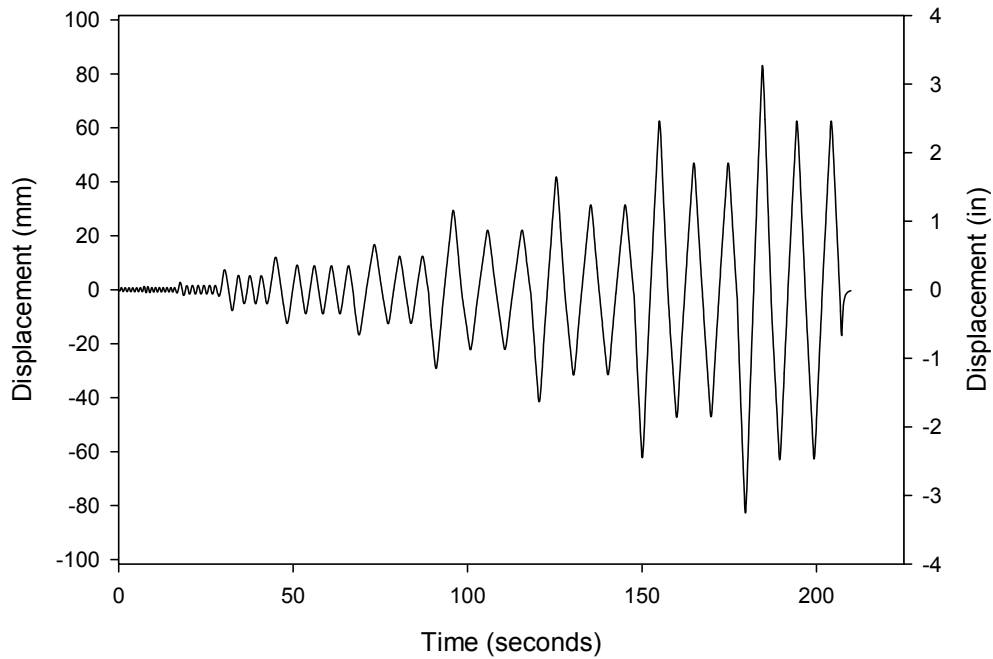


Figure B.8 Time history for Test WOOD4-1

Table B.2 Test WOOD4-1 Energy and damping data

Cycle Number	Cycle Maximums				Hysteretic Energy	Strain Energy	EVDR, ζ_{eq} (radians)	
	Load (kN)		Deflection (mm)		W_D (kN-mm)	U (kN-mm)		
	Positive	Negative	Positive	Negative				
Initiation	1	1.89	-0.80	0.56	-0.13	-0.04	0.05	-0.06
	2	1.76	-1.12	0.51	-0.23	-0.03	0.53	0.00
	3	1.70	-1.18	0.48	-0.25	0.00	0.45	0.00
	4	1.71	-1.20	0.48	-0.25	-0.03	0.41	-0.01
	5	1.71	-1.22	0.48	-0.28	-0.06	0.41	-0.01
	6	1.71	-1.21	0.48	-0.28	-0.12	0.41	-0.02
Primary	7	1.69	-1.20	0.48	-0.28	-0.10	0.41	-0.02
	8	2.56	-1.83	0.89	-0.58	-0.34	1.14	-0.02
	9	2.35	-1.71	0.79	-0.53	-0.25	0.92	-0.02
	10	1.68	-1.37	0.48	-0.38	-0.01	0.41	0.00
	11	1.70	-1.35	0.53	-0.36	-0.10	0.45	-0.02
	12	1.78	-1.35	0.53	-0.38	-0.09	0.48	-0.01
	13	1.81	-1.35	0.53	-0.38	-0.11	0.48	-0.02
	14	1.80	-1.37	0.56	-0.38	0.01	0.50	0.00
	15	1.79	-1.37	0.53	-0.38	-0.12	0.48	-0.02
	16	1.79	-1.96	0.53	-0.64	0.03	0.48	0.00
Primary	17	4.13	-3.45	1.93	-1.75	2.05	3.99	0.04
	18	2.49	-2.78	0.91	-1.30	0.16	1.14	0.01
	19	2.65	-2.78	0.99	-1.27	0.22	1.31	0.01
	20	2.62	-2.80	0.99	-1.27	0.24	1.30	0.01
	21	2.62	-2.79	0.99	-1.24	0.15	1.30	0.01
	22	2.64	-2.79	0.99	-1.24	0.23	1.31	0.01
Primary	23	2.67	-3.86	0.99	-2.01	0.43	1.32	0.03
	24	7.65	-9.47	6.22	-6.71	27.89	23.81	0.09
	25	5.80	-5.81	4.29	-4.39	10.31	12.45	0.07
	26	5.70	-5.86	4.19	-4.45	9.64	11.95	0.06
Primary	27	5.65	-5.88	4.19	-4.45	9.51	11.84	0.06
	28	10.77	-9.43	10.67	-12.14	93.83	57.42	0.13
	29	7.38	-6.93	7.72	-8.64	38.15	28.50	0.11
	30	7.13	-7.02	7.57	-8.74	34.78	26.97	0.10
Primary	31	7.17	-7.02	7.52	-8.76	34.11	26.94	0.10
	32	7.14		7.57	0.00	15.31	27.01	0.05
	33	10.01	-7.28	16.76	-16.71	169.09	83.89	0.16
	34	7.51	-5.30	12.80	-12.22	66.66	48.05	0.11
Primary	35	7.45	-5.34	12.70	-12.22	64.06	47.30	0.11
	36	12.05	-9.11	30.10	-29.51	380.04	181.35	0.17
Primary	37	8.65	-6.00	23.95	-22.91	193.20	103.62	0.15
	38	8.56	-5.98	23.93	-22.94	183.21	102.40	0.14
	39	12.33	-8.19	37.90	-41.20	548.76	233.64	0.19
	38	7.53	-5.26	33.30	-32.41	266.41	125.38	0.17
	39	7.44	-5.34	32.72	-32.44	247.66	121.76	0.16

Total Estimated Energy

2394.75 kN-mm

Table B.3 Test WOOD4-2 Summary

Specimen WOOD4-2
Sill Plate Type Pressure-treated wood
Date April 25, 2005

	Units	
Area Under Envelope Curve	<i>kN-mm</i>	427
	<i>lbf-in</i>	3781
Area Enclosed by Hysteresis	<i>kN-mm</i>	2446
	<i>lbf-in</i>	21,648
Maximum absolute load, P_{peak}	<i>kN</i>	11.0
	<i>lbf</i>	2482
Maximum absolute displacement, Δ_{peak}	<i>mm</i>	28
	<i>in</i>	1.10
Failure Load, $0.80 \cdot P_{peak}$	<i>kN</i>	8.8
	<i>lbf</i>	1986
Ultimate Displacement, cyclic, Δ_u	<i>mm</i>	44
	<i>in</i>	1.75
$0.40 \cdot P_{peak}$	<i>kN</i>	4.4
	<i>lbf</i>	993
Displacement, $\Delta_{0.4peak}$	<i>mm</i>	3
	<i>in</i>	0.10
P_{yield}	<i>kN</i>	10.3
	<i>lbf</i>	2316
Yield Displacement, cyclic, Δ_{yield}	<i>mm</i>	6
	<i>in</i>	0.23
Shear Strength, v_{peak}	<i>kN/m</i>	4.5
	<i>lbf/ft</i>	310
Secant Shear Modulus, $G' @ 0.4P_{peak}$	<i>kN/mm</i>	1.8
	<i>lbf/in</i>	10,086
Secant Shear Modulus, $G' @ P_{peak}$	<i>kN/mm</i>	0.4
	<i>lbf/in</i>	2257
Elastic Shear Stiffness, K_e	<i>kN/mm</i>	1.8
	<i>lbf/in</i>	10,086

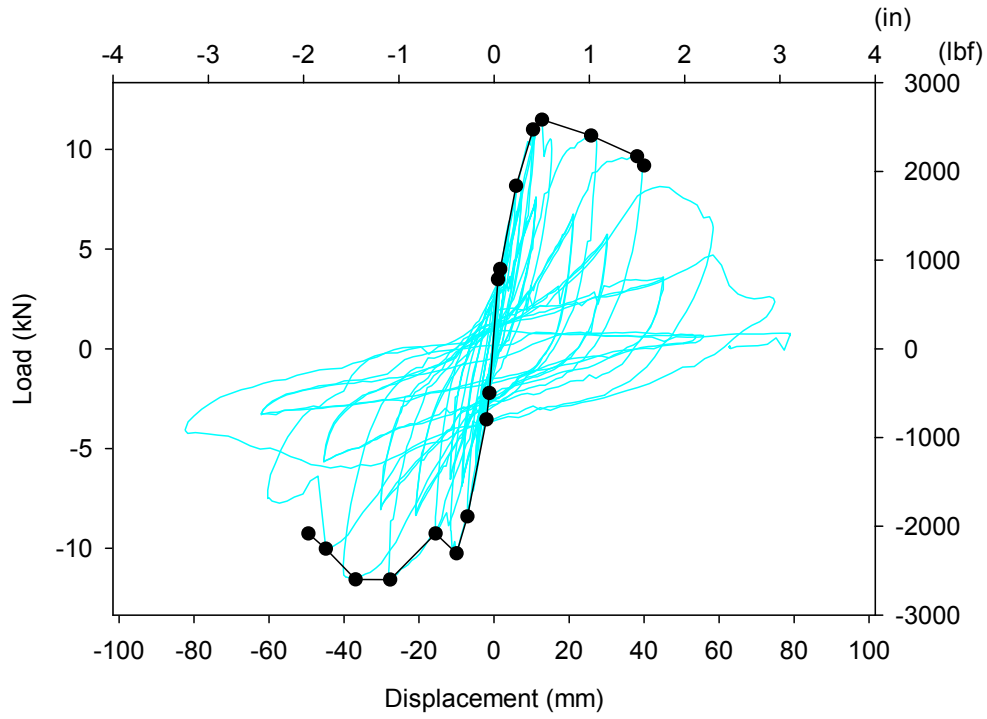


Figure B.9 Test WOOD4-2 Hysteresis: Reference Displacement = 41 mm (1.61 in)

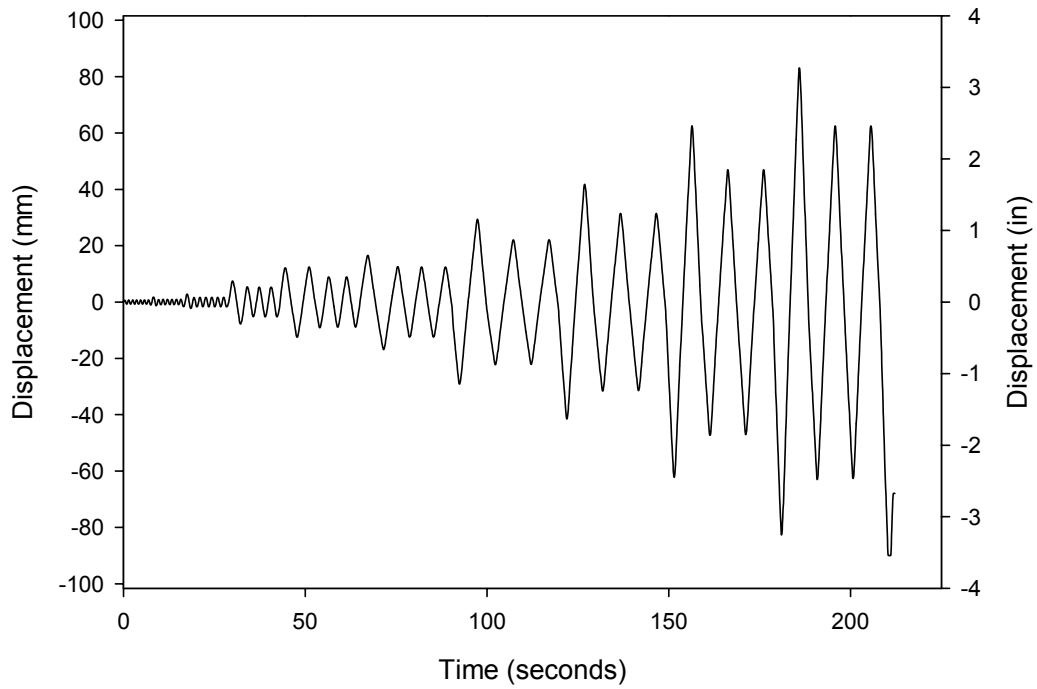


Figure B.10 Time history for Test WOOD4-2

Table B.4 Test WOOD4-2 Energy and damping data

Cycle Number	Cycle Maximums				Hysteretic Energy W_D (kN-mm)	Strain Energy U (kN-mm)	EVDR, ζ_{eq} (radians)	
	Load (kN)		Deflection (mm)					
	Positive	Negative	Positive	Negative				
Initiation	1	1.39	-1.39	0.18	-0.74	-0.07	0.12	-0.05
	2	1.74	-1.18	0.23	-0.74	0.02	0.20	0.01
	3	1.80	-1.35	0.25	-0.74	0.17	0.23	0.06
	4	1.81	-1.29	0.23	-0.74	0.03	0.21	0.01
	5	1.84	-1.30	0.23	-0.76	0.08	0.21	0.03
	6	1.83	-1.31	0.23	-0.74	0.07	0.23	0.02
	7	1.84	-1.80	0.25	-1.04	0.44	0.21	0.16
	8	3.49	-2.22	0.23	-1.24	0.79	1.82	0.03
Primary	9	2.03	-1.54	1.04	-0.99	0.38	0.28	0.11
	10	2.22	-1.57	0.28	-0.99	0.12	0.39	0.02
	11	2.23	-1.54	0.36	-0.97	-0.31	0.40	-0.06
	12	2.22	-1.57	0.36	-0.99	0.03	0.39	0.01
	13	2.22	-1.54	0.36	-0.97	0.29	0.39	0.06
	14	2.24	-2.58	0.36	-1.50	0.09	0.40	0.02
	15	4.00	-3.54	0.36	-2.03	3.10	3.30	0.07
Primary	16	3.08	-2.78	1.65	-1.60	0.67	1.33	0.04
	17	3.21	-2.72	0.86	-1.60	0.48	1.47	0.03
	18	3.22	-2.75	0.91	-1.63	0.62	1.47	0.03
	19	3.22	-2.74	0.91	-1.63	0.70	1.47	0.04
	20	3.23	-2.74	0.91	-1.63	0.47	1.52	0.02
	21	3.21	-2.79	0.94	-1.60	0.51	1.47	0.03
	22	8.17	-8.41	0.91	-7.09	34.85	23.97	0.12
Primary	23	6.24	-5.77	5.87	-4.80	14.75	12.51	0.09
	24	6.17	-5.86	4.01	-4.85	13.24	11.75	0.09
	25	6.14	-5.90	3.81	-4.88	13.01	11.77	0.09
	26	10.99	-10.25	3.84	-10.01	96.66	56.95	0.14
Primary	27	10.90	-6.87	10.36	-8.53	56.17	58.44	0.08
	28	7.94	-6.72	10.72	-8.33	38.81	29.36	0.11
	29	7.98	-6.69	7.39	-8.33	39.12	29.58	0.11
	30	11.48	-9.26	7.42	-15.57	161.09	73.37	0.17
Primary	31	7.61	-6.54	12.78	-11.63	66.22	42.80	0.12
	32	7.59	-6.54	11.25	-11.68	63.52	42.29	0.12
	33	7.59		11.15		26.14	42.23	0.05
Primary		10.69	-11.57	11.13	-27.71	331.25	138.19	0.19
	34	6.74	-8.35	25.86	-20.88	153.48	71.16	0.17
	35	6.75	-8.35	21.11	-20.85	144.88	71.19	0.16
Primary	36	9.65	-11.57	21.08	-36.93	462.02	184.15	0.20
	37	5.74	-8.01	38.15	-30.23	215.16	86.69	0.20
	38	5.74	-8.07	30.23	-30.23	198.25	86.20	0.18
	39		-10.02		-44.86	308.59	224.79	0.11
	40		-5.64		-45.26			
	41		-5.67		-45.42			

Total Estimated Energy

2445.92 kN-mm

Table B.5 Test PE3-1 Summary

Specimen PE3-1
Sill Plate Type PE solid section
Date April 26, 2005

	Units	
Area Under Envelope Curve	<i>kN-mm</i>	338
	<i>lbf-in</i>	2989
Area Enclosed by Hysteresis	<i>kN-mm</i>	1592
	<i>lbf-in</i>	14,095
Maximum absolute load, P_{peak}	<i>kN</i>	11.4
	<i>lbf</i>	2565
Maximum absolute displacement, Δ_{peak}	<i>mm</i>	23
	<i>in</i>	0.90
Failure Load, $0.80 \cdot P_{peak}$	<i>kN</i>	9.1
	<i>lbf</i>	2052
Ultimate Displacement, cyclic, Δ_u	<i>mm</i>	35
	<i>in</i>	1.39
$0.40 \cdot P_{peak}$	<i>kN</i>	4.6
	<i>lbf</i>	1026
Displacement, $\Delta_{0.4peak}$	<i>mm</i>	2.7
	<i>in</i>	0.11
P_{yield}	<i>kN</i>	10.54
	<i>lbf</i>	2369
Yield Displacement, cyclic, Δ_{yield}	<i>mm</i>	6.4
	<i>in</i>	0.25
Shear Strength, V_{peak}	<i>kN/m</i>	4.7
	<i>lbf/ft</i>	321
Secant Shear Modulus, $G' @ 0.4P_{peak}$	<i>kN/mm</i>	1.7
	<i>lbf/in</i>	9439
Secant Shear Modulus, $G' @ P_{peak}$	<i>kN/mm</i>	0.5
	<i>lbf/in</i>	2850
Elastic Shear Stiffness, K_e	<i>kN/mm</i>	1.7
	<i>lbf/in</i>	9439

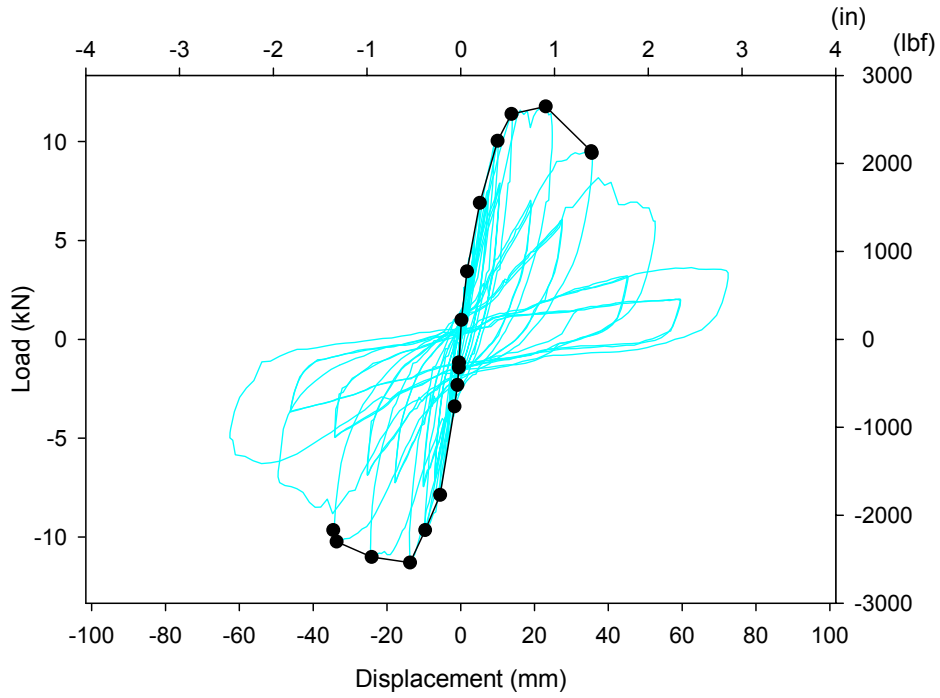


Figure B.11 Test PE3-1 Hysteresis: Reference Displacement = 36 mm (1.40 in)

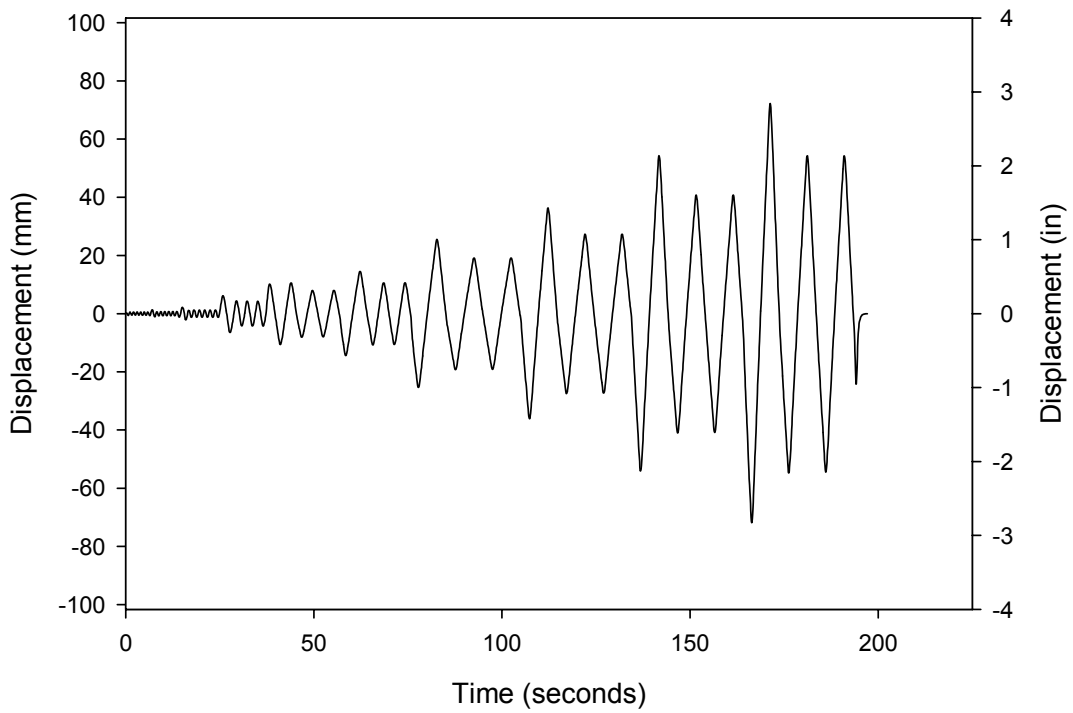


Figure B.12 Time history for Test PE3-1

Table B.6 Test PE3-1 Energy and damping data

Cycle Number	Cycle Maximums				Hysteretic Energy W_D (kN-mm)	Strain Energy U (kN-mm)	EVDR, ζ_{eq} (radians)	
	Load (kN)		Deflection (mm)					
	Positive	Negative	Positive	Negative				
Initiation	1	0.54	-1.17	0.05	-0.46	0.00	0.01	0.00
	2	0.98	-1.16	0.18	-0.43	0.06	0.09	0.06
	3	1.02	-1.19	0.18	-0.43	-0.05	0.09	-0.04
	4	1.02	-1.24	0.18	-0.43	-0.07	0.09	-0.06
	5	1.03	-1.23	0.18	-0.43	-0.04	0.09	-0.03
	6	1.04	-1.18	0.18	-0.43	0.05	0.09	0.04
	7	1.02	-1.43	0.18	-0.53	0.01	0.10	0.00
Primary	8	2.31	-2.31	0.20	-0.89	-0.15	1.56	-0.01
	9	1.07	-1.54	1.35	-0.58	0.02	0.14	0.01
	10	1.29	-1.55	0.25	-0.56	-0.05	0.21	-0.02
	11	1.32	-1.36	0.33	-0.56	-0.07	0.24	-0.02
	12	1.29	-1.47	0.36	-0.56	-0.07	0.23	-0.02
	13	1.29	-1.51	0.36	-0.56	0.11	0.23	0.04
	14	1.33	-2.48	0.36	-0.99	0.00	0.24	0.00
Primary	15	3.43	-3.40	0.36	-1.68	1.80	2.92	0.05
	16	2.45	-1.85	1.70	-0.91	-0.26	1.12	-0.02
	17	2.64	-1.85	0.91	-0.89	-0.10	1.34	-0.01
	18	2.61	-1.89	1.02	-0.89	0.18	1.33	0.01
	19	2.61	-1.92	1.02	-0.89	-0.20	1.32	-0.01
	20	2.62	-1.90	1.02	-0.89	0.23	1.33	0.01
	21	2.60	-1.92	1.02	-0.89	-0.16	1.32	-0.01
Primary	22	6.90	-7.87	1.02	-5.61	22.09	17.79	0.10
	23	5.04	-5.03	5.16	-3.53	8.82	9.21	0.08
	24	4.86	-5.15	3.66	-3.63	6.80	8.71	0.06
	25	4.95	-5.16	3.58	-3.68	7.41	8.80	0.07
Primary	26	9.77		3.56		82.54	43.80	0.15
	27	10.04	-9.65	9.96	-9.63	14.66	49.97	0.02
	28	7.53	-7.12	7.44	-6.93	33.96	28.02	0.10
Primary	29	7.33	-7.12	7.29	-6.93	29.84	26.72	0.09
	30	11.40	-11.29	13.74	-13.77	130.19	78.29	0.13
	31	7.90	-7.45	10.59	-10.08	68.24	41.86	0.13
Primary	32	7.75	-7.45	10.46	-10.13	63.84	40.55	0.13
	33	11.78	-11.01	23.01	-24.16	297.79	135.49	0.17
	34	7.03	-7.25	18.85	-17.81	104.20	66.22	0.13
Primary	35	6.87	-7.25	18.95	-17.75	100.01	65.07	0.12
	36	9.51	-10.24	35.36	-33.63	335.73	168.17	0.16
	37	6.05	-6.84	27.41	-25.30	145.02	82.96	0.14
	37	6.06	-6.89	27.46	-25.30	140.10	83.23	0.13

Total Estimated Energy

1592.48 kN-mm

Table B.7 Test PE3-2 Summary

Specimen PE3-2
Sill Plate Type PE solid section
Date April 27, 2005

	Units	
Area Under Envelope Curve	<i>kN-mm</i>	354
	<i>lbf-in</i>	3129
Area Enclosed by Hysteresis	<i>kN-mm</i>	1611
	<i>lbf-in</i>	14,258
Maximum absolute load, P_{peak}	<i>kN</i>	12.3
	<i>lbf</i>	2770
Maximum absolute displacement, Δ_{peak}	<i>mm</i>	17
	<i>in</i>	0.66
Failure Load, $0.80 \cdot P_{peak}$	<i>kN</i>	9.9
	<i>lbf</i>	2216
Ultimate Displacement, cyclic, Δ_u	<i>mm</i>	36
	<i>in</i>	1.40
$0.40 \cdot P_{peak}$	<i>kN</i>	5.0
	<i>lbf</i>	1108
Displacement, $\Delta_{0.4peak}$	<i>mm</i>	4
	<i>in</i>	0.15
P_{yield}	<i>kN</i>	11.3
	<i>lbf</i>	2543
Yield Displacement, cyclic, Δ_{yield}	<i>mm</i>	9
	<i>in</i>	0.34
Shear Strength, v_{peak}	<i>kN/m</i>	5.1
	<i>lbf/ft</i>	346
Secant Shear Modulus, $G' @ 0.4P_{peak}$	<i>kN/mm</i>	1.3
	<i>lbf/in</i>	7575
Secant Shear Modulus, $G' @ P_{peak}$	<i>kN/mm</i>	0.7
	<i>lbf/in</i>	4196
Elastic Shear Stiffness, K_e	<i>kN/mm</i>	1.3
	<i>lbf/in</i>	7575

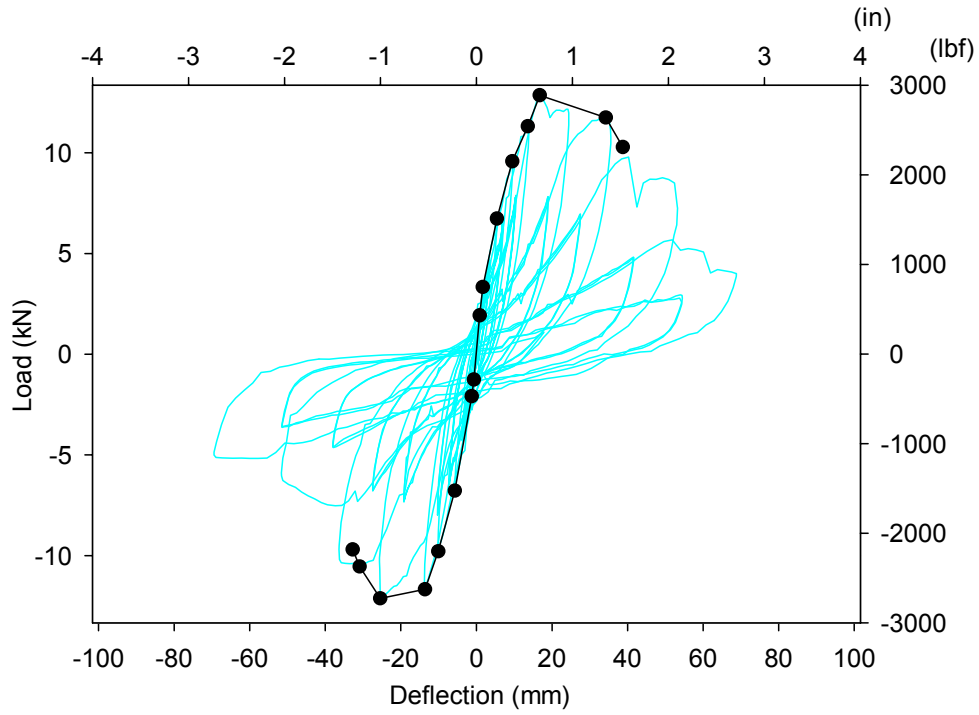


Figure B.13 Test PE3-2 Hysteresis: Reference Displacement = 36 mm (1.40 in)

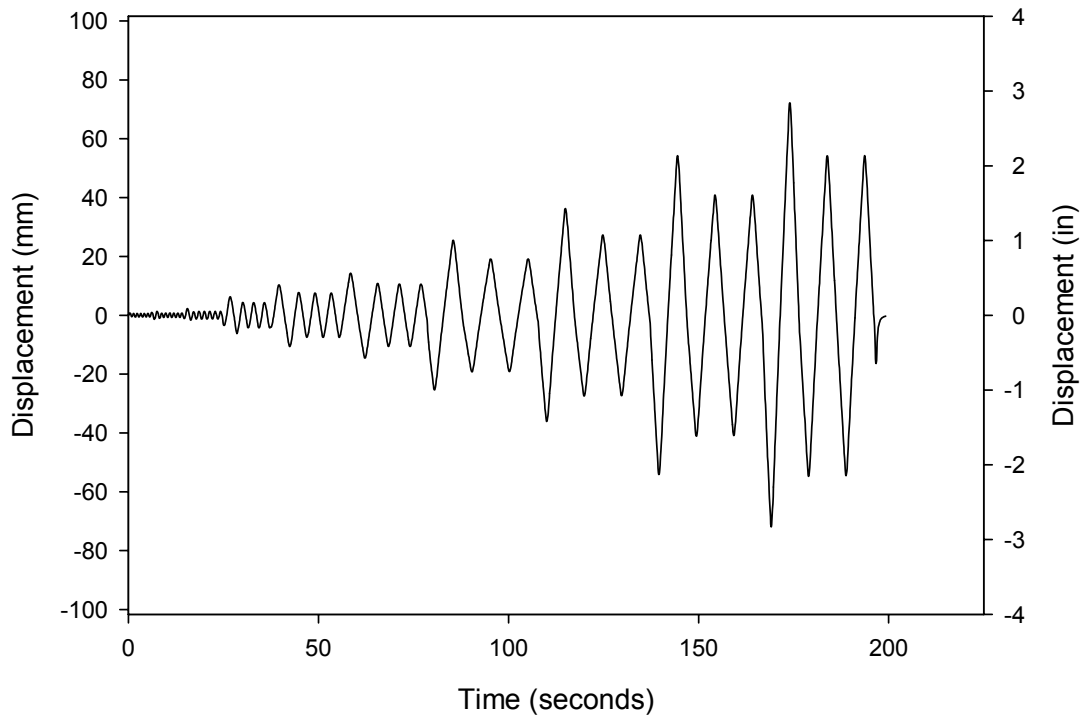


Figure B.14 Time history for Test PE3-2

Table B.8 Test PE3-2 Energy and damping data

Cycle Number	Cycle Maximums				Hysteretic Energy W_D (kN-mm)	Strain Energy U (kN-mm)	EVDR, ζ_{eq} (radians)	
	Load (kN)		Deflection (mm)					
	Positive	Negative	Positive	Negative				
Initiation	1	1.05	-0.73	0.38	-0.30	0.09	0.20	0.04
	2	0.83	-0.83	0.23	-0.36	0.08	0.10	0.07
	3	0.83	-0.81	0.20	-0.38	0.03	0.08	0.03
	4	0.83	-0.82	0.23	-0.38	0.06	0.09	0.05
	5	0.87	-0.82	0.23	-0.38	0.01	0.10	0.01
	6	0.84	-0.81	0.23	-0.38	0.12	0.10	0.10
	7	1.31	-1.64	0.56	-0.97	0.40	0.37	0.09
Primary	8	1.92	-1.27	0.86	-0.69	0.37	0.83	0.04
	9	0.96	-0.93	0.36	-0.46	0.09	0.17	0.04
	10	1.05	-0.91	0.41	-0.43	0.11	0.21	0.04
	11	1.03	-0.91	0.41	-0.43	0.10	0.21	0.04
	12	1.04	-0.92	0.43	-0.46	0.00	0.22	0.00
	13	1.04	-0.89	0.41	-0.46	0.10	0.21	0.04
	14	1.05	-1.36	0.41	-0.74	0.29	0.21	0.11
Primary	15	3.33	-2.09	1.70	-1.24	0.94	2.83	0.03
	16	1.46	-1.65	0.81	-0.94	0.56	0.60	0.07
	17	1.62	-1.63	0.89	-0.94	0.31	0.72	0.03
	18	1.66	-1.63	0.91	-0.91	0.31	0.76	0.03
	19	1.65	-1.61	0.89	-0.91	0.56	0.73	0.06
	20	1.65	-1.60	0.91	-0.91	0.27	0.76	0.03
	21	1.63	-3.72	0.91	-2.79	1.08	0.75	0.12
Primary	22	6.72	-6.78	5.41	-5.72	24.39	18.18	0.11
	23	4.66	-4.29	3.48	-3.63	8.25	8.11	0.08
	24	4.65	-4.28	3.45	-3.68	6.86	8.02	0.07
	25	4.59	-4.32	3.48	-3.68	7.22	7.99	0.07
Primary	26	9.56		9.50		69.46	45.43	0.12
	27	6.77	-6.30	7.16	-7.09	34.93	24.25	0.11
	28	6.64	-6.48	6.96	-7.16	32.87	23.10	0.11
	29	6.63	-6.47	6.99	-7.14	32.64	23.16	0.11
Primary	30	11.30	-11.68	13.61	-13.61	113.44	76.95	0.12
	31	7.88	-7.90	10.49	-10.24	57.77	41.33	0.11
	32	7.76	-8.00	10.31	-10.26	54.06	40.00	0.11
Primary		7.76	0.00	10.31	0.00	25.49	39.99	0.05
	33	12.84	-12.12	16.76	-25.48	297.86	107.66	0.22
	34	7.81	-7.24	18.97	-19.18	104.39	74.10	0.11
	35	7.79	-7.34	18.87	-19.18	99.21	73.49	0.11
Primary	36	11.74	-10.55	34.24	-30.91	357.00	201.02	0.14
	37	6.96	-6.78	27.51	-27.41	141.65	95.67	0.12
	38	6.91	-6.79	27.33	-27.43	137.53	94.48	0.12

Total Estimated Energy

1610.90 kN-mm

Table B.9 Test PP5-1 Summary

Specimen PP5-1
Sill Plate Type PP Three-box hollow section
Date April 28, 2005

	Units	
Area Under Envelope Curve	<i>kN-mm</i>	221
	<i>lbf-in</i>	1958
Area Enclosed by Hysteresis	<i>kN-mm</i>	982
	<i>lbf-in</i>	8695
Maximum absolute load, P_{peak}	<i>kN</i>	15.8
	<i>lbf</i>	3552
Maximum absolute displacement, Δ_{peak}	<i>mm</i>	16
	<i>in</i>	0.64
Failure Load, $0.80 \cdot P_{peak}$	<i>kN</i>	12.6
	<i>lbf</i>	2842
Ultimate Displacement, cyclic, Δ_u	<i>mm</i>	20
	<i>in</i>	0.81
$0.40 \cdot P_{peak}$	<i>kN</i>	6.3
	<i>lbf</i>	1421
Displacement, $\Delta_{0.4peak}$	<i>mm</i>	4
	<i>in</i>	0.15
P_{yield}	<i>kN</i>	13.6
	<i>lbf</i>	3053
Yield Displacement, cyclic, Δ_{yield}	<i>mm</i>	8
	<i>in</i>	0.33
Shear Strength, v_{peak}	<i>kN/m</i>	6.5
	<i>lbf/ft</i>	444
Secant Shear Modulus, $G' @ 0.4P_{peak}$	<i>kN/mm</i>	1.6
	<i>lbf/in</i>	9254
Secant Shear Modulus, $G' @ P_{peak}$	<i>kN/mm</i>	1.0
	<i>lbf/in</i>	5551
Elastic Shear Stiffness, K_e	<i>kN/mm</i>	1.6
	<i>lbf/in</i>	9254

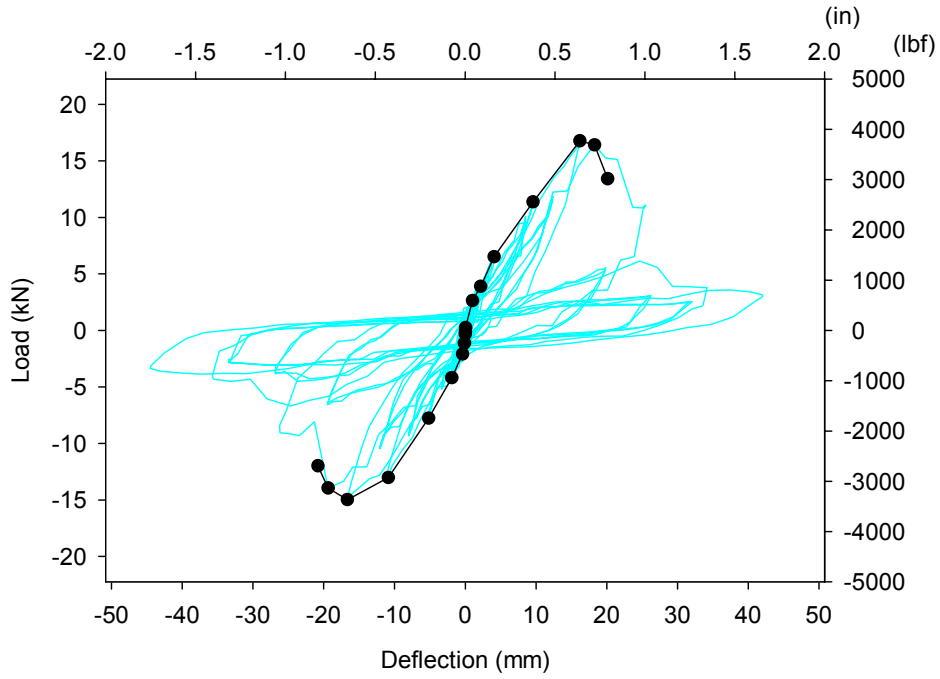


Figure B.15 Test PP5-1 Hysteresis (Reference Displacement = 18 mm (0.70 in))

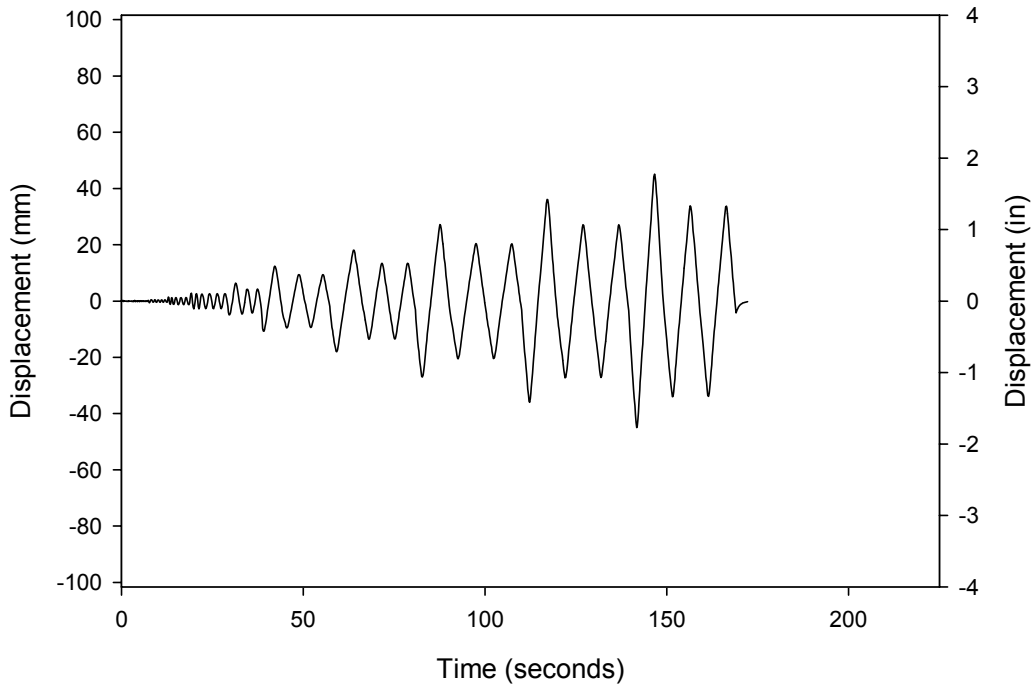


Figure B.16 Time history for Test PP5-1

Table B.10 Test PP5-1 Energy and damping data

Cycle Number	Cycle Maximums				Hysteretic Energy W_D (kN-mm)	Strain Energy U (kN-mm)	EVDR, ζ_{eq} (radians)	
	Load (kN)		Deflection (mm)					
	Positive	Negative	Positive	Negative				
Initiation	1	0.10	-0.09	0.05	0.03	0.00	0.00	0.00
	2	0.19	-0.10	0.03	0.05	0.00	0.00	0.03
	3	0.22	-0.15	0.05	0.03	0.00	0.01	-0.01
	4	0.09	-0.19	0.03	0.03	0.00	0.00	0.00
	5	0.17	-0.08	0.03	0.05	0.00	0.00	0.03
	6	0.23	-0.14	0.05	0.05	0.00	0.01	0.00
Primary	7	0.31	-0.32	0.03	0.03	0.01	0.00	0.29
	8	0.21	-0.25	0.05	0.05	0.00	0.01	0.03
	9	0.34	-0.21	0.05	0.05	0.00	0.01	0.00
	10	0.33	-0.22	0.05	0.05	0.00	0.01	0.00
	11	0.34	-0.20	0.05	0.08	0.00	0.01	0.00
	12	0.31	-0.11	0.08	0.05	0.00	0.01	0.00
	13	0.33	-0.23	0.05	0.05	0.00	0.01	0.00
Primary	14	0.25	-1.12	0.08	-0.10	-0.13	0.01	-1.11
	15	0.82	-0.72	0.25	0.03	-0.02	0.10	-0.02
	16	0.82	-0.85	0.20	0.03	0.09	0.08	0.08
	17	0.80	-0.78	0.20	0.03	0.10	0.08	0.09
	18	0.71	-0.84	0.18	0.05	0.01	0.06	0.01
	19	0.82	-0.70	0.23	0.10	0.06	0.09	0.05
Primary	20	2.64	-2.09	1.04	-0.36	-3.47	1.37	-0.20
	21	2.16	-2.19	0.61	-0.46	-2.07	0.66	-0.25
	22	2.20	-2.48	0.86	-0.61	-1.17	0.95	-0.10
	23	2.34	-2.50	0.79	-0.64	-0.77	0.92	-0.07
	24	2.41	-2.44	0.89	-0.56	-1.80	1.07	-0.13
Primary	25	3.90	-4.18	2.21	-1.88	-7.77	4.31	-0.14
	26	3.93	-4.05	1.75	-1.85	-8.37	3.45	-0.19
	27	3.58	-4.28	1.88	-1.93	-2.04	3.36	-0.05
	28	3.66	-4.21	1.96	-1.78	-1.78	3.58	-0.04
	29	3.99	-4.09	1.91	-1.93	0.28	3.80	0.01
Primary		4.00		1.96		-1.73	3.91	-0.04
	31	6.51	-7.77	-5.16	3.78	9.10	13.31	0.05
	32	6.16	-5.05	-3.28	3.48	1.63	11.66	0.01
	33	5.78	-5.21	-3.28	0.00	1.33	10.06	0.01
Primary	34	11.36	-13.02	9.60	-10.85	43.63	54.56	0.06
	35	10.09	-9.28	8.56	-7.98	31.83	43.19	0.06
	36	9.58	-9.32	8.41	-7.95	29.77	40.29	0.06
Primary	37	16.77	-14.97	16.23	-16.64	142.05	136.06	0.08
	38	11.85	-10.44	12.40	-12.04	57.85	73.43	0.06
	39	11.73	-10.47	12.32	-12.04	48.01	72.24	0.05
Primary	40	16.41	-13.94	-12.04	18.29	398.20	150.09	0.21
	41	5.58	-6.58	18.29	-19.35	126.21	55.53	0.18
	42	5.40	-6.38	-19.35	19.89	123.43	53.61	0.18

Total Estimated Energy

982 kN-mm

Table B.11 Test PP5-2 Summary

Specimen PP5-2
Sill Plate Type PP Three-box hollow section
Date April 29, 2005

	Units	
Area Under Envelope Curve	<i>kN-mm</i>	384
	<i>lbf-in</i>	3397
Area Enclosed by Hysteresis	<i>kN-mm</i>	2082
	<i>lbf-in</i>	18,429
Maximum absolute load, P_{peak}	<i>kN</i>	18.0
	<i>lbf</i>	4043
Maximum absolute displacement, Δ_{peak}	<i>mm</i>	23
	<i>in</i>	0.92
Failure Load, $0.80 \cdot P_{peak}$	<i>kN</i>	14.4
	<i>lbf</i>	3234
Ultimate Displacement, cyclic, Δ_u	<i>mm</i>	30
	<i>in</i>	1.17
$0.40 \cdot P_{peak}$	<i>kN</i>	7.2
	<i>lbf</i>	1617
Displacement, $\Delta_{0.4peak}$	<i>mm</i>	5
	<i>in</i>	0.20
P_{yield}	<i>kN</i>	15.9
	<i>lbf</i>	3575
Yield Displacement, cyclic, Δ_{yield}	<i>mm</i>	11
	<i>in</i>	0.43
Shear Strength, V_{peak}	<i>kN/m</i>	7.4
	<i>lbf/ft</i>	505
Secant Shear Modulus, $G' @ 0.4P_{peak}$	<i>kN/mm</i>	1.5
	<i>lbf/in</i>	8287
Secant Shear Modulus, $G' @ P_{peak}$	<i>kN/mm</i>	0.8
	<i>lbf/in</i>	4394
Elastic Shear Stiffness, K_e	<i>kN/mm</i>	1.5
	<i>lbf/in</i>	8287

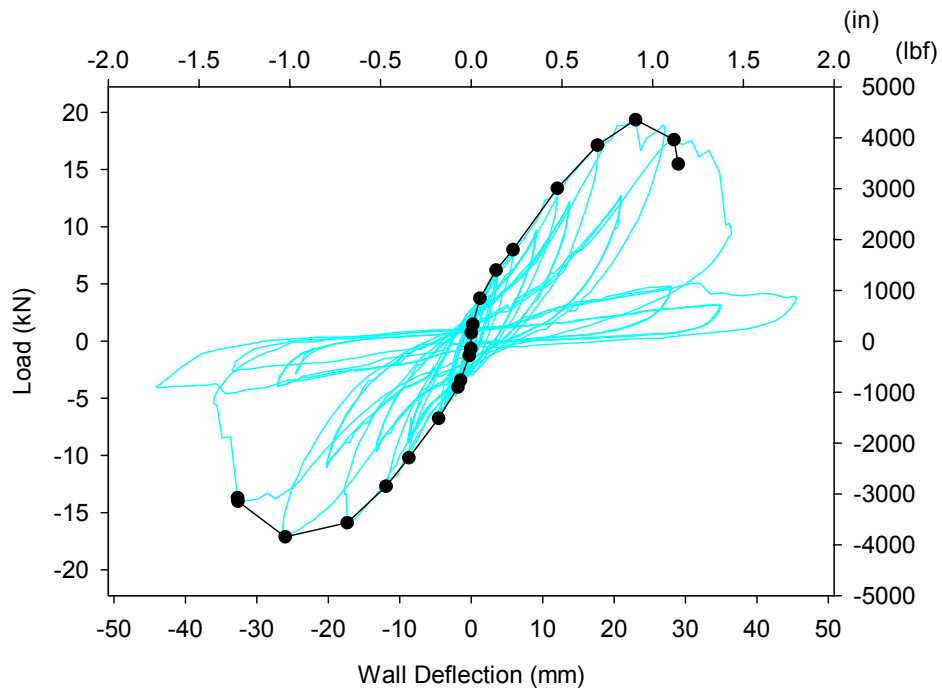


Figure B.17 Test PP5-2 Hysteresis (Reference Displacement = 18 mm (0.70 in))

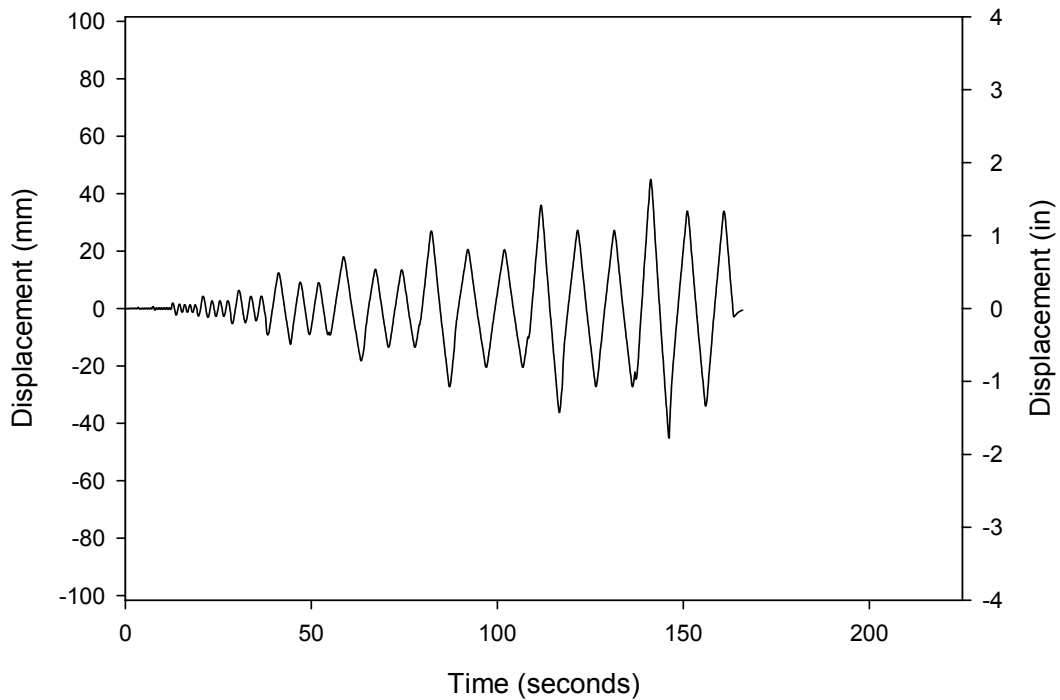


Figure B.18 Time history for Test PP5-2

Table B.12 Test PP5-2 Energy and damping data

Cycle Number	Cycle Maximums				Hysteretic Energy W_D (kN-mm)	Strain Energy U (kN-mm)	EVDR, ζ_{eq} (radians)	
	Load (kN)		Deflection (mm)					
	Positive	Negative	Positive	Negative				
Initiation	1	0.13	-0.22	-0.03	-0.03	0.00	0.00	0.14
	2	0.21	-0.15	-0.03	-0.03	0.00	0.00	0.00
	3	0.22	-0.16	-0.03	0.00	0.00	0.00	0.00
	4	0.22	-0.15	-0.03	-0.03	0.00	0.00	-0.02
	5	0.25	-0.19	-0.03	-0.03	0.00	0.00	0.00
	6	0.22	-0.16	-0.03	0.00	0.01	0.00	-0.20
Primary	7	0.75	-0.64	0.00	-0.05	0.00	0.00	0.00
	8	0.13	-0.41	-0.05	-0.05	0.03	0.00	-0.70
	9	0.19	-0.37	-0.05	-0.05	0.00	0.00	0.00
	10	0.23	-0.36	-0.05	-0.05	0.00	-0.01	0.00
	11	0.23	-0.36	-0.05	-0.05	0.00	-0.01	0.00
	12	0.24	-0.36	-0.05	-0.05	0.00	-0.01	0.00
Primary	13	0.21	-0.37	-0.05	-0.05	0.03	-0.01	-0.43
	14	1.47	-1.25	0.20	-0.25	0.18	0.15	0.09
	15	0.46	-0.75	-0.13	-0.15	0.01	-0.03	-0.04
	16	0.66	-0.68	-0.08	-0.13	0.02	-0.03	-0.07
	17	0.67	-0.67	-0.05	-0.10	0.05	-0.02	-0.22
	18	0.68	-0.68	-0.05	-0.10	0.00	-0.02	-0.02
Primary	19	0.67	-0.69	-0.05	-0.10	0.02	-0.02	-0.07
	20	0.68	-0.65	-0.05	-0.10	0.22	-0.02	-1.01
	21	3.75	-3.42	1.22	-1.50	2.20	2.29	0.08
	22	3.35	-2.36	0.86	-0.84	0.59	1.45	0.03
	23	2.97	-2.44	0.69	-0.86	0.49	1.02	0.04
	24	2.97	-2.46	0.69	-0.86	0.51	1.02	0.04
Primary	25	2.95	-4.01	0.69	-1.85	3.07	1.01	0.24
	26	6.22	-4.84	3.48	-2.18	12.53	10.82	0.09
	27	4.37	-4.29	1.91	-1.91	4.61	4.16	0.09
	28	4.56	-4.29	2.01	-1.91	4.59	4.57	0.08
Primary	29	4.57	-6.75	2.03	-4.57	13.86	4.64	0.24
	30	8.01	-6.34	5.87	-4.32	33.25	23.48	0.11
	31	5.86	-5.56	3.63	-3.68	19.13	10.65	0.14
	32	5.84	-10.19	3.71	-8.74	39.17	10.83	0.29
Primary	33	13.36	-12.68	12.07	-11.91	103.67	80.62	0.10
	34	9.71	-8.85	9.12	-8.71	55.55	44.25	0.10
	35	9.54	-8.90	8.99	-8.74	54.48	42.90	0.10
	36	17.14	-15.86	17.68	-17.35	202.38	151.51	0.11
Primary	37	12.23	-9.58	13.77	-13.13	84.79	84.19	0.08
	38	12.04	-9.65	13.64	-13.26	83.29	82.10	0.08
	39	19.36	-17.10	23.01	-26.04	343.30	222.76	0.12
	40	12.73	-10.98	20.98	-20.19	124.48	133.56	0.07
Primary	41	12.71	-11.02	20.96	-20.22	115.64	133.15	0.07
	42	17.63	-14.00	28.37	-32.64	540.11	250.03	0.17
	43	4.85	-3.94	27.99	-27.13	123.23	67.82	0.14
	44	4.75	-3.96	27.84	-27.13	116.77	66.18	0.14

Total Estimated Energy

2082 kN-mm

Table B.13 Test PP10-1 Summary

Specimen PP10-1
Sill Plate Type PP Hollow section
Date April 30, 2005

	Units	
Area Under Envelope Curve	<i>kN-mm</i>	1732
	<i>lbf-in</i>	15329
Area Enclosed by Hysteresis	<i>kN-mm</i>	5133
	<i>lbf-in</i>	45,433
Maximum absolute load, P_{peak}	<i>kN</i>	28.7
	<i>lbf</i>	6456
Maximum absolute displacement, Δ_{peak}	<i>mm</i>	46
	<i>in</i>	1.82
Failure Load, $0.80 \cdot P_{peak}$	<i>kN</i>	23.0
	<i>lbf</i>	5165
Ultimate Displacement, cyclic, Δ_u	<i>mm</i>	76
	<i>in</i>	3.01
$0.40 \cdot P_{peak}$	<i>kN</i>	11.5
	<i>lbf</i>	2582
Displacement, $\Delta_{0.4peak}$	<i>mm</i>	9
	<i>in</i>	0.36
P_{yield}	<i>kN</i>	26.2
	<i>lbf</i>	5897
Yield Displacement, cyclic, Δ_{yield}	<i>mm</i>	21
	<i>in</i>	0.81
Shear Strength, v_{peak}	<i>kN/m</i>	11.8
	<i>lbf/ft</i>	807
Secant Shear Modulus, $G' @ 0.4P_{peak}$	<i>kN/mm</i>	1.3
	<i>lbf/in</i>	7254
Secant Shear Modulus, $G' @ P_{peak}$	<i>kN/mm</i>	0.6
	<i>lbf/in</i>	3547
Elastic Shear Stiffness, K_e	<i>kN/mm</i>	1.3
	<i>lbf/in</i>	7254

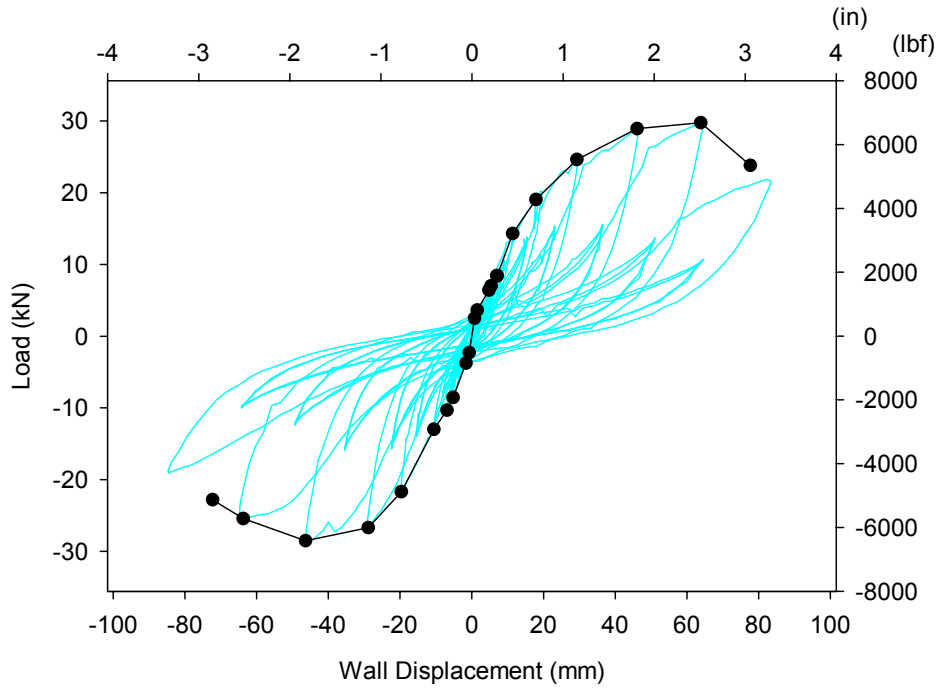


Figure B.19 Test PP10-1 Hysteresis (Reference Displacement = 35 mm (1.39 in))

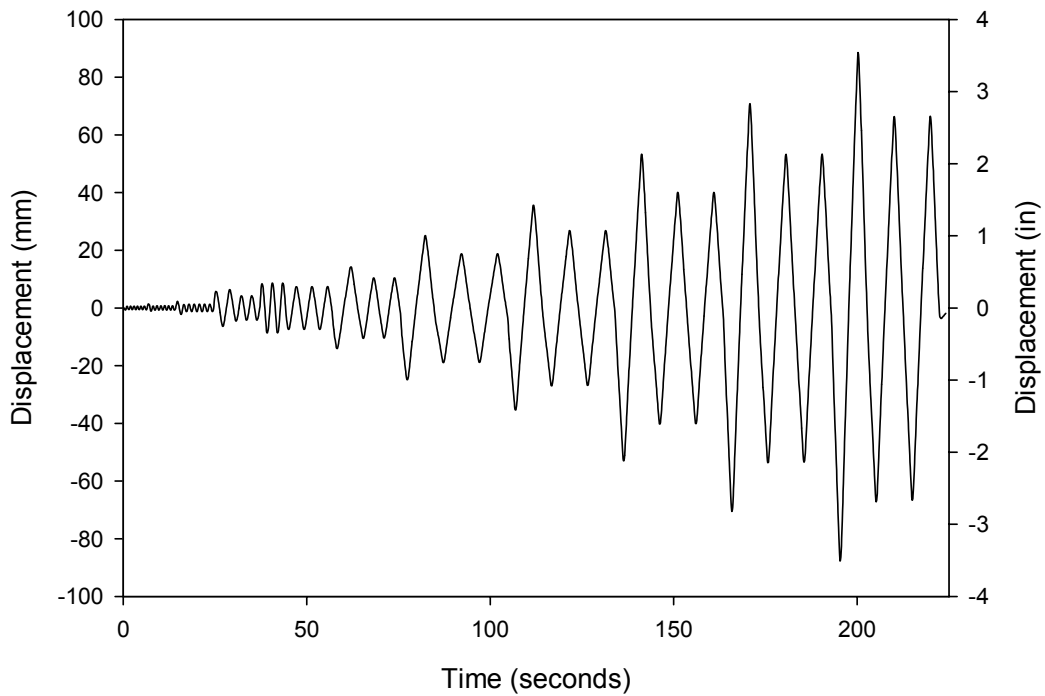


Figure B.20 Time history for Test PP10-1

Table B.14 Test PP10-1 Energy and damping data

Cycle Number	Cycle Maximums				Hysteretic Energy W_D (kN-mm)	Strain Energy U (kN-mm)	EVDR, ζ_{eq} (radians)	
	Load (kN)		Deflection (mm)					
	Positive	Negative	Positive	Negative				
Initiation	1	1.01	-1.31	0.03	-0.33	0.07	0.01	0.44
	2	1.07	-1.31	0.05	-0.33	0.02	0.03	0.07
	3	1.05	-1.28	0.05	-0.33	0.07	0.03	0.21
	4	1.09	-1.30	0.05	-0.33	0.10	0.03	0.28
	5	1.09	-1.31	0.05	-0.33	0.08	0.03	0.24
	6	1.11	-1.45	0.08	-0.38	0.08	0.04	0.15
Primary	7	2.47	-2.32	0.71	-0.74	0.68	0.88	0.06
	8	1.18	-1.61	0.13	-0.46	0.05	0.08	0.05
	9	1.39	-1.55	0.20	-0.43	0.06	0.14	0.04
	10	1.39	-1.55	0.20	-0.43	-0.08	0.14	-0.04
	11	1.40	-1.57	0.20	-0.43	0.04	0.14	0.02
	12	1.41	-1.55	0.23	-0.41	0.10	0.16	0.05
Primary	13	1.40	-1.57	0.23	-0.43	0.07	0.16	0.04
	14	3.62	-3.78	1.50	-1.65	3.00	2.71	0.09
	15	2.14	-2.35	0.56	-0.86	0.69	0.60	0.09
	16	2.34	-2.34	0.69	-0.84	0.49	0.80	0.05
	17	2.35	-2.36	0.69	-0.86	0.46	0.81	0.05
	18	2.33	-2.36	0.69	-0.86	0.39	0.80	0.04
Primary	19	2.30	-2.36	0.69	-0.86	0.55	0.79	0.06
	20	2.32	-2.36	0.69	-0.86	0.31	0.79	0.03
	21	6.40	-8.57	4.75	-5.28	20.07	15.20	0.11
	22	6.99	-6.07	5.33	-3.81	15.86	18.64	0.07
	23	4.72	-5.63	3.38	-3.51	8.83	7.98	0.09
	24	4.72	-5.62	3.43	-3.48	10.32	8.09	0.10
Primary	25	8.39	-10.33	6.91	-6.99	16.18	28.99	0.04
	26	8.41	-10.06	7.04	-6.96	19.95	29.60	0.05
	27	8.32	-8.43	7.09	-6.07	18.88	29.50	0.05
	28	7.23	-8.44	6.35	-6.07	21.30	22.97	0.07
	29	7.23	-8.42	6.35	-6.07	19.97	22.96	0.07
	30	7.20	-8.42	6.35	-6.07	10.27	22.87	0.04
Primary	31	14.29	-12.99	11.35	-10.64	71.34	81.12	0.07
	32	10.55	-8.41	9.04	-8.13	38.54	47.70	0.06
	33	10.36	-8.44	8.94	-8.13	35.58	46.32	0.06
Primary	34	19.02	-21.70	17.86	-19.69	253.66	169.82	0.12
	35	13.58	-13.85	15.32	-15.37	106.06	103.97	0.08
	36	13.78	-13.99	15.34	-15.44	94.36	105.68	0.07
Primary	37	24.59	-26.70	29.26	-28.93	496.46	359.74	0.11
	38	15.37	-15.66	23.06	-22.33	184.79	177.25	0.08
	39	15.29	-15.70	23.09	-22.45	163.42	176.50	0.07
Primary	40	28.90	-28.54	46.05	-46.38	1022.14	665.50	0.12
	41	15.61	-15.73	36.40	-35.38	310.25	284.10	0.09
	42	15.48	-15.89	36.53	-35.43	270.04	282.74	0.08
Primary	43	29.74	-25.45	63.80	-63.80	1273.65	948.62	0.11
	44	13.70	-12.33	51.03	-49.35	350.75	349.56	0.08
	45	13.36	-12.38	50.83	-49.40	293.37	339.57	0.07

Total Estimated Energy

5133 kN-mm

Table B.15 Test PP10-2 Summary

Specimen PP10-2
Sill Plate Type PP Hollow section
Date May 2, 2005

	Units	
Area Under Envelope Curve	<i>kN-mm</i>	1764
	<i>lbf-in</i>	15,610
Area Enclosed by Hysteresis	<i>kN-mm</i>	7663
	<i>lbf-in</i>	67,826
Maximum absolute load, P_{peak}	<i>kN</i>	28
	<i>lbf</i>	6393
Maximum absolute displacement, Δ_{peak}	<i>mm</i>	43
	<i>in</i>	1.68
Failure Load, $0.80 \cdot P_{peak}$	<i>kN</i>	22.8
	<i>lbf</i>	5114
Ultimate Displacement, cyclic, Δ_u	<i>mm</i>	78
	<i>in</i>	3.07
$0.40 \cdot P_{peak}$	<i>kN</i>	11.4
	<i>lbf</i>	2557
Displacement, $\Delta_{0.4peak}$	<i>mm</i>	9
	<i>in</i>	0.37
P_{yield}	<i>kN</i>	26.2
	<i>lbf</i>	5899
Yield Displacement, cyclic, Δ_{yield}	<i>mm</i>	22
	<i>in</i>	0.86
Shear Strength, v_{peak}	<i>kN/m</i>	11.7
	<i>lbf/ft</i>	799
Secant Shear Modulus, $G' @ 0.4P_{peak}$	<i>kN/mm</i>	1.2
	<i>lbf/in</i>	6885
Secant Shear Modulus, $G' @ P_{peak}$	<i>kN/mm</i>	0.7
	<i>lbf/in</i>	3805
Elastic Shear Stiffness, K_e	<i>kN/mm</i>	1.2
	<i>lbf/in</i>	6885

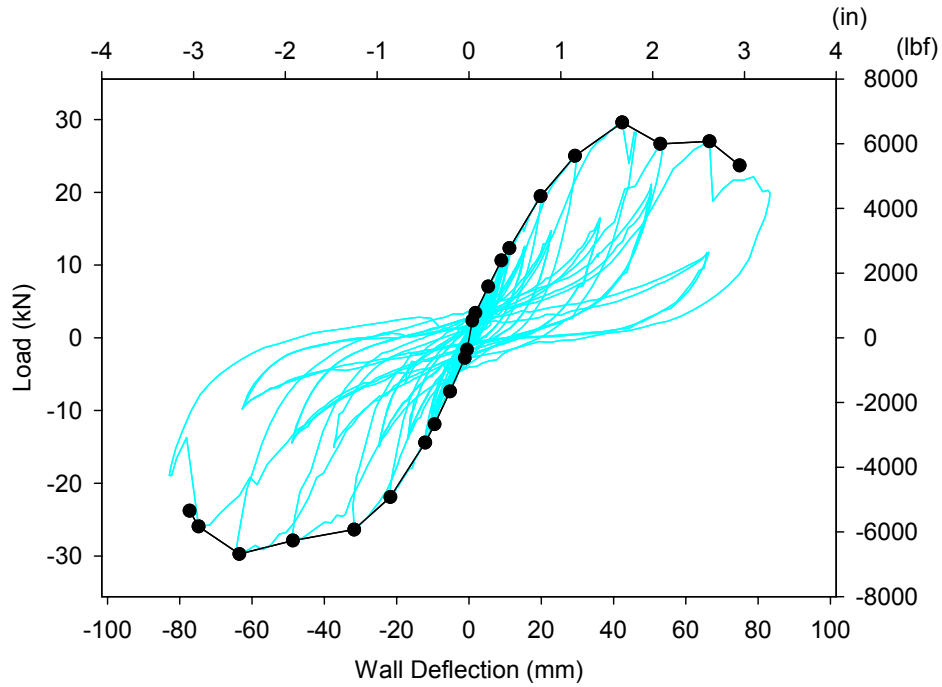


Figure B.21 Test PP10-2 Hysteresis (Reference Displacement = 35 mm (1.39 in))

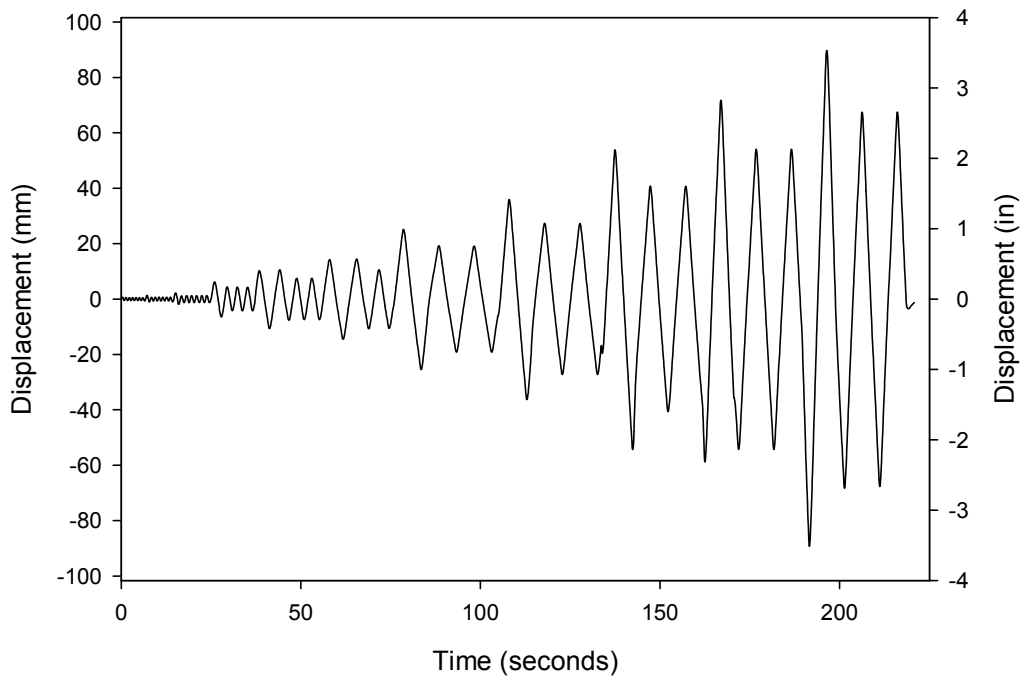


Figure B.22 Time history for Test PP10-2

Table B.16 Test PP10-2 Energy and damping data

Cycle Number	Cycle Maximums				Hysteretic Energy W_D (kN-mm)	Strain Energy U (kN-mm)	EVDR, Z_{eq} (radians)	
	Load (kN)		Deflection (mm)					
	Positive	Negative	Positive	Negative				
Initiation	1	1.31	-0.81	0.330	-0.203	0.00	0.22	0.00
	2	1.07	-0.92	0.229	-0.229	0.04	0.12	0.03
	3	1.08	-0.91	0.229	-0.254	0.01	0.12	0.01
	4	1.10	-0.90	0.229	-0.229	0.02	0.13	0.02
	5	1.08	-0.91	0.229	-0.254	0.03	0.12	0.02
	6	1.06	-0.92	0.229	-0.254	0.03	0.12	0.02
	7	1.07	-1.14	0.229	-0.356	0.13	0.12	0.08
Primary	8	2.35	-1.61	0.940	-0.533	0.08	1.10	0.01
	9	1.06	-1.12	0.330	-0.305	0.10	0.17	0.05
	10	1.29	-1.12	0.406	-0.305	-0.02	0.26	-0.01
	11	1.32	-1.11	0.432	-0.305	0.06	0.29	0.02
	12	1.28	-1.13	0.406	-0.305	-0.03	0.26	-0.01
	13	1.31	-1.12	0.432	-0.305	0.04	0.28	0.01
	14	1.30	-1.50	0.406	-0.483	0.12	0.26	0.04
Primary	15	3.42	-2.76	1.803	-1.143	0.93	3.08	0.02
	16	1.85	-1.87	0.838	-0.660	0.24	0.78	0.03
	17	2.02	-1.84	0.940	-0.635	0.09	0.95	0.01
	18	2.04	-1.88	0.940	-0.610	0.19	0.96	0.02
	19	2.05	-1.88	0.940	-0.610	0.04	0.97	0.00
	20	2.03	-1.90	0.940	-0.635	0.16	0.95	0.01
	21	2.03	-1.86	0.940	-0.635	0.13	0.95	0.01
Primary	22	7.04	-7.36	5.359	-5.258	16.16	18.88	0.07
	23	5.11	-4.47	3.734	-2.870	4.69	9.55	0.04
	24	4.96	-4.62	3.683	-2.946	3.45	9.14	0.03
	25	4.94	-4.63	3.632	-2.946	4.15	8.97	0.04
Primary	26	10.63	-11.88	8.992	-9.525	43.06	47.79	0.07
	27	10.63	-8.02	9.246	-7.061	26.76	49.16	0.04
	28	6.69	-7.75	6.350	-6.858	13.63	21.23	0.05
	29	6.80	-7.73	6.401	-6.858	12.86	21.77	0.05
Primary	30	12.31	-14.41	11.201	-12.116	63.82	68.96	0.07
	31	11.92	-11.51	11.278	-10.465	47.80	67.22	0.06
	32	8.63	-11.13	8.865	-10.236	29.62	38.24	0.06
Primary	33	19.46	-21.89	19.812	-21.742	270.73	192.81	0.11
	34	12.60	-13.71	15.418	-16.789	96.65	97.15	0.08
	35	12.51	-13.86	15.392	-16.789	87.16	96.27	0.07
Primary	36	25.03	-26.37	29.337	-31.750	542.11	367.13	0.12
	37	14.70	-14.82	22.835	-24.816	175.32	167.85	0.08
	38	14.72	-14.96	22.606	-24.790	153.37	166.37	0.07
Primary	39	29.61	-27.87	42.393	-48.692	1018.08	627.69	0.13
	40	16.49	-15.04	36.297	-37.414	336.03	299.33	0.09
	41	16.44		36.170		153.87	297.35	0.04
Primary	42	26.66	-29.73	52.934	-63.525	1032.83	705.69	0.12
	43	21.13	-14.47	50.470	-48.946	481.58	533.25	0.07
	44	20.41	-14.47	50.521	-48.997	402.83	515.58	0.06
Primary	45	27.01	-25.94	66.548	-74.778	1807.76	898.77	0.16
	46	11.77	-9.68	66.319	-62.636	461.01	390.17	0.09
	47	11.70	-9.84	65.837	-62.713	375.60	385.10	0.08

Total Estimated Energy

7663 kN-mm

B.4 Cyclic Stiffness

Initial stiffness values for each primary were calculated based on maximum load and associated displacement for each cycle. Data was used as an estimate for comparison of stiffness degradation.

Table B.17 Cyclic stiffness values

Test WOOD4-1			Test WOOD4-2			Test PE3-1			Test PE3-2		
Primary Cycle Number	Positive Hysteresis Stiffness	Negative Hysteresis Stiffness	Primary Cycle Number	Positive Hysteresis Stiffness	Negative Hysteresis Stiffness	Primary Cycle Number	Positive Hysteresis Stiffness	Negative Hysteresis Stiffness	Primary Cycle Number	Positive Hysteresis Stiffness	Negative Hysteresis Stiffness
	<i>kN/mm</i>	<i>kN/mm</i>		<i>kN/mm</i>	<i>kN/mm</i>		<i>kN/mm</i>	<i>kN/mm</i>		<i>kN/mm</i>	<i>kN/mm</i>
1	2.9	3.1	1	3.4	1.8	1	5.5	2.6	1	2.2	1.9
2	2.1	2.0	2	2.4	1.7	2	2.0	2.7	2	2.0	1.7
3	1.2	1.4	3	1.4	1.2	3	1.3	2.6	3	1.2	1.2
4	1.0	0.8	4	1.1	1.0	4	1.0	2.0	4	1.0	1.0
5	0.6	0.4	5	0.9	0.6	5	0.8	1.4	5	0.8	0.9
6	0.4	0.3	6	0.4	0.4	6	0.5	1.0	6	0.8	0.5
7	0.3	0.2	7	0.3	0.3	7	0.3	0.8	7	0.3	0.3
8	0.2	0.2	8	0.2	0.2	8	0.2	0.5	8	0.2	0.2
			9		93	9		0.3			
						10		0.3			

Test PP5-1			Test PP5-2			Test PP10-1			Test PP10-2		
Primary Cycle Number	Positive Hysteresis Stiffness	Negative Hysteresis Stiffness	Primary Cycle Number	Positive Hysteresis Stiffness	Negative Hysteresis Stiffness	Primary Cycle Number	Positive Hysteresis Stiffness	Negative Hysteresis Stiffness	Primary Cycle Number	Positive Hysteresis Stiffness	Negative Hysteresis Stiffness
	<i>kN/mm</i>	<i>kN/mm</i>		<i>kN/mm</i>	<i>kN/mm</i>		<i>kN/mm</i>	<i>kN/mm</i>		<i>kN/mm</i>	<i>kN/mm</i>
1	3.3	21.0	1	21.8	12.7	1	3.5	3.1	1	2.5	3.0
2	2.5	12.7	2	7.2	4.9	2	2.4	2.3	2	1.9	2.4
3	1.8	11.0	3	3.1	2.3	3	1.3	1.6	3	1.3	1.4
4	1.6	5.9	4	1.8	2.2	4	1.3	1.5	4	1.2	1.2
5	1.2	2.2	5	1.4	1.5	5	1.2	1.2	5	1.1	1.2
6	1.0	1.5	6	1.1	1.2	6	1.2	1.1	6	1.0	1.0
7	0.9	1.2	7	1.0	1.1	7	1.3	0.9	7	0.9	0.8
8	0.2	0.9	8	0.8	0.9	8	1.1	0.6	8	0.7	0.6
9		0.7	9	0.6	0.7	9	0.8	0.4	9	0.5	0.5
10		0.3	10	0.2	0.4	10	0.6	0.2	10	0.4	0.3
			11		0.1	11	0.5		11	0.3	0.2

B.5 Load Washer

Load washer data has been included to document load distribution throughout the length of sills, throughout testing. Both monotonic and cyclic results are included here. Figures B.25-B.28 plot monotonic time histories for load washers, whereas Figures B.29-B.31 plot the displacement-load history to compare how individual washers gain load as load is applied.

Cyclic results plot time histories for load washers for each test. The applied load is plotted behind all three load washer data plots for comparison. Initial load offset for load washers exists from tightening bolts prior to testing. The “loss” of this prestress and the resulting shift in the offset for individual washers exists as sill fibers compress and material splits, causing the force on bolts to reduce.

Monotonic Results

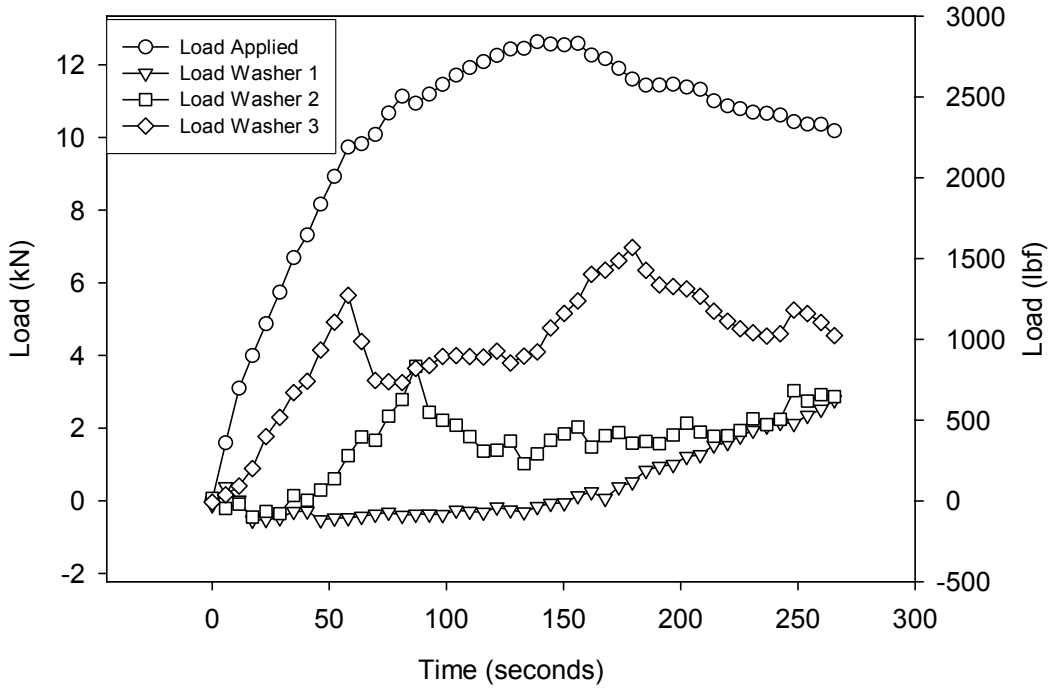


Figure B.25 Test WOOD4-M load washer data

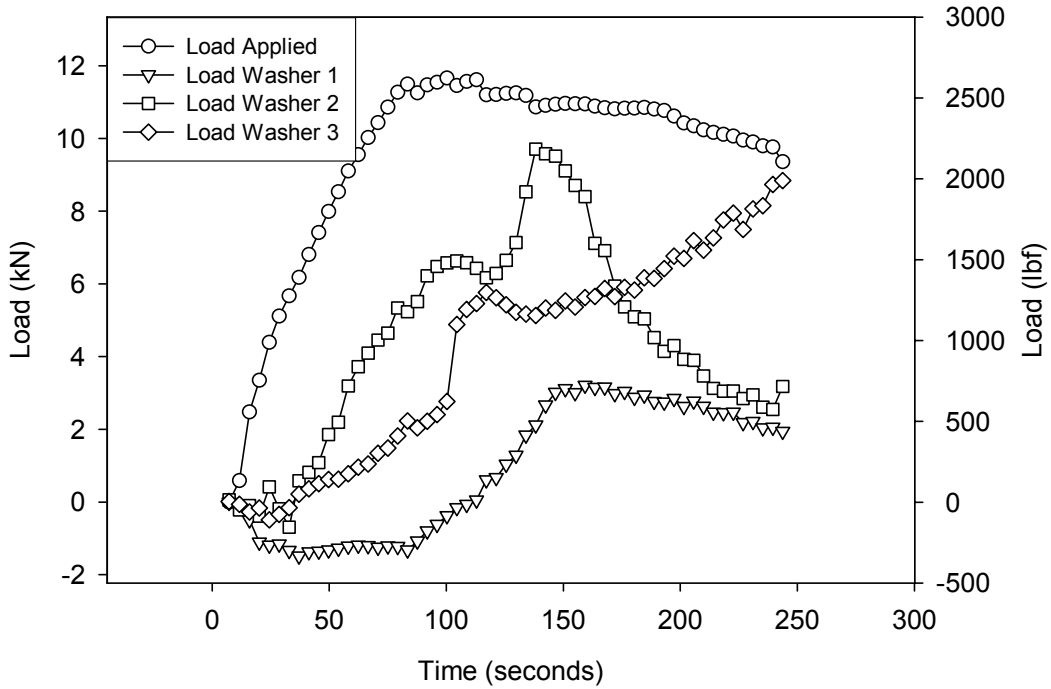


Figure B.26 Test PE3-M load washer data

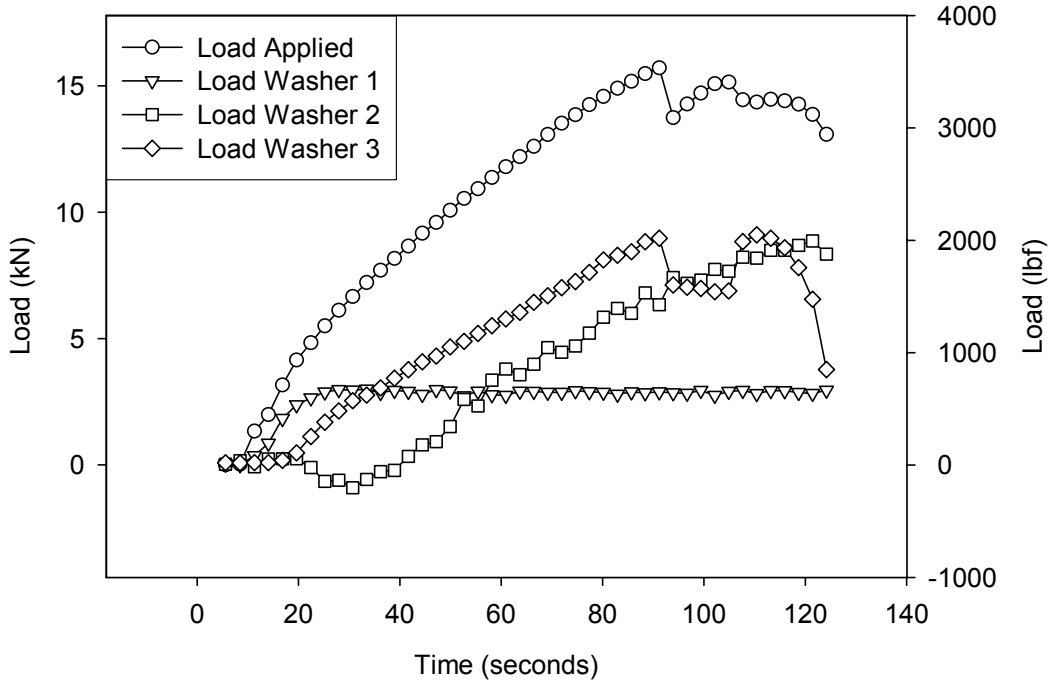


Figure B.27 Test PP5-M load washer data

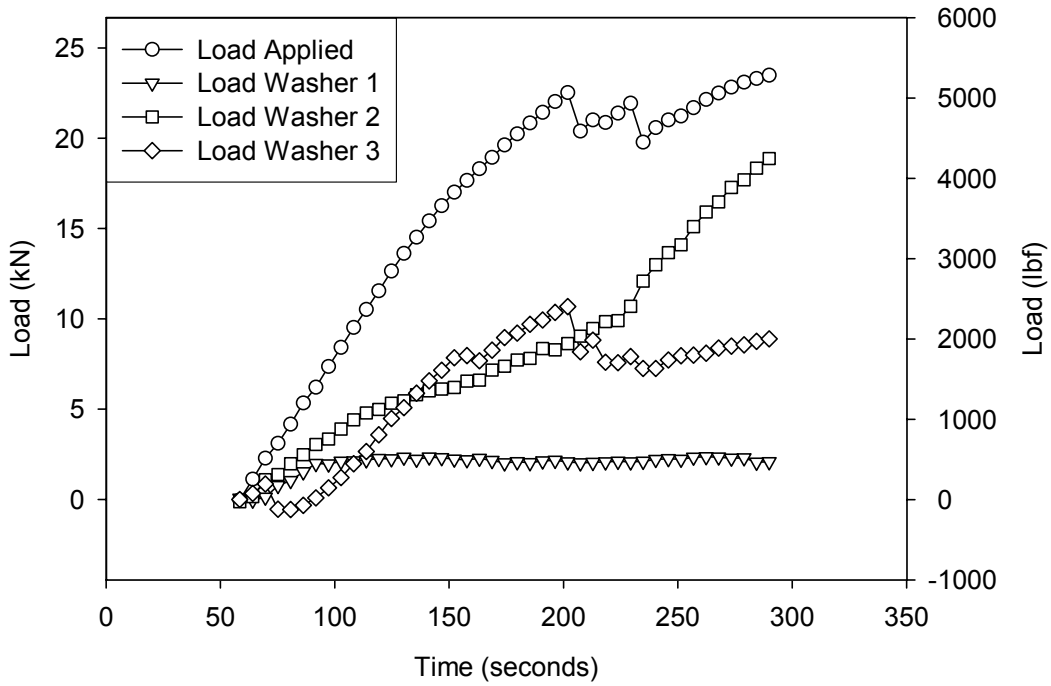


Figure B.28 Test PP10-M load washer data

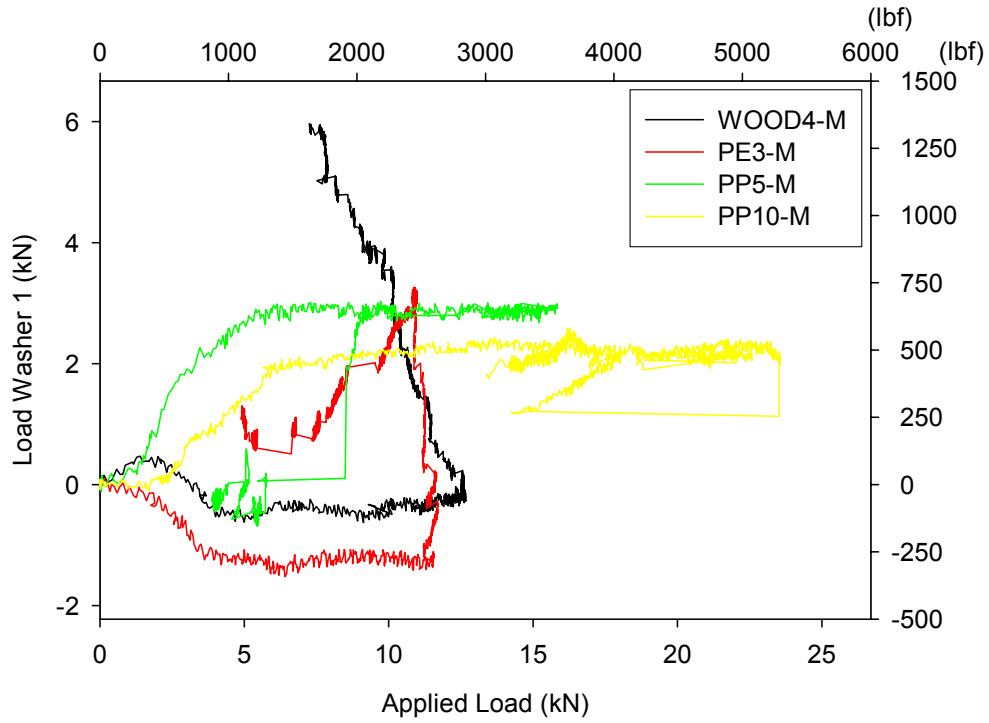


Figure B.29 Load washer 1 test data

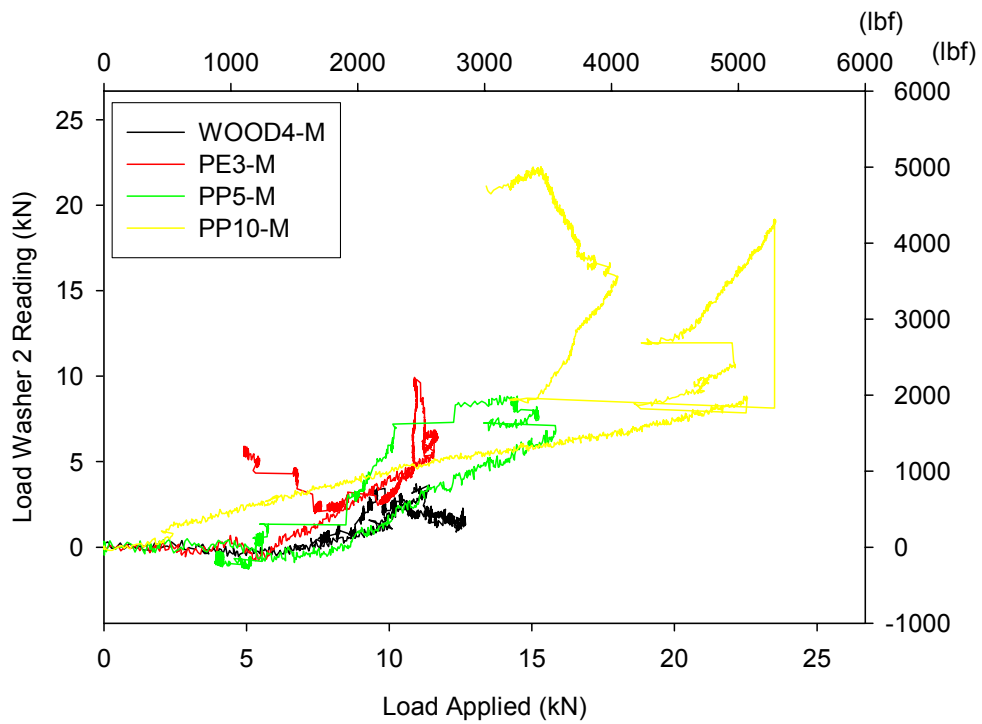


Figure B.30 Load washer 2 test data

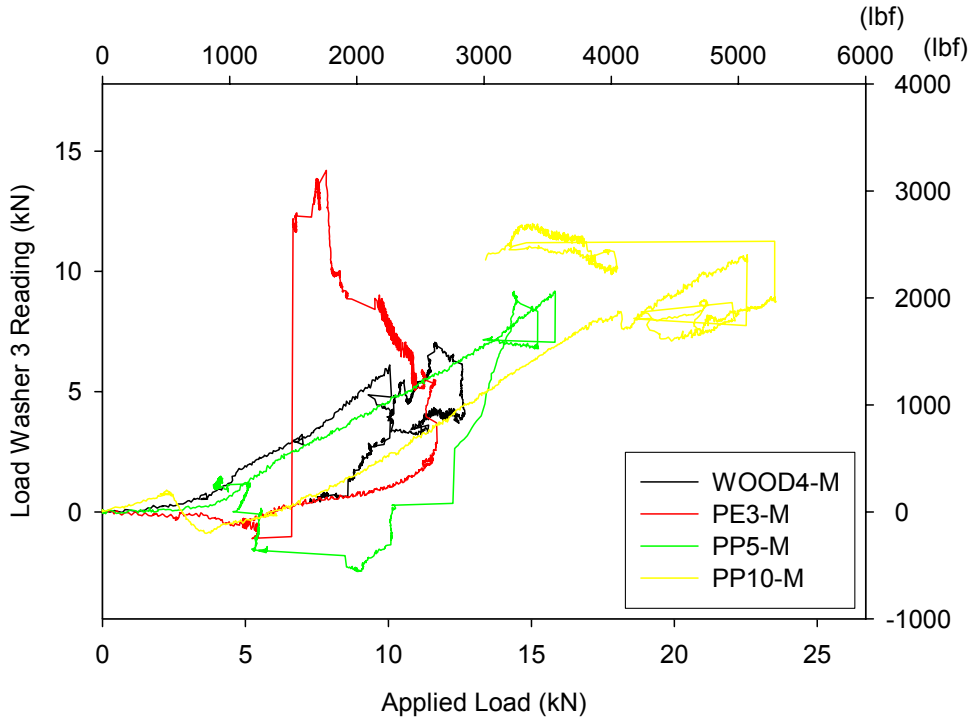


Figure B.31 Load washer 3 test data

Cyclic Results

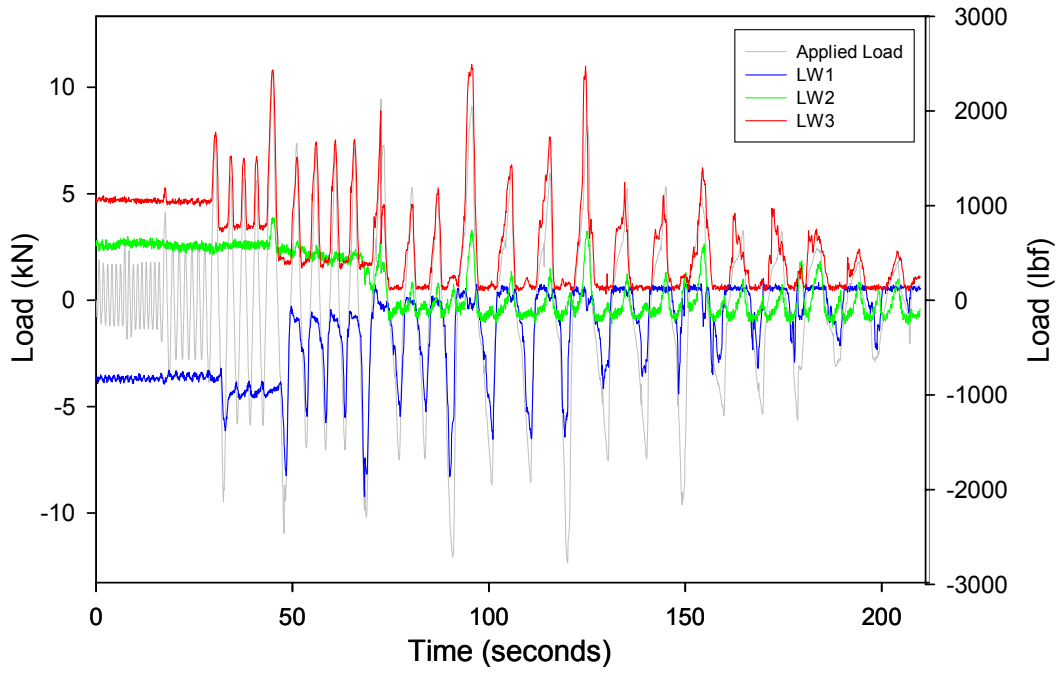


Figure B.32 Test WOOD4-1 load washer time history

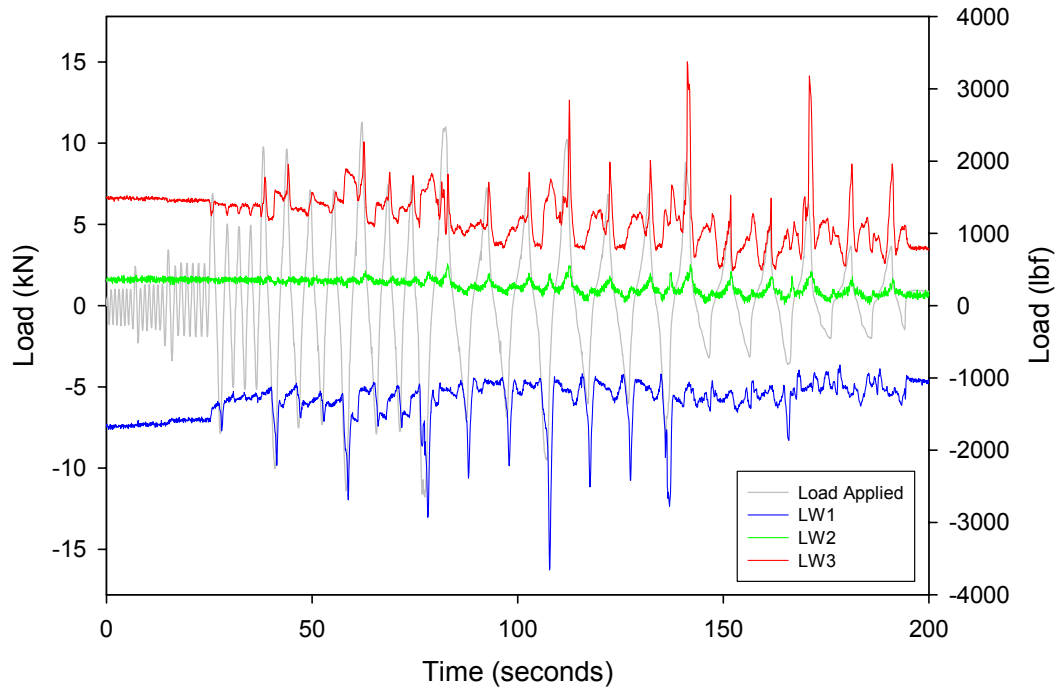


Figure B.33 Test WOOD4-2 load washer time history

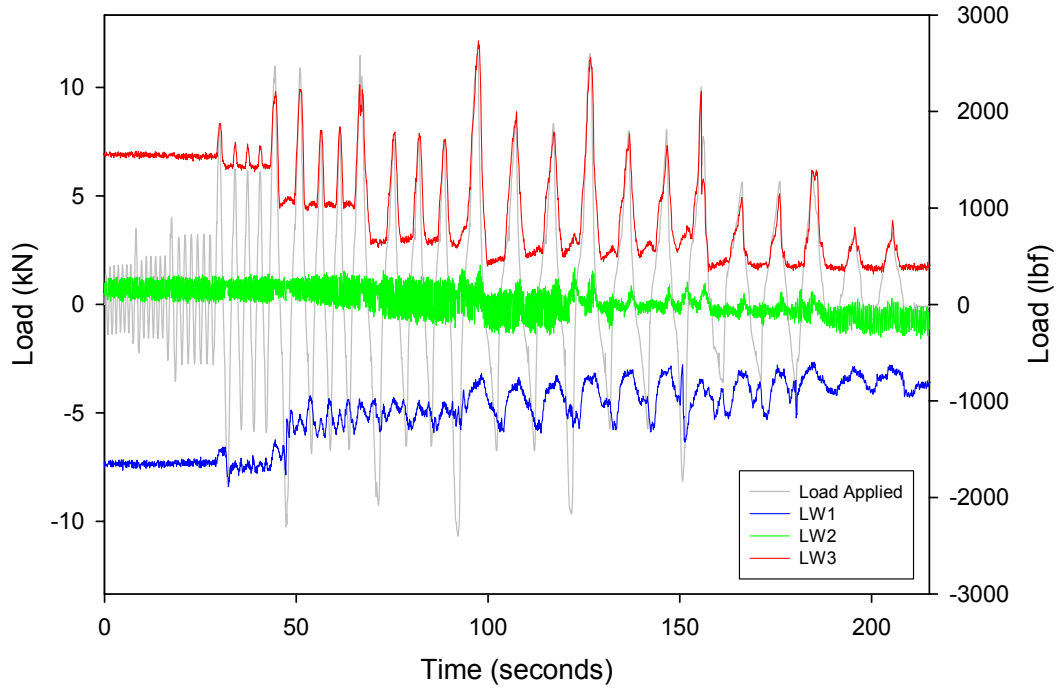


Figure B.34 Test PE3-1 load washer time history

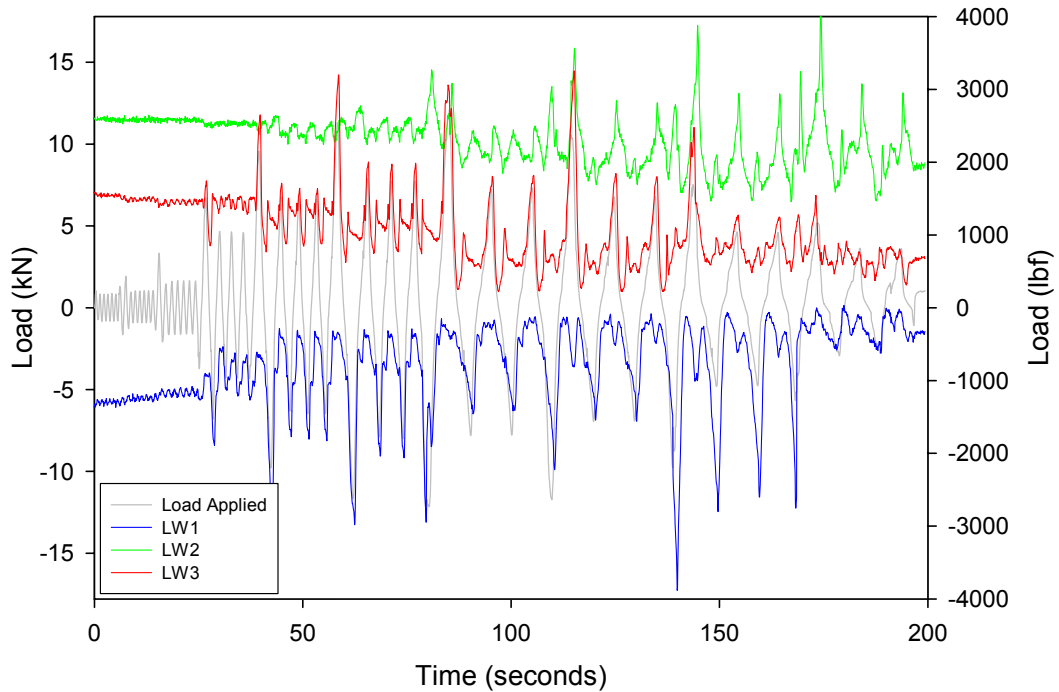


Figure B.35 Test PE3-2 load washer time history

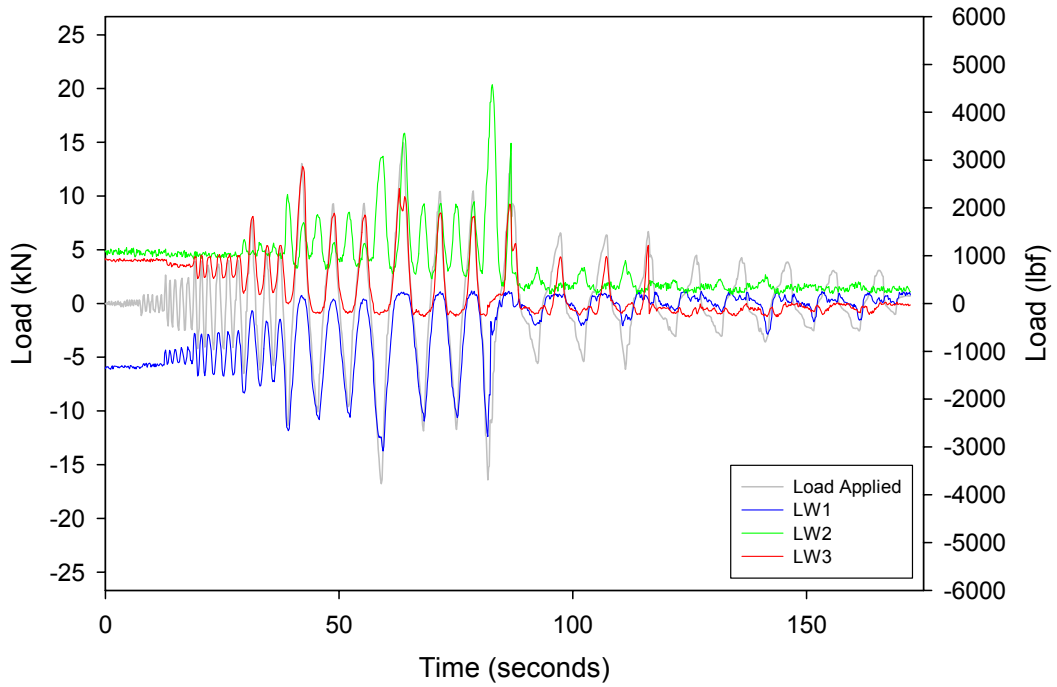


Figure B.36 Test PP5-1 load washer time history

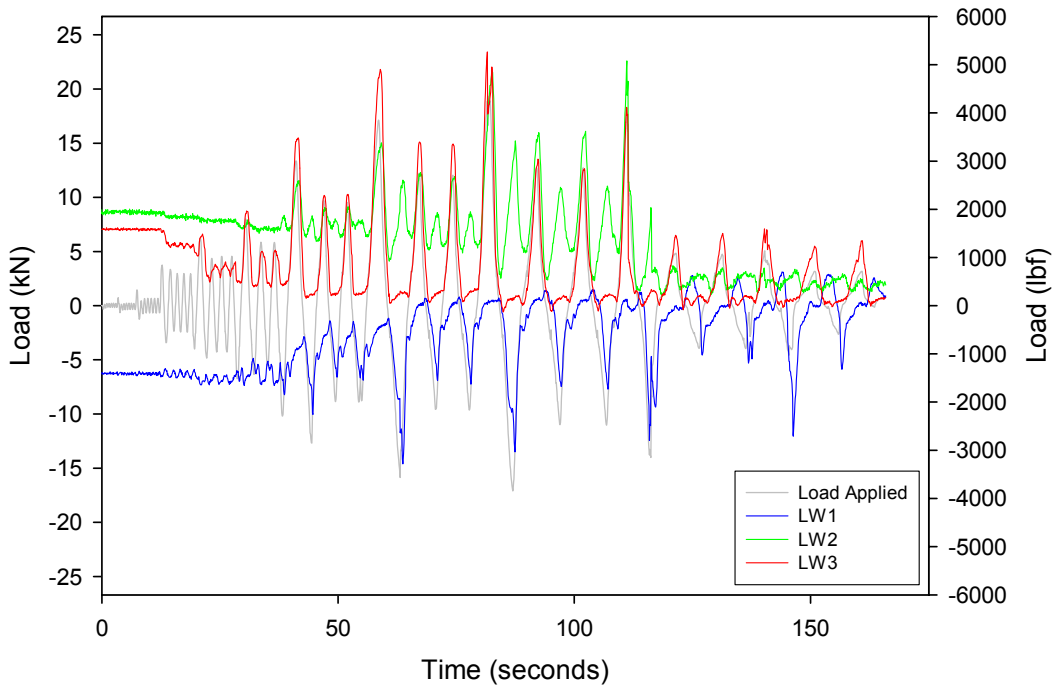


Figure B.37 Test PP5-2 load washer time history

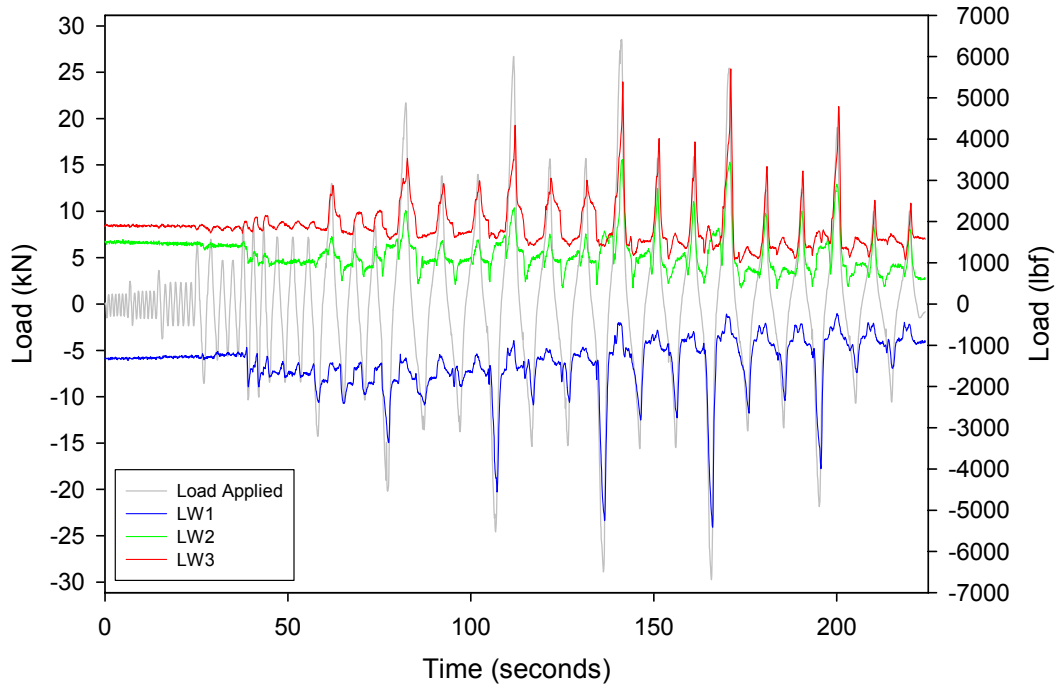


Figure B.38 Test PP10-1 load washer time history

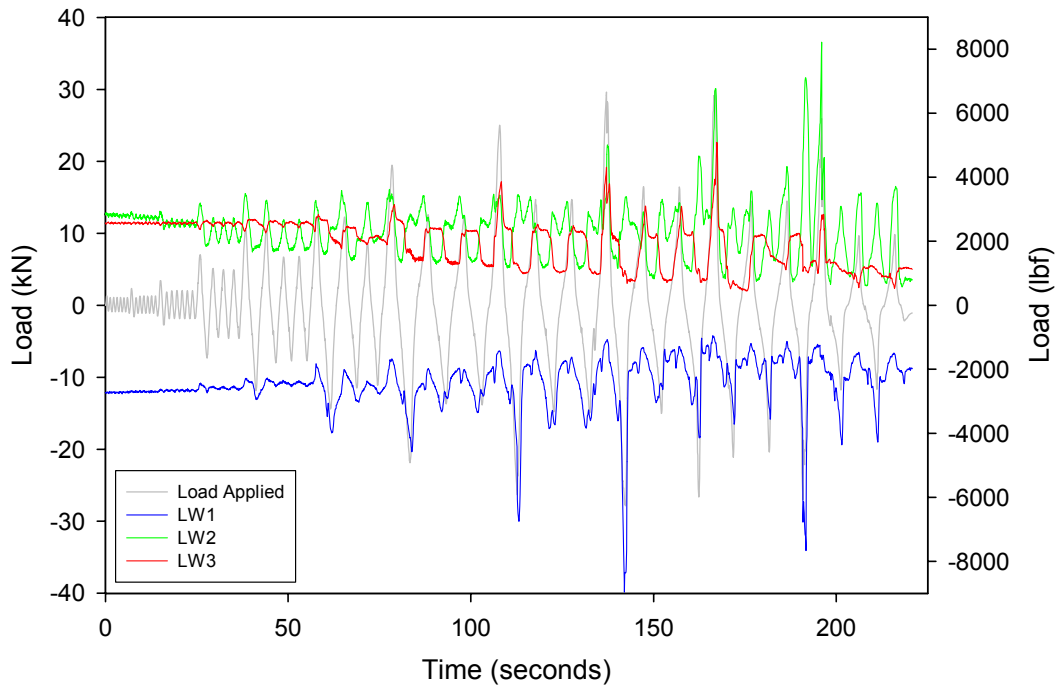


Figure B.39 Test PP10-2 load washer time history